

**INAUGURAL – DISSERTATION**  
zur  
Erlangung der Doktorwürde  
der  
Naturwissenschaftlich-Mathematischen  
Gesamtfakultät  
der  
Ruprecht-Karls-Universität  
Heidelberg

Vorgelegt von:  
Master of Science Chunyu Dong  
aus: Qingzhou, China  
Tag der mündlichen Prüfung:  
8. Juli 2016



## THEMA

Assessing the availability of remote sensing, hydrological modeling  
and in situ observations in snow cover research

Gutachter: Prof. Dr. Lucas Menzel (Ruprecht-Karls-Universität Heidelberg)  
Prof. Dr. habil. Britta Schmalz (Technische Universität Darmstadt)



## Zusammenfassung

Schnee ist ein wichtiger Bestandteil des Wasserkreislaufs. Als Teil der Kryosphäre ist die Schneedecke eine wertvolle terrestrische Ressource von Wasser. Im Kontext des Klimawandels spielt die Variabilität der Schneedecke eine entscheidende Rolle bei den Veränderungen des globalen Energie- und Wasserhaushalts. Die Fernerkundung, die hydrologische Modellierung und Feldbeobachtungen sind die drei wichtigsten Methoden zur Untersuchung von Schneedecken. Unsicherheiten die durch systematische Fehler, Skalenprobleme und den physikalischen Eigenschaften von Schnee entstehen, begrenzen aber die Verfügbarkeit von schneebezogenen Datensätzen. Diese Dissertation zielt auf die Verknüpfung der drei Methoden ab, um hierdurch unser Verständnis des räumlich- zeitlichen Verhaltens der saisonalen Schneedecke auf regionaler Ebene zu erhöhen. Dafür wurde auf Basis von vier Fallstudien in Südwestdeutschland ein neuartiger Algorithmus für die Verbesserung der Qualität von Fernerkundungsdaten mit Hilfe von bodengestützten meteorologischen Beobachtungen entwickelt. Insbesondere bodengestützte Schneehöhenmessungen dienten zur Validierung der Fernerkundungsdaten und zur Reduzierung von Wolken aus MODIS (*Moderate Resolution Imaging Spectroradiometer*) Schneedeckenprodukten. Ein häufiges Problem bei den Satellitendaten ist die Überschätzung von Schneedecken infolge von Wolken, da diese ähnliche Strahlungseigenschaften wie Schnee aufweisen. Daher wurde anhand von Temperatur-, Niederschlags- und Schneehöhendaten ein meteorologischer Filter entwickelt, der diese Überschätzung deutlich reduzieren kann. Im Anschluss wurden mit dem hydrologischen Modell TRAIN die saisonalen Schneedecken simuliert. Die Modellrechnungen wurden mit den verbesserten MODIS Daten und den real gemessenen Schneehöhen validiert und zeigen gute Ergebnisse. Die langfristigen Trends des simulierten Schneewasseräquivalents, der beobachteten Lufttemperatur und des Niederschlages wurden mit dem Mann-Kendall Test und der Theil-Sen Methode statistisch analysiert. Die Ergebnisse zeigen einen signifikanten Rückgang der Schneedecke in den höheren Berglagen Südwestdeutschlands und einen intensiven Erwärmungstrend im März innerhalb der Periode 1961-2008. Ein weiteres Ziel dieser Arbeit war das Verständnis von schneehydrologischen Prozessen zu verbessern und dieses Verständnis in die hydrologische Modellierung einfließen zu lassen. Hierzu wurde eine automatische Wetterstation installiert, mit der anhand von Zeitrafferaufnahmen und manuellen Messungen die komplexen Schneeprozesse im Mittelgebirge (Nordschwarzwald) untersucht werden konnten. Insbesondere die

Zeitraffermethode zeigte sich als gut geeignet um quantitative Informationen von Prozessen, wie z.B. der Schneeeinterzeption von Baumkronen zu erfassen.

Die in dieser Arbeit durchgeführte, kombinierte Anwendung von Fernerkundung, hydrologischer Modellierung und Feldbeobachtung zeigt gute Ergebnisse und die entwickelten Verfahren können einen wichtigen Beitrag bei künftigen Untersuchungen leisten.

## **Abstract**

Snow is an important component of the hydrological cycle. As a major part of the cryosphere, snow cover also represents a valuable terrestrial water resource. In the context of climate change, the dynamics of snow cover play a crucial role in rebalancing the global energy and water budgets. Remote sensing, hydrological modeling and in situ observations are three techniques frequently utilized for snowpack investigation. However, the uncertainties caused by systematic errors, scale issues, snow physics limit the availability of the three approaches in snow studies. This dissertation aims at the linkage of the three methods, seeking for a more effective way to understand the spatial-temporal behavior of seasonal snow cover at regional scales. Four case studies have been conducted in the Upper Rhine Region, southwestern Germany. A novel algorithm has been developed to improve the data quality of remotely sensed snow datasets with the help of ground-based meteorological observations. In particular, in situ snow depth measurements were involved into the cloud-gap-filling schemes of MODIS (Moderate Resolution Imaging Spectroradiometer) snow cover products with a conditional probability method. Meteorological filters generated by temperature, precipitation and snow depth data showed high performance in rejecting the overestimation errors of remotely sensed snow maps. A distributed hydrological model (TRAIN) was employed to simulate the seasonal snow cover, which was then validated against the improved cloud-free MODIS snow products and station-derived snow depth data, indicating a well model performance. The long-term trends of the simulated snow water equivalent as well as the recorded air temperature and precipitation were detected using Mann-Kendall trend test and Theil-Sen estimator, which showed a significant snow retreat at the high elevations and an intense warming trend in March during the study period of 1961-2008. Moreover, a snow monitoring network consisting of automatic weather stations, time-lapse photography and manual measurement was applied to reveal the complex snow processes in montane forest environments. Time-lapse photography proved great ability in collecting quantitative snow process information, such as snow canopy interception and blowing snow, suggesting a potential contribution to snow modeling. Finally, it was concluded that a synergistic application of remote sensing, hydrological modeling (with data assimilation) and field observations should be strengthened for the snow cover research in the future.



# Contents

<b>Zusammenfassung</b> .....	<b>i</b>
<b>Abstract</b> .....	<b>iii</b>
<b>List of Figures</b> .....	<b>ix</b>
<b>List of tables</b> .....	<b>xi</b>
<b>Mathematical and physical notations</b> .....	<b>xii</b>
<b>Abbreviations</b> .....	<b>xiii</b>
<b>Chapter 1 Introduction</b> .....	<b>1</b>
1.1 Snow cover properties .....	2
1.2 Snow cover parameters and measurements .....	2
1.3 In situ monitoring of snow .....	5
1.4 Remote sensing of snow .....	6
1.5 Hydrological modeling of snow .....	8
1.6 Outline of the thesis .....	9
<b>Chapter 2 Improvement and application of MODIS 8-day snow products</b> .....	<b>11</b>
2.1 Introduction .....	11
2.2 Study area.....	13
2.3 Data sources .....	15
2.3.1 MODIS data .....	15
2.3.2 Meteorological data and DEM .....	16
2.4 Methodology .....	17
2.4.1 Aqua & Terra Combination.....	17
2.4.2 Min. Ground-T Correction.....	18
2.4.3 Neighborhood Analysis .....	19
2.4.4 Precipitation & Temperature Filter .....	19
2.4.5 Spatial and temporal analysis of snow cover .....	20
2.5 Results.....	20
2.5.1 Reduction of cloud obstruction.....	20
2.5.2 Improved representation of snow cover .....	23
2.6 Validation .....	25

2.7 Spatio-temporal analysis of snow cover.....	30
2.7.1 Spatial variation of snow cover and snow duration .....	30
2.7.2 Temporal variation of snow cover and snow duration .....	33
2.7.3 Influence of spatial factors on snow cover .....	37
2.8 Discussion and conclusions .....	37
<b>Chapter 3 Improvement and application of MODIS daily snow products .....</b>	<b>41</b>
3.1 Introduction .....	41
3.2 Study region and data.....	43
3.2.1 Study area .....	43
3.2.2 MODIS data .....	44
3.2.3 Meteorological data and DEM .....	45
3.3 Methodology .....	45
3.3.1 Aqua/Terra Combination.....	46
3.3.2 Temporal Combination .....	46
3.3.3 Spatial Combination .....	47
3.3.4 Meteorological Interpolation.....	47
3.3.5 Meteorological Correction .....	49
3.4 Results.....	51
3.4.1 Reduction of cloud contamination .....	51
3.4.2 Improvement of snow cover mapping .....	52
3.5 Validation.....	55
3.6 Snow cover in southwestern Germany .....	58
3.7 Discussion and conclusions .....	61
<b>Chapter 4 Simulation of snow cover with TRAIN model .....</b>	<b>65</b>
4.1 Introduction .....	65
4.2 Data .....	67
4.2.1 MODIS snow cover products .....	67
4.2.2 Climatic and hydrologic data.....	67
4.3 Method.....	68
4.3.1 Study area .....	68
4.3.2 Hydrological Model .....	69
4.3.3 Model evaluation .....	69
4.3.4 Trend and correlation analysis.....	70

4.4 Results.....	71
4.4.1 Simulation of snow covered area (SCA) .....	71
4.4.2 Simulation of snow water equivalent (SWE) .....	74
4.5 Snow cover trends under a changing climate .....	77
4.5.1 Trend analysis of snow water equivalent and climate variables.....	77
4.5.2 Seasonal and spatial dynamics of the long-term trends .....	81
4.5.3 Correlation between SWE and climate variables .....	82
4.6 Discussion and conclusions .....	83
<b>Chapter 5 Monitoring of snow processes with time-lapse photography.....</b>	<b>87</b>
5.1 Introduction .....	87
5.2 Methodology .....	89
5.2.1 Study area .....	89
5.2.2 Observation setup.....	90
5.2.3 Digital camera .....	92
5.2.4 Image analysis .....	93
5.3 Results.....	97
5.3.1 Snow depth and validation .....	97
5.3.2 Snow canopy interception .....	100
5.3.3 Snow accumulation and ablation .....	101
5.4 Discussion and conclusions .....	107
<b>Chapter 6 Summary and concluding remarks.....</b>	<b>109</b>
<b>Appendix A Selected snow observation projects, remote sensing sensors and snow models .....</b>	<b>113</b>
<b>Appendix B Relations between ground observations, remote sensing and snow models .....</b>	<b>117</b>
<b>Bibliography.....</b>	<b>119</b>
<b>Acknowledgment .....</b>	<b>138</b>



## List of figures

<b>Figure 1.1</b>	Representative spectral reflectance of snow, clouds, soil and vegetation. ....	7
<b>Figure 2.1</b>	Topography of Rhineland-Palatinate and the network of meteorological stations.....	14
<b>Figure 2.2</b>	Flow chart of 8-day MODIS data processing and validation. ....	18
<b>Figure 2.3</b>	Average and median of the cloud coverage in the original and improved MODIS images.....	21
<b>Figure 2.4</b>	Snow and cloud cover maps of original 8-day MODIS Terra and Aqua images and after implementation of the four steps. 29 Sep. - 6 Oct. 2008 .....	22
<b>Figure 2.5</b>	Snow and cloud cover maps of original 8-day MODIS Terra and Aqua images and after implementation of the four steps. 10 - 17 Feb. 2013.....	22
<b>Figure 2.6</b>	Average and median of the 8-day snow coverage. ....	24
<b>Figure 2.7</b>	Temporal variation in snow cover and snow depth.....	25
<b>Figure 2.8</b>	Over- and underestimation error as well as accuracy of the improve MODIS snow data .....	28
<b>Figure 2.9</b>	Annual overestimation error, underestimation error and accuracy for the improved MODIS snow data.....	29
<b>Figure 2.10</b>	Elevation dependent relationships for snow coverage and snow depth....	31
<b>Figure 2.11</b>	Spatial distribution of snow onset date, end date and snow duration.....	32
<b>Figure 2.12</b>	Temporal variation of MODIS snow coverage at three altitudes .....	34
<b>Figure 2.13</b>	Temporal variation of in situ snow depth at three altitudes .....	35
<b>Figure 2.14</b>	Temporal variation of snow onset date, end date and snow duration. ....	35
<b>Figure 2.15</b>	Spatial distribution of the snow occurrence.....	36
<b>Figure 3.1</b>	Topography of the study area and the locations of snow stations. ....	44
<b>Figure 3.2</b>	Flow chart of daily MODIS snow data processing. ....	46
<b>Figure 3.3</b>	Snow and cloud maps of the original and improved MODIS images .....	51
<b>Figure 3.4</b>	Cloud coverage of the original and improved MODIS images.....	52
<b>Figure 3.5</b>	Snow coverage of the original and improved MODIS images.....	53
<b>Figure 3.6</b>	Temporal variation in snow coverage and snow depth.....	54
<b>Figure 3.7</b>	Validation indices for the original and improved MODIS snow data .....	56
<b>Figure 3.8</b>	Spatial distribution of the validation indices for MODIS snow maps .....	58
<b>Figure 3.9</b>	Temporal variation of the snow coverage for the final MODIS data. ....	59
<b>Figure 3.10</b>	Snow onset dates, end dates and duration days derived from MODIS snow maps and from DWD snow depth observations .....	59
<b>Figure 3.11</b>	Monthly snow occurrence during the snow season .....	61
<b>Figure 4.1</b>	Topography of the study region Rhineland-Palatinate.....	68
<b>Figure 4.2</b>	Simulated snow cover by TRAIN model and MODIS snow maps .....	72

<b>Figure 4.3</b> Simulated SCA by TRAIN model and observed MODIS SCA.....	72
<b>Figure 4.4</b> Simulated SWE by TRAIN model and observed snow depth for the snow season of 2003/2004 .....	75
<b>Figure 4.5</b> Same as Figure 4.4, but for the snow season of 2004/2005. ....	75
<b>Figure 4.6</b> Trends of simulated SWE by TRAIN model in different elevations and months .....	76
<b>Figure 4.7</b> Same as Figure 4.6, but for recorded air temperature .....	78
<b>Figure 4.8</b> Same as Figure 4.6, but for recorded precipitation .....	79
<b>Figure 4.9</b> Spatial distribution of the simulated SWE trends .....	80
<b>Figure 4.10</b> Same as Figure 4.9, but for recorded air temperature .....	80
<b>Figure 4.11</b> Same as Figure 4.9, but for recorded precipitation .....	80
<b>Figure 4.12</b> Spatial distribution of the recorded air temperature, precipitation and simulated SWE.....	82
<b>Figure 4.13</b> Temporal dynamics of the SWE, air temperature and precipitation.....	82
<b>Figure 5.1</b> The two study catchments of Schwarzbach and Murg. ....	90
<b>Figure 5.2</b> Locations and views of the digital cameras at three sites. ....	91
<b>Figure 5.3</b> Camera Canon EOS 1100D and the timer remote control.....	93
<b>Figure 5.4</b> Hourly photos of snow stake at Hundseck.....	93
<b>Figure 5.5</b> Snow interception as observed by time-lapse photography. ....	94
<b>Figure 5.6</b> Thresholds of different binary classification methods .....	96
<b>Figure 5.7</b> Digital-image based snow depths from a semi-automatic procedure and from manually interpreted results at Hundseck.....	98
<b>Figure 5.8</b> Same as Figure 5.5, but for results at Hortenkopf.....	99
<b>Figure 5.9</b> Automatically versus manually interpreted snow depths at Hundseck .....	99
<b>Figure 5.10</b> Snow interception dynamics at Hundseck.....	99
<b>Figure 5.11</b> Same as Figure 8, but for the results at Hortenkopf .....	100
<b>Figure 5.12</b> Snow depth dynamics at Hundseck .....	101
<b>Figure 5.13</b> The differences between snow depths at Hundseck high open and forest sites for the winter season 2014/2015.....	102
<b>Figure 5.14</b> Same as Figure 5.12, but for snow interception.....	105
<b>Figure 6.1</b> Relations between in situ observations, hydrological models and remote sensing in snow cover research. ....	110
<b>Figure A1</b> Relations between ground snow observations, hydrological modeling and remote sensing (Sturm, 2015).....	117

## List of tables

<b>Table 1.1</b> Snow cover parameters investigated in this study.....	3
<b>Table 2.1</b> Parameters of the used MODIS products. ....	16
<b>Table 2.2</b> Elevation zones of MODIS and in situ snow data. ....	20
<b>Table 2.3</b> Cloud coverage for original and improved MODIS snow maps .....	21
<b>Table 2.4</b> Snow coverage for original and improved MODIS images .....	23
<b>Table 2.5</b> Confusion matrix comparing snow depth with MODIS snow cover .....	26
<b>Table 2.6</b> <i>MO</i> error, <i>MU</i> error and accuracy of the improved MODIS snow data .....	27
<b>Table 2.7</b> Correlations between the number of snow days and spatial factors. ....	36
<b>Table 3.1</b> Criterion of PT filters. ....	50
<b>Table 3.2</b> Criterion of SD filters.....	50
<b>Table 3.3</b> Confusion matrix comparing snow depth with MODIS snow cover. ....	54
<b>Table 3.4</b> Parameters of the ten elevation zones.....	60
<b>Table 4.1</b> Evaluation indices of MAE, NSE, Bias and R for simulated SCA by TRAIN model verified using MODIS snow cover maps from November to April.....	73
<b>Table 4.2</b> Evaluation indices of MAE, NSE, Bias and R for simulated SCA by TRAIN model verified using MODIS snow cover maps for the 9 elevation zones .....	74
<b>Table 4.3</b> Correlation coefficients of SWE with air temperature and precipitation.....	83
<b>Table 5.1</b> Parameters of the Canon cameras.....	92
<b>Table 5.2</b> Thresholds of different binary classifications .....	97
<b>Table 5.3</b> Snow accumulation and ablation on the ground.....	103
<b>Table 5.4</b> Snow loading and unloading in canopy cover .....	105
<b>Table A1</b> Selected projects and datasets including in situ snow observations .....	113
<b>Table A2</b> Characteristics of optical sensors for snow detection .....	114
<b>Table A3</b> Characteristics of passive and active microwave snow sensors.....	115
<b>Table A4</b> Selected snow hydrological models .....	116

## Mathematical and physical notations

$\xi$	cm	Threshold of snow depth
$\rho_s$	kg m <sup>-3</sup>	Density of a snowpack
$\rho_w$	kg m <sup>-3</sup>	Density of liquid water
$\gamma$	°C km <sup>-1</sup>	Temperature lapse rate
$H$	m.a.s.l.	Elevation from DEM
$H_0$	m.a.s.l.	Interpolated elevation
$k$	%	MODIS overall accuracy
$MO$	%	MODIS overestimation error
$MU$	%	MODIS underestimation error
$N_s$	-	Numbers of snow pixels on a snow cover map
$N_t$	-	Total cloud-free pixels on a snow cover map
$N_{x,y}$	-	Number of snow days at a station and a pixel
$p$	-	P-value (test for significance)
$P_i$	-	Total pixel number of the corresponding ROI
$P^l$	-	Conditional probability for land
$P^s$	-	Conditional probability for snow
$R$	-	Correlation Coefficient
$SCA$	%	Snow Covered Area
$SCD$	d	Snow Cover Duration
$SD$	cm	Snow Depth
$SED$	JD	Snow End Date
$S_i$	-	Snow pixel number in the foreground of one ROI
$SII$	%	Snow Interception Index
$S_{n,t}$	-	Snow condition for a station $n$ at time $t$
$SOD$	JD	Snow Onset Date
$SWE$	mm	Snow Water Equivalent
$S_{x,y,t}$	-	Snow condition for a pixel $x,y$ at time $t$
$T$	°C	Corrected air/ground temperature
$T_0$	°C	Interpolated air/ground temperature

## Abbreviations

AMSR-E	Advanced Microwave Scanning Radiometer-EOS
AVHRR	Advanced Very High Resolution Radiometer
AWS	Automatic Weather Station
CI	Confidence Interval
CP	Conditional Probability
DEM	Digital Elevation Model
DSLR	Digital Single-Lens Reflex Cameras
DWD	German Weather Service
EnKF	Ensemble Kalman Filter
EOSDIS	Earth Observing System Data and Information System
GAMs	Generalized Additive Models
IPCC	Intergovernmental Panel on Climate Change
IR	Infrared Rays
LiDAR	Light Detection and Ranging
MAE	Mean Absolute Error
MC	Meteorological Composite Filters
MK	Mann-Kendall Test
MO	MODIS Overestimation Error
MODIS	Moderate Resolution Imaging Spectroradiometer
MU	MODIS Underestimation Error
NDSI	Normalized Difference Snow Index
NDVI	Normalized Difference Vegetation Index
NOAA	National Oceanic and Atmospheric Administration
NSE	Nash Sutcliffe Efficiency
PT	Precipitation-Temperature Filters
RMSE	Root Mean Square Error
ROI	Regions Of Interest
RSLE	Regional Snowline Elevation
SMMR	The Scanning Multichannel Microwave Radiometer
SOD	Snow Onset Date
SRTM	The Shuttle Radar Topography Mission
TRAIN	TRAnspiration and INterception evaporation model
VIS	Visible Light
WMO	World Meteorological Organization



# Chapter 1

## Introduction

Snow is precipitation in the form of ice crystals, which fall to Earth and become snow cover. The process of snowfall represents a water transfer from the atmosphere to the ground surface, involved in the natural water cycle. As a main component of the cryosphere, snow cover plays an important role in the Earth's climate system through its impact on the surface energy budget, the water cycle, primary productivity, and surface gas exchange (IPCC, 2013). Snow cover is also an indicator to a changing climate, especially because snow accumulation and ablation are closely related to temperature (Brown and Mote, 2009). Besides, with more than one-sixth of the Earth's population relying on glaciers and seasonal snow packs for their water supply, the consequences of the removing snow cover are likely to be severe with the global warming (Barnett et al., 2005). It is thus imperative and of great significance to decipher the current changes in snow covers at various scales using our knowledge in hydrology and climatology.

According to previous estimations based on observations, reanalysis products and model simulations (Hirabayashi et al., 2008; Hoinkes, 1967), the global percentage of snowfall in total precipitation ranges from 5% to 11%. The significant disagreement between various estimating approaches reveals the large uncertainties in our understanding of the snow distribution. In the context of climate change, the rise in temperature has led to a general reduction in the fraction of precipitation that falls as snow rather than rain, as well as an earlier retreat of snow cover, followed by a shift from springtime snowmelt to winter runoff, which may be expected to increase risks of winter flooding and summer drought (Arnell, 1999; Feng and Hu, 2007; Knowles et al., 2005; Mote, 2003).

Snow cover in temperate regions (e.g. central and western Europe) is generally thin and often close to the melting point; consequently, both continental and alpine snow covers have high sensitivity to climate change (Fitzharris, 1996). However, even though statistically significant snow recession at least since the early 1980s or late 1970s has been reported in many locations of the globe (Brown, 2000; Brown et al., 2010; Brown and Robinson, 2011; Estilow et al., 2015; IPCC, 2013; Laternser and Schneebeli, 2003), the snow cover dynamics both in spatial and temporal dimensions are still not well quantified, not only because of the high heterogeneity of snow distribution, but

also the incompatibility of different snow data sources. Moreover, it is difficult to measure the exact impact of changing temperatures and precipitation on snow due to the potentially substantial variation of the impact through time and region (Serquet et al., 2011). Therefore, large efforts with the supports of state-of-the-art techniques are still required to investigate snow cover and snow processes, as well as the response of snow to climate change.

## 1.1 Snow cover properties

A number of variables such as density, albedo, specific surface area, crystal size and shape, thermal conductivity, permeability, diffusivity and shear resistance are required for a complete physical description of the snowpack (Domine, 2011). The understanding of snow properties, physical, thermal and optical, is essential to hydrologic research of snow (Singh and Singh, 2001). Much attention has been paid to the studies of snow properties within the literature (e.g. Brucker et al., 2010; Gallet et al., 2009; Jin et al., 2008; Koenig et al., 2007; Montpetit et al., 2011; Warren, 1982).

Due to the special properties of snow, as summarized by Pomeroy and Brun (2001), snow cover functions as an energy bank, a radiation shield, an insulator, a reservoir and a water transport medium in the global climate system and ecosystem. In detail, snow cover stores latent heat and crystal bonding forces during its formation and releases energy through fusion and sublimation. Because of the high albedo, most shortwave radiation can be reflected by a fresh snow cover, though the albedo decreases with snowmelt. As a near blackbody, cold snow absorbs and reemits most long-wave radiation, but the emission is limited to a snow surface temperature of below 0 °C, and thus snow cover hampers a fast warming of the adjacent air relative to a snow-free surface (Street and Melnikov, 1990). Snow cover also acts as an insulator, which constrains the thaws of permafrost and protects microorganisms and plants from wind and severe winter temperatures. Consequently, snow cover plays an important role in influencing the surface radiative exchange and heat transfer. Besides, as a solid water resource, snow directly participates into the natural water distribution and redistribution through a series of processes. Since environmental factors interact with snow in complex ways, making it difficult to investigate the snow processes, e.g. snowfall, snowmelt, sublimation, interception, snow drift, snow avalanche and rain-on-snow etc.

## 1.2 Snow cover parameters and measurements

A number of snow cover parameters are applied to study the behavior of snowpack at different spatial and temporal scales. Table 1.1 shows some snow cover parameters that are normally used in hydrological applications, which are investigated in this study.

Snow covered area (SCA, %) is an index quantifying the extent of snow cover over a region, which is generally derived from snow cover maps and calculated as follows:

$$SCA = (N_s / N_t) \times 100\% \quad (1.1)$$

where  $N_s$  and  $N_t$  are the numbers of snow pixels and total cloud-free pixels respectively over the study area or a sub-region on a snow cover map. Though SCA only demonstrates the extent of snow presence over a region, the information of snow mass or volume cannot be interpreted from this index. However, SCA maps have high value in investigating the spatial and temporal variations of snow cover, especially when it is difficult to estimate the snow mass over a large area because of the varied topography and inhomogeneous snowfall. Besides, SCA information is also essential in studying the land-air coupling system, because snow cover extent instead of snow mass has more influence on the interactions between snow surface and the atmosphere. The high albedo and lower aerodynamic roughness heights of snow cover compared to land surface play important roles in changing the thermal and motion states of the atmosphere through direct and indirect feedbacks.

**Table 1.1** Snow cover parameters investigated in this study.

Parameters	Abbreviation	Unit
Snow covered area	SCA	%
Snow depth	SD	cm
Snow water equivalent	SWE	mm
Snow cover duration	SCD	day
Snow onset date	SOD	Julian day
Snow end date	SED	Julian day

For hydrologists, snow mass and volume parameters are more valuable, from which the water resource stored in the snowpack and the followed snowmelt runoff can be estimated. Snow water equivalent (SWE, mm) and snow depth (SD, cm) are normally measured and applied for this purpose. There is a relation between snow water equivalent (SWE, mm) and snow depth (SD, cm), which can be described by the followed equation:

$$SWE = 10 \times SD \times (\rho_s / \rho_w) \quad (1.2)$$

where  $\rho_s$  is the snowpack density ( $\text{kg m}^{-3}$ ), and  $\rho_w$  is the density of liquid water, approximately  $1 \times 10^3 \text{ kg m}^{-3}$ .

To monitor the temporal variations of snowpack, snow cover duration (SCD, d), snow onset date (SOD) and snow end date (SED) are three indices which show the seasonal behavior of snow cover. SOD and SED are often recorded in Julian dates in hydrological applications, which mean the date of the first snowfall and the date of the last snow presence during a snow season. SCD indicates the number of days between SOD and SED during a snow season. For the regions which have persistent snow cover, a hydrological year should be defined in advance, e.g. 1<sup>st</sup> August to 31<sup>st</sup> July. Then SED indicates the date of the last snowfall during a hydrological year. For the rarely snowed regions, it may be more appropriate to both calculate Julian dates of SOD and SED based on 1<sup>st</sup> January of the beginning year of a hydrological year, which means SOD and SED may have values higher than 366, indicating a delayed snow onset or early snow ending.

The six snow cover parameters listed in Table 1.1 contain the information of both the spatial and temporal distribution of a snow cover (SCA, SCD, SOD and SED), as well as the quantity of a snowpack (SWE and SD). Therefore, the continuous time series of the six parameters can be utilized to investigate the spatio-temporal dynamics of snow cover and to estimate the water storage in snowpack, which has critical significance for climate-change assessment and water resource management.

Currently, three approaches are frequently used to derive the above snow parameters. The first is the traditional, ground-based and mostly manual process of monitoring snow characteristics; these data are typically collected with other variables at meteorological stations. However, the limited number of meteorological stations with appropriate snow monitoring protocols hinders a detailed snow survey at a large spatial scale. As a result, traditional snow measurement cannot provide sufficient snowpack information for water resource management at the basin scale, despite its point-scale accuracy. To obtain the basin-scale information about a snow cover, one can use remote sensing as a substitute. Remotely sensed images have the advantage of monitoring the snow cover over a large area in near-real time. Recently, remote sensing of snow hydrology has experienced vigorous development all over the world. However, compared with in situ snow measurements, remotely sensed snow data is limited by the short observation term. The premier remotely sensed dataset for snow cover, which dates back to 1966, is the NOAA weekly snow cover maps for the Northern Hemisphere, and it is also the longest satellite-based environmental data of any kind (Robinson et al., 1993), while some climate stations have snow records more than 100 years (e.g. Armstrong, 2001; CDIAC et al., 1991). A second limitation for remotely sensed snow information is the high number of pixels overlain by clouds. Besides, the remote-sensing snow data also have more errors than ground-based snow archives. Due to the spectral confusion of different land surface features and the signal interference of severe atmospheric conditions, misclassifications widely existed in

remote sensing based hydrological datasets. Hydrological model, which consists of physically-based model, conceptual model and black-box model, is also a robust approach in snow estimation. Based on the input of climatic, geomorphologic and other environmental information, snow cover can be simulated by numerical models. In addition, snowpack models also have the capability to predict the snow cover variations in the future under a changing climate, which is impossible for in situ and remotely sensed snow observations. Nevertheless, snow models are regularly limited by the poor availability of reliable meteorological observations as the model input, which is a common problem for high-latitude studies (Essery et al., 2013). Moreover, the physical and empirical relations between various hydrological variables are still incompletely understood, which restrained the performance of hydrological models in snow cover simulations.

Therefore, each snow measurement approach among in situ observations, remote sensing and hydrological modeling possesses its obvious advantages compared to the others and also shortcomings at the same time. Thus, it is necessary to compare the availability of field monitoring, remote sensing and snow modeling in snow cover research and to seek the possibility to integrate the three methods to improve our capability of studying snow cover in the future.

### **1.3 In situ monitoring of snow**

Before remote sensing and hydrological modeling, in situ snow monitoring has a long history of being used for snowfall and snow cover measurement. During 1500s to 1800s, modern meteorologic observations began in Europe with the invention of meteorological instruments, with the daily snow depth and new snowfall being observed by various methods in many countries (e.g., Switzerland, USA and Finland). The national rainfall and snowfall archives of the Qing Dynasty of China date back to 1693, which systematically recorded the rainfall and snow depth in 268 counties until 1911. Snow depth and snow water equivalent (SWE) measurements became widespread by 1950 in the mountain regions of western North America and Europe (IPCC, 2007).

With the global warming attracted much attention in the second half of the 20<sup>th</sup> century, large-scale snow studies called for data exchange of snow observations among different countries. The inconsistent monitoring criterions limited the comparability of the snow measurements from various stations and regions. In support of improving the quality and consistency of in situ snowfall, snow depth and water equivalent observations, a number of international and national projects have been implemented worldwide and several station-based snow data datasets have been set up (Table A1). In addition, a global SYNOP (surface synoptic observations) network is sponsored by the World Meteorological Organization (WMO), responsible for the data collection and

exchange of coordinated international weather observations from the RBSCNs (Regional Basic Synoptic/Climatological Network) stations. In situ snow depth measurements from the station network are provided by the SYNOP reports in near real time.

At meteorological stations, snow depth is generally observed one or two times per day by a surveyor while snow water equivalent is measured in very low frequency. In the past years, automatic snow stations, e.g. equipped with ultrasonic snow height sensors or weighting SWE system, have been widely used to monitor SD and SWE in high temporal resolution (e.g. hourly). In addition, time-lapse photography recently also has shown the capability to collect SD data (Parajka, 2012a) and quantify snow canopy interception (Garvelmann, 2013), which is a low-cost and feasible method to monitor snow processes in remote mountain area.

For the regions that have an adequate density of point observations, the spatial distribution of snow hydrological variables can be estimated using geostatistical interpolation techniques (Foppa et al., 2007), such as inverse distance weighting (Jarvis and Stuart, 2001), kriging (Carrera-Hernández and Gaskin, 2007) and regression tree models (Molotch et al., 2005). However, estimating the areal spatial distribution of snow cover with point-scale snow monitoring is particularly difficult in mountainous environments given the complex topography, vegetation transition, and scarce meteorological stations. López-Moreno and Nogués-Bravo (2006) evaluated the performance of several local, geostatistical and global interpolation methods for mapping the snowpack distribution in the Iberian Peninsula, and they concluded that local and geostatistical interpolators did not provide satisfactory predictions of snow depth while generalized additive models (GAMs) achieved better estimations, but remarkable overestimation still occurred for some regions. Meromy et al. (2013) validated the representativeness of the SD and SWE observations at 15 snow stations in USA; more than 30,000 field snow observations at the surrounding area were interpolated using regression tree models and then compared with the station data; it was found that the biases over all sites ranged from 74% overestimates to 77% underestimates, indicating a poor relationship between the point-scale and regional-scale snow measurements in mountainous regions. Therefore, remote sensing and hydrological simulations possess more potential to provide more accurate predictions of snowpack distribution at large scales.

#### **1.4 Remote sensing of snow**

The technology of remote sensing has shown a major impact on data collection for measuring snow accumulation and ablation (DeWalle and Rango, 2008). During the last several decades, a large number of remotely sensed snow products, including both SCA and SWE data, have been developed to investigate snow cover.

Table A2 shows some optical satellite sensors that have been widely used in snow cover mapping. Optical sensors loaded on satellites or aircraft can distinguish the objects on the ground by examining the reflected visible light (VIS, 0.39 - 0.70  $\mu\text{m}$ ) and infrared rays (IR, 0.70  $\mu\text{m}$  - 1.00 mm). Figure 1.1 demonstrates the spectral reflectance of several land features in the VIS and IR range, indicating a high VIS reflectance and low IR reflectance for snow. Thus, normalized difference snow index (NDSI) has been developed to detect snow cover in optical remote sensing data. For example, MODIS (or Moderate Resolution Imaging Spectroradiometer) band 4 (0.545-0.565  $\mu\text{m}$ ) and band 6 (1.628-1.652  $\mu\text{m}$ ) are used to calculate the NDSI and map snow cover. This method can discriminate snow from most land-cover classes and water clouds since they have different features in the electromagnetic spectrum. However, ice clouds (upper tropospheric cirrus clouds) have reflection characteristics similar to those of snow, which is why the NDSI is prone to incorrectly label ice clouds as snow. In mountain regions where cloud cover is a typical and predominant feature, the confusion of snow and cloud occurs frequently. In addition, dense cloud cover can also seriously block the snow observations of space-based optical sensors. Microwave remote sensing is an appropriate substitute in this situation.

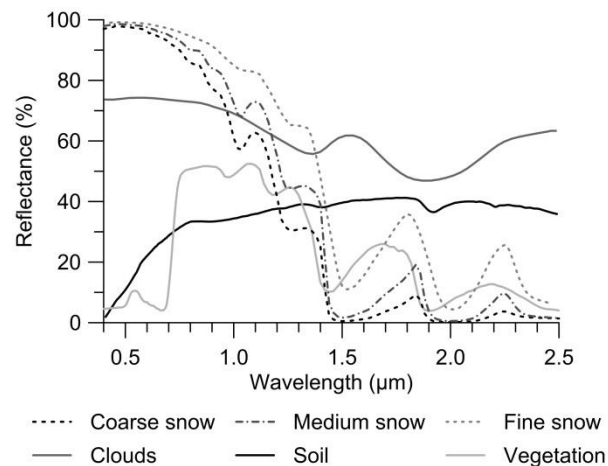


**Figure 1.1** Representative spectral reflectance of snow, clouds, soil and vegetation in the VIS and IR range.

The emitted microwave radiation (with wavelength of 0.1-100 cm) from the underlying surface can be attenuated by snow cover, from which a passive microwave (PM) sensor on a remote-sensing platform may quantify the snow mass (e.g. SWE) of a snowpack by analyzing the characteristics of the received microwave signal. Since 1978, space-borne passive microwave sensors (e.g. SMMR) have made it possible to globally monitor not just snow cover, but also snow depth (SD) and snow water equivalent (SWE), without being affected by cloud cover and winter darkness (IPCC, 2007). The

parameters of five representative satellite-based passive microwave sensors are given in Table A3. Since the microwave radiation emitted from the Earth's surface itself is in low level, passive microwave sensors cannot provide detailed snow parameter distribution, though high temporal resolution can be achieved. This gives an advantage to active microwave (AM) remote sensing, which can map snow properties in high spatial resolution through continuously transmitting microwave signal to the ground surface and receiving the reflected signal, but at the expense of repeat-pass interval (Table A3). However, microwave reflectivity and scattering characteristics of snow depend on many different factors such as snow depth and water equivalent, grain size and shape, liquid water content, impurity of snow, temperature and stratification, ice content and the terrains beneath the snow cover (Dietz et al., 2012; Hall and Martinec, 1985; Kelly et al., 2003; Foster et al., 2005; Painter et al., 2009). The multi-influence on the microwave signal from a snowpack leads to large uncertainty and low accuracy of SWE measurements with microwave remote sensing. Therefore, microwave remote sensing of snow needs more efforts to improve the algorithms used for quantify the relations between snow cover parameters and microwave signals.

In the recent past, some state-of-art remote-sensing techniques have been developed to carry out snow measurements, such as GPS-reflectometry (e.g. McCreight et al., 2014; Jin et al., 2016) and airborne LiDAR (Deems et al., 2013; Kirchner et al., 2014). GPS-reflectometry utilizes active microwave reflectometry in bistatic geometry to derive snow depth, rather than monostatic geometry which is typical for satellite-based remote sensing (McCreight et al., 2014). Airborne LiDAR uses a laser scanning system to detect snow depth by analyzing the change of signal return time for snow covered and snow-free conditions. Both the two approaches have the potential to provide accurate snow depth and snow water equivalent information with high spatial resolution in the future.

## **1.5 Hydrological modeling of snow**

Since 1960s, the application of digital computers has given hydrologists the capacity to simulate the snow accumulation and ablation processes with numerical models, i.e. one set of equations depicting the relationships between various environmental elements (Armstrong and Brun, 2008). Hydrological models have experienced the development from lumped conceptual models (e.g. Snow-17 model) to physically based distributed models (e.g. NOAH-LSM and VIC model). Table A4 shows some selected hydrological models that have a snow module. Due to the sparse observation network of meteorological stations, snowpack models have played an important role in estimating seasonal snow cover distribution and simulating snowmelt runoff. Besides, more and more snow parameters can be simulated with hydrological models, such as snow water equivalent (e.g. TRAIN), snow depth (e.g. CRHM), snow covered

fraction (e.g. JULES), snow interception (e.g. SWAP), snow albedo (e.g. NCEP) and snowmelt runoff (e.g. VIC).

However, snow models still have a great potential for improvement. Slater et al. (2001) compared the snow simulations by 21 land surface models, and systematic differences between the models' simulations were suggested, though the models showed the ability to capture the broad features of the snow regime. Rutter et al. (2009) conducted a similar project, and the simulations of 33 forest snowpack models was evaluated, concluding that there was no universal "best" model for all sites or locations because of the high complexity of snow processes in forest environments, and the model performance showed large differences between individual models as well as between forest and open sites.

Data assimilation (DA) provides an outstanding solution for improving hydrological modeling with its innovative approach of accounting for uncertainties in model, observation, and forcing data (Samuel et al., 2014). An ensemble Kalman filter (EnKF) was applied by Slater and Clark (2006) to assimilate in situ SWE data into SNOW-17 model, and evident improvements in the resulting SWE were achieved during the accumulation and melt periods. Thirel et al. (2013) successfully improved the modeled SCA and discharges by assimilating MODIS snow cover products into a distributed hydrological model with a particle filter (PF). Liu et al. (2013) assimilated satellite-based snow products into the Noah land surface model, which includes the standard MODIS SCA and AMSR-E SD data as well as the bias-adjusted versions against in situ observations; they concluded that the assimilation of bias-corrected snow data showed more consistent improvement on snow and streamflow predictions. Therefore, it is an essential procedure to improve the data quality of snow observations before assimilating them to hydrological models; otherwise, the model performance can even deteriorate, which is supported by the study of Molotch and Margulis (2008).

## **1.6 Outline of the thesis**

As discussed above, each approach of in situ monitoring, remote sensing and hydrological modeling has its specific advantages and disadvantages in snow cover studies. The best solution for this issue is to integrate the three methods, which can strengthen our ability to monitor, estimate and predict snow cover variation and snow-related processes in the future hydrological researches. Thus, the major objective of this thesis is to carry out some attempts in the context of this topic. The three approaches are jointly applied to investigate the snow cover and snow processes in the Upper Rhine Region of southwestern Germany.

In chapter 2 and 3, ground-based meteorological data are used to improve remotely sensed MODIS 8-day and daily snow cover products, respectively. Removal of cloud fractions and correction of snow misclassification are both involved in the efforts.

Considering the specific characteristics of 8-day and daily MODIS snow cover maps, different algorithms were developed and applied. As composite SCA data, MODIS 8-day snow products have lower cloud obscuration and more snow overestimation than daily data. Therefore, a relatively conservative cloud reduction algorithm was utilized to process MODIS 8-day data in chapter 2, while in situ snow depth data were used to reclassify the normally aggregated clouds in daily MODIS snow data in chapter 3. The false snow in MODIS 8-day products were reduced using two meteorological filters derived from in situ minimum ground temperature, air temperature and precipitation. A composite meteorological filter generated with air temperature, precipitation and snow depth was applied to reject the overestimated snow on daily MODIS snow cover maps. Both the two algorithms showed high efficiency in improving the data quality of MODIS snow information.

In chapter 4, the seasonal snow cover during the period 1961-2008 was simulated with a distributed hydrological model TRAIN. Then the improved cloud-free MODIS daily snow cover images were used to evaluate the SCA simulations, while the modeled SWE results were compared with in situ snow depth (SD) observations.

In chapter 5, a time-lapse photography network and automatic weather stations were employed to monitor the mountain snow processes, such as snow accumulation and melt in open area and forest sites, snow canopy interception loading and unloading.

Finally, a critical appraisal of the eligibility of integrating in situ monitoring, remote sensing and hydrologic modeling for snow cover research is given. The superior performance of utilizing ground-based meteorological data to improve remotely sensed snow measurements is highlighted. The potential contribution of fusing multi-source snow observations towards updating snow hydrological models with data assimilation schemes is discussed.

## Chapter 2

# Improvement and application of MODIS 8-day snow products

### 2.1 Introduction

Deriving the spatial and temporal distribution of snow cover is important for accurately estimating the stored water resources and for forecasting flood or drought conditions. The limited number of meteorological stations with appropriate snow monitoring protocols hinders a comprehensive snow survey at a large spatial scale. Thus, traditional snow measurement cannot provide sufficiently detailed information for snow parameters (e.g., snow cover extent, snow duration), despite its point-scale accuracy. To obtain basin-scale information about snow cover, one can instead use satellite data to remotely sense snow cover (König et al., 2001).

Remote sensing images have the advantage of monitoring the snow cover extent over a large area in near-real time. As a remote sensing technique that unites high temporal resolution (1 day) and relatively high spatial resolution (500 m), MODIS snow products have attracted a great deal of attention over the past ten years. The high number of studies concerning MODIS demonstrates the vital role of this sensor for snow-related research. In particular, recent studies have focused on the processing and validation of MODIS snow data (Ault et al., 2006; Gafurov and Bárdossy, 2009; Hall et al., 2002; Hall and Riggs, 2007; Hall et al., 2010; Liang et al., 2008a; Maurer et al., 2003; Parajka et al., 2012b; Parajka and Blöschl, 2006, 2008a; Wang et al., 2009) or the spatio-temporal variation of snow parameters (Dietz et al., 2012; Foppa and Seiz, 2012; Paudel and Andersen, 2011; Pu et al., 2007; Sauter et al., 2009; Wang et al., 2008). Further applications are the combination or comparison of MODIS snow information with other remote sensing snow products (Lee et al., 2005; Liang et al., 2008b; Simic et al., 2004; Zhou et al., 2013) and the use of MODIS snow data to calibrate or drive hydrologic models (Homan et al., 2011; Parajka and Blöschl, 2008b; Powell et al. 2011; Sauter et al. 2010; Shrestha et al., 2014).

There are two independent satellite platforms that carry MODIS optical sensors (Terra and Aqua). Terra was launched in December 1999; Aqua followed in May 2002. Therefore, MODIS data have a short observation term of about 16 years, i.e., the long-term analysis of snow cover development is limited to the years since about 2000. A

second limitation is the high number of pixels overlain by clouds. Parajka and Blöschl (2008a) reported that the medians of annual cloud coverage of Terra and Aqua snow products over Austria were 66.1% and 70.1% during 2003-2005, respectively. During winter (November to February), the values were even higher. Cloud obstruction seriously influences the ability of the user to extract information from MODIS snow data. A number of investigations have contributed to the improvement of cloud removal techniques from MODIS snow images. Riggs and Hall (2003) developed a liberal cloud mask from the MODIS cloud-mask threshold tests, which showed high performance in eliminating false clouds in some areas of the globe. Since the liberal cloud mask might miss some clouds in other areas and increase the cloud/snow confusion errors in the resulting snow maps, it was not included in the global algorithm of MODIS Collection-5 snow products (Hall et al., 2010). As an alternative, a conservative cloud mask was used, leading to a relatively high cloud fraction in MODIS Collection-5 snow maps (Riggs et al., 2006). Parajka and Blöschl (2008a) introduced three methods to markedly reduce the cloud coverage of MODIS snow products, including the combination of Terra and Aqua data, a spatial filter that considers the adjacent 8 pixels, and a temporal filter that replaces the cloud pixels with the information from images from the past several days. Gafurov and Bárdossy (2009) presented another two steps to remove all the residual cloud pixels. They used the timing of the onset and melting of snow cover to determine if cloud pixels obscured land (i.e., snow free) or snow. Moreover, they also utilized the snow transition elevation to reject the cloud covered pixels above the maximum snow lines or below the minimum snow lines. However, these steps led to a decline of accuracy. Krajčí et al. (2014) improved the detection of regional snowline elevation (RSLE) from MODIS images, which contributes to the cloud reduction in MODIS snow products.

MODIS snow data is further limited by the misclassification of snow, which corresponds to an over- and underestimation of snow cover. Patchy snow is possibly an important reason for the underestimation of snow pixels, especially in forest-covered mountain regions with complex topography. The confusion of snow and cloud can lead to overestimation errors, and false snow detection along cloud fringes is frequently reported. The MODIS snow products are generated based on the calculation of NDSI (Normalized Difference Snow Index). This method can distinguish between most cloud types and snow since they have different features in the near-infrared part of the electromagnetic spectrum. However, cirrus clouds (upper tropospheric ice clouds) have reflection characteristics similar to those of snow, which is why the NDSI is prone to incorrectly label cirrus clouds as snow. In mountain regions where cloud cover is a typical and predominant feature, the confusion of snow and cloud occurs frequently. Moreover, the snow errors of commission (i.e., an incorrect identification of snow) from the daily MODIS data are propagated into the eight-day MODIS snow

products (Riggs et al. 2006). Klein and Barnett (2003) reported that the errors in MODIS daily snow products from mapping extra and/or missing snow were comparable, with MODIS missing snow in approximately 12% of the cases and mapping too much snow in 15% of the cases. Parajka and Blöschl (2006) studied the misclassification of MODIS based snow information over Austria and concluded that the average overestimation errors were about 10% and 5% on cloud-free days in November and December, respectively. Dong and Peters-Lidard (2010) reported that the MODIS snow images showed a false alarm ratio of 8.5% in the studied mountainous regions in western USA, and the error had a steadily increasing trend with temperature rise. Gao et al. (2011) suggested monthly mean snow underestimation errors of up to 31% on daily MODIS Terra snow maps over the Pacific Northwest USA. The above researches indicate that snow misclassification of MODIS snow products is a severe issue in many regions. Overestimation errors in MODIS snow data are visually detectable because they appear as a lot of snow pixels in the summer images of temperate regions. Such errors obstruct the analysis of snow duration and the assessment of snow distribution.

As indicated in this review, most of the previous studies about MODIS snow products have focused on three issues: validation of snow mapping, removal of cloud obstruction, and spatio-temporal variation of snow cover. Reducing the misclassification error of the MODIS snow products has not yet drawn much attention. The omission error (underestimation) of snow classification is difficult to reduce because it is a kind of spatial information loss. Besides, no alternative remote sensing snow data are available to supplement the MODIS snow images. However, the commission error (overestimation) of MODIS snow data can be reduced because it is a kind of spatial information redundancy. By combining the MODIS snow products with meteorological data such as temperature and precipitation, a part of the false snow can be excluded. The aim of this study is therefore to develop a methodology for reducing the overestimation error of MODIS 8-day snow products with the help of ground-based meteorological data. The improved MODIS snow data were validated with observations of in situ snow depth taken at 60 stations in Rhineland-Palatinate. Both the spatial and temporal variations of MODIS snow covered area and in situ snow depth were investigated. Then the results from the two kinds of snow data were compared. Additionally, the influence of spatial factors on the number of snow days was evaluated using correlation analysis.

## **2.2 Study area**

Rhineland-Palatinate (Figure 2.1, 49.0-51.0° N, 6.1-8.5° E) is one of the 16 states of the Federal Republic of Germany. It covers an area of 19,853 km<sup>2</sup> and is located in southwestern Germany. The Rhine is the region's largest river and is fed by several large tributaries, including the Mosel, Lahn and Nahe rivers. The deeply eroded Rhine

Valley and its tributaries separate the northeast-trending highlands into a number of isolated massifs and plains, of which the extended Upper Rhine Valley is the most remarkable. From north to south, the mountains of the Eifel, the Hunsrück and the Palatinate forest follow in close succession on the west bank of the Rhine, divided by the Mosel and Nahe rivers. The Westerwald and the Taunus mountains are located on the east bank and are bounded by the Lahn River. As a representative low mountain region in central Europe, the elevations in Rhineland-Palatinate range between 10 and 817 m a.s.l., with an average elevation between 400 and 600 m a.s.l. A total of 42% of the state area – mostly in the highlands – is covered by mixed woodland, while intense agriculture extends across the lowlands and along the transitions from the mountains to the deep valleys. Agglomerations can mainly be found along the Rhine (with the city of Mainz as the state capital) and Mosel valleys.

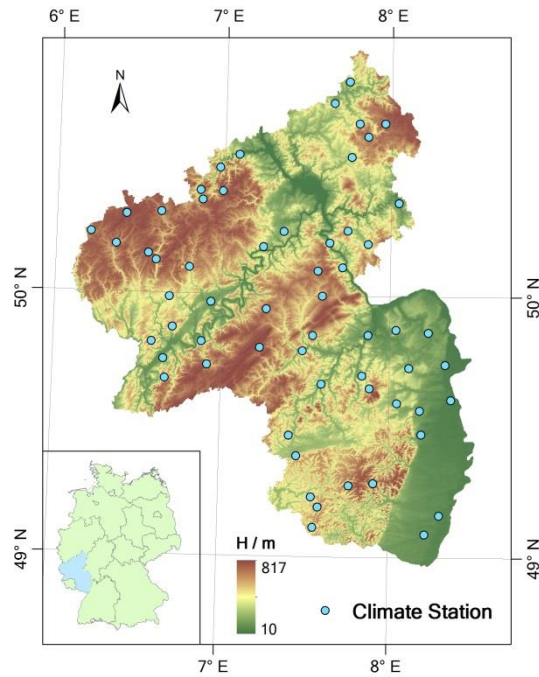


**Figure 2.1** Topography of Rhineland-Palatinate and the network of meteorological stations (operated by the German Weather Service DWD) with in situ snow depth measurements.

The climatic conditions in Rhineland-Palatinate are humid temperate, with warm summers and cool winters. The region is mostly dominated by frequently alternating low pressure systems and anticyclones, feeding air masses from different origin, but mostly of maritime character. Mean annual air temperature is about 6°C at the highest elevations and exceeds 10°C in the warm valleys. During summer, mean air temperatures reach 14-15°C; during winter, they fall to between -2 and +2°C.

Prevailing westerly winds from the Atlantic Ocean provide precipitation evenly distributed throughout the year (Sauter et al., 2010). Mean annual precipitation in Rhineland-Palatinate is 800 mm. The complex terrains significantly increased the climate heterogeneity. In the highlands, it reaches approximately 1400 mm, whereas some parts of the Upper Rhine Valley receive less than 500 mm, which is located on the leeward side of the mountains. At the same time, the potential evapotranspiration in the plains is far higher than that at the mountain tops, partly because of the varied vegetation and the agricultural activities in the low elevations. Typical values of mean annual snow duration (observed at meteorological stations run by the German Weather Service) range between less than 20 days at the lowest elevations to up to 80 days in the mountains. Typically, these numbers result from fragmented snow periods that are frequently interrupted by thaw periods, which may affect even the highest elevations. Due to the complex topography of the region (Figure 2.1), snow cover in Rhineland-Palatinate has a high temporal and spatial variability. This area is often covered by dense clouds in winter, which screens the land surface from the satellite view, adding to the difficulties of remotely sensed snow observations.

## **2.3 Data sources**

### **2.3.1 MODIS data**

The MODIS (Moderate Resolution Imaging Spectroradiometer) sensor collects data for a suite of products for which it is equipped with 36 spectral bands, from the visible spectrum to thermal infrared. Since MODIS resides on the Terra and Aqua satellites, which have distinct orbits, it delivers images of a specific area on Earth for two different points of time during a day. Thus, the user can combine the Aqua and Terra images to optimize a cloud-free view of the surface. MODIS snow products are available at a 500 x 500 m spatial resolution on a daily basis (MOD10A1 and MYD10A1), as well as for an aggregated 8-day period (MOD10A2 and MYD10A2). Each 8-day MODIS snow cover tile is combined with 8 daily MODIS snow tiles. A grid cell is labeled as snow-covered during an 8-day interval when snow is detected for at least one day of the 8-day period. Therefore MOD10A2 and MYD10A2 data represent the maximum snow cover occurrence for the 8-day period.

The algorithm of the MODIS snow products is based on the reflection characteristics of snow (Jedlovec, 2009), i.e., snow has a high reflectance in the visible band (band 4, 0.545-0.565  $\mu\text{m}$ ) and a low reflectance in the near-infrared band (band 6, 1.628-1.652  $\mu\text{m}$ ). Cloud reflectance, in contrast, is high in both bands (Hall et al., 2002). Thus, the normalized difference snow index (NDSI) was established to distinguish between snow and snow-free surfaces or other features in MODIS images:

$$NDSI = \frac{Band4 - Band6}{Band4 + Band6} \quad (2.1)$$

In the calculation of the NDSI for the Aqua data, band 6 is replaced by band 7 because the Aqua MODIS instrument shows mostly non-functional detectors in band 6. A pixel is classified as snow-covered when the following conditions are fulfilled:  $NDSI \geq 0.4$ , reflectance in MODIS band 2 (0.841-0.876  $\mu\text{m}$ )  $> 11\%$  and reflectance in MODIS band 4  $> 10\%$  (Hall et al., 2002).

In this study, a total of 1,992 MODIS Terra and Aqua 8-day snow cover images (MOD10A2 and MYD10A2, respectively, Collection 5) were collected over the study area from 4 July 2002 to 30 April 2013. MODIS NDVI products (MOD13A3), as well as the albedo products (MCD43B3) were also applied in this study to detect the relations between snow cover and environmental variables. All the MODIS data were downloaded from the website of NASA's Earth Observing System Data and Information System (EOSDIS, <http://reverb.echo.nasa.gov/>). The parameters of the four products are shown in Table 2.1 Preprocessing, which consists of image-mosaic, reprojection and format conversion, was carried out with the MODIS Reprojection Tool (MRT, 2008).

**Table 2.1** Parameters of the used MODIS products.

MODIS products	Data content	Spatial resolution	Temporal resolution	Data period
MOD10A2	snow cover	500 m	8 day	Jul. 2002- Apr. 2013
MYD10A2	snow cover	500 m	8 day	Jul. 2002- Apr. 2013
MOD13A3	NDVI	1 km	monthly	Jan. 2002- Jul. 2014
MCD43B3	albedo	1 km	16 day	Jul. 2002- Apr. 2013

### 2.3.2 Meteorological data and DEM

The meteorological data used in this study come from the network of the German Weather Service (DWD, [www.dwd.de](http://www.dwd.de)) and include daily time series (4 July 2002 - 30 April 2013) of precipitation (P) at 158 stations, air temperature (T) at 60 stations, minimum soil surface temperature (min. ground-T) at 52 stations, and snow depth at 60 stations (Figure 2.1). There have been few data gaps which could be removed through interpolation with data from adjacent stations. Gridded data of daily precipitation and air temperature in the study area from 2002-2008 were also used in this analysis (Hinterding, 2003). The grid has a cell size of  $1 \times 1$  km and was based on observed time series interpolated using the Kriging method; see Hinterding (2003) for details. The gridded data was supplied by LUWG, the state agency for the environment and water management in Rhineland-Palatinate. During snow-free

periods, the minimum ground temperature (min. ground-T) data were applied to remove false snow pixels on MODIS snow products. During the snow season, precipitation and temperature data were used to generate snow masks, which were then applied to exclude the remaining misclassified snow pixels from the MODIS images.

The Digital Elevation Model (DEM) used in this study has a spatial resolution of  $90 \times 90$  m and comes from the Shuttle Radar Topography Mission (SRTM), downloaded from the Consultative Group on International Agricultural Research (CGIAR, <http://srtm.csi.cgiar.org/>). The purpose of the DEM was to develop daily elevation gradients for the min. ground-T that could then be interpolated with the individual pixels. The DEM, as well as the gridded precipitation and temperature data, was resampled to the cell size of the MODIS data.

## **2.4 Methodology**

All the 8-day MODIS snow data were imported from HDF-EOS format to GEO-TIFF format, transformed to the projection WGS1984-UTM32N (Universal Transverse Mercator), and clipped to the extent of the study area. Then the MODIS data were processed with a new four-step method that was developed to reduce snow misclassifications and cloud cover in the images (Figure 2.2). The individual steps of the method are described in the following sections.

### **2.4.1 Aqua & Terra Combination**

The first step is the combination of MODIS Aqua and Terra snow data (Figure 2.2). Since the MODIS instruments on Terra and Aqua image pass through a region of interest at two individual points in time during a day (Terra at approx. 10:40 AM, Aqua at approx. 1:30 PM), melting snow that is present in the morning but disappears around noon can be retrieved from the combined pixels, i.e., such days count as “snow days”. This frequently applies during late autumn/early winter and during springtime. The 8-day MOD10A2 and MYD10A2 data are produced from daily MOD10A1 and MYD10A1 images. For an 8-day period, the individual cells are examined as follows: If snow cover is present on any day in the period, the cell in the "Maximum Snow Extent" (MOD10A2 and MYD10A2) is labeled as snow-covered (Riggs et al. 2006).

A number of investigations have compared the cloud cover in daily MODIS data and in 8-day composite products (Liang et al. 2008b). They found that the combination of the two products enables a reduction in cloud obstruction based on the variation of the cloud cover on the images.

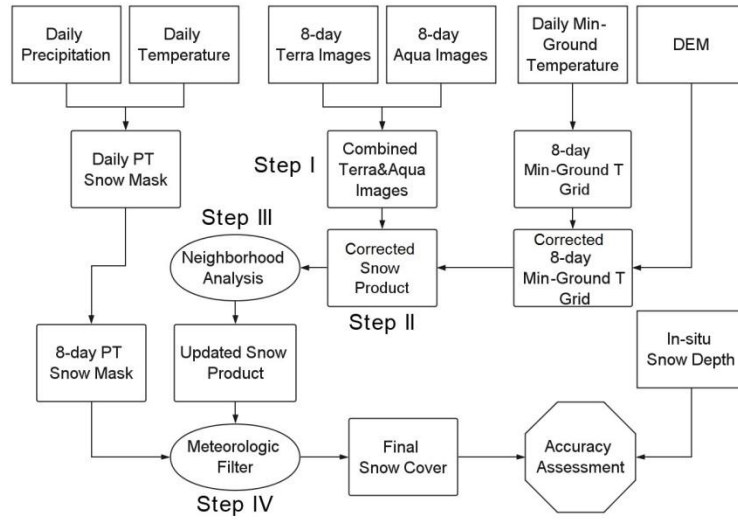


Figure 2.2 Flow chart of MODIS data processing and validation.

#### 2.4.2 Min. Ground-T Correction

The second step of the proposed methodology (Figure 2.2) applies especially when the combined Aqua and Terra product reports snow cover during summer, which is most unlikely in the study region. In order to remove such cases of false snow detection, the daily minimum ground temperature (min. ground-T), which is routinely measured at meteorological stations, is introduced. Firstly, the daily min. ground-T observed at 52 stations was interpolated to a regular grid (having the same spatial resolution as the MODIS pixels) using ordinary Kriging. Secondly, the daily min. ground-T gradient that was calculated from the station data was applied in combination with the DEM to modify the spatially interpolated min. ground-T data with respect to elevation, which can be regarded as a scale transformation procedure for upscaling point-scale temperature data to areal scale. In detail, the correction procedure was performed according to the following equation:

$$T = T_0 - \gamma (H - H_0)/1000 \quad (2.2)$$

Where  $T$  is the corrected min. ground-T ( $^{\circ}\text{C}$ );  $T_0$  is the interpolated min. ground-T with Kriging ( $^{\circ}\text{C}$ );  $\gamma$  is the min. ground-T lapse rate ( $^{\circ}\text{C}/\text{km}$ ), which was calculated on daily time steps with data from four representative stations situated at high and low elevations;  $H$  is the real elevation of each pixel on the DEM (m);  $H_0$  is the elevation of each pixel interpolated from the elevation of the meteorological stations (m). Then the 8-day min. ground-T of a pixel was determined as the minimum of the 8 individual daily min. ground-T data of the respective grid cell. Finally, this product was used to correct the MODIS snow cover from step I of the methodology. If the 8-day min.

ground-T of a pixel classified as snow-covered was higher than 0°C, then the snow information was classified as false and the pixel labelled as “land” (i.e., not snow-covered). This step assumes that snow cannot occur or stay on the ground for a period of one or more days if the ground temperature exceeds a certain limit.

### **2.4.3 Neighborhood Analysis**

A further reduction of cloud obstruction is performed in the third step of the methodology, which uses neighborhood analysis (Figure 2.2). When a pixel is classified as cloud-covered, the information of its 8 closest neighbors is analyzed. If the majority of the neighboring pixels have been assigned to a class other than cloud (i.e., snow-covered or land), then the grid cell under investigation is also assigned to this class. This procedure mostly applies during cases of scattered clouds, when a pixel is cloud-covered or when the pixel is situated along cloud fringes while its proximity is cloud-free. This step is not successful during times of extensive cloud cover.

### **2.4.4 Precipitation & Temperature Filter**

The fourth step of the methodology aims at further reducing the number of misclassified snow pixels (Figure 2.2), especially during the snow season. Since min. ground-T is low during winter, the applicability of step II is restricted during this period. Therefore, precipitation P and air temperature T data that are regularly observed at meteorological stations were applied to complement the min. ground-T filter from step II. First, the P and T data were interpolated to a grid with a cell size identical to that of the MODIS data. Topographical correction was utilized to upscale the point air temperature to areal scales using the same method as presented in section 2.4.2, while the upscaling of precipitation was not conducted in this study because of the extreme complexity of the precipitation patterns in the mountainous area.

Then, a daily PT snow mask was created with the fixed thresholds of 0.5 mm and 0.0°C; that is, if the daily precipitation exceeds 0.5 mm and the daily mean air temperature is equal to or below 0°C, the probability of a snow day is high. In this case, the respective pixel was valued 1 (true); otherwise, it was allocated 0 (false). Next, the 8-day PT snow mask was generated in the same way as described for the MODIS data in section 2.4.1. If the daily PT snow mask was valued 1 on one or more days during an 8-day period, the resulting 8-day PT snow mask was valued 1 (true) as well; it was valued 0 (false) otherwise. Finally, an overlay analysis between the processed 8-day MODIS snow data and the 8-day PT snow mask was carried out. If the value of one pixel on the PT snow mask was 0 but was rated as snow-covered in the MODIS data, then this pixel value was corrected to land (i.e., not snow-covered). To assess the accuracy of steps I-IV of this method (Figure 2.2), the final images were compared to measured snow depth at a

total of 60 meteorological stations (Figure 2.1). The respective results are presented in section 2.6.

#### 2.4.5 Spatial and temporal analysis of snow cover

Upon the updated MODIS snow data and in situ snow depth, the main snow parameters of snow coverage, snow onset time, snow end time and snow duration were obtained. Then the temporal and spatial variation of snow cover in Rhineland-Palatinate during 2002-2013 was analyzed. All the MODIS snow data was classified into 9 elevation zones based on DEM, while the in situ snow measurements were divided into 10 elevation zones according to the station locations (Table 2.2). The snow parameters were finally plotted, and their relationships with spatial factors were tested through curve fitting and correlation analysis.

**Table 2.2** Elevation zones of MODIS and in situ snow data.

<u>MODIS snow products</u>			<u>In situ snow depth data</u>		
Range (m)	Mean Altitude (m)	Area (km <sup>2</sup> )	Range (m)	Mean Altitude (m)	No. of stations
< 145	110,6	2499,7	< 110	95,6	8
146-214	180,4	2014,7	110-150	127,6	7
215-276	248,4	2699,5	150-200	176,3	8
277-331	304,3	3151,5	200-250	229,1	7
332-385	357,8	2950,8	250-290	267,8	9
386-442	413,1	2586,2	290-320	309,4	7
443-503	471,1	2181,2	320-390	362,3	7
504-583	535,8	1340,3	390-450	421,0	7
> 584	630,3	440,7	450-510	480,4	7
			> 510	554,7	7

## 2.5 Results

### 2.5.1 Reduction of cloud obstruction

Table 2.3 summarizes the cloud cover fractions of the original MODIS Aqua and Terra snow products, as well as the cloud cover fractions after Aqua-Terra combination (step I) and neighborhood analysis (step III) for Rhineland-Palatinate during the period 2002-2013. The mean annual cloud coverage in the original MODIS Aqua and Terra images is 13.7% and 13.1%, respectively, with the highest cloud obstructions (> 20%) occurring during the winter months (November-February). This is a clear indication

that, given the climatic conditions of the study region, investigations on snow cover extent and variability using original MODIS data are very much limited. However, an examination of the results in Table 2.3 shows that step I of the method reduces cloud obstruction in winter to values below 20% (the medians decline to less than 10%). Following step III, the percentage of pixels obstructed by clouds is further reduced to about 11% on average. Figure 2.3 clearly illustrates the concentration of cloud cover between late autumn and early spring, and the strong decline of cloud-covered pixels following steps I and III.

**Table 2.3** Mean cloud coverage (% , period 2002-2013) over Rhineland-Palatinate as indicated by Aqua, Terra, combined Aqua-Terra (step I), and neighborhood-analyzed Aqua-Terra (step III) MODIS Snow Maps<sup>a</sup>

Month	Aqua	Terra	step I	step III
Jan	32.0/23.5	28.0/20.4	18.3/7.6	13.4/2.9
Feb	24.1/21.7	21.8/12.4	12.8/5.0	8.4/1.3
Mar	7.5/0.1	6.8/0.0	2.8/0.0	1.2/0.0
Apr	4.1/0.1	3.6/0.0	0.9/0.0	0.3/0.0
May	11.0/0.5	10.3/0.0	4.3/0.0	2.0/0.0
Jun	6.3/1.0	5.3/0.1	1.9/0.0	0.9/0.0
Jul	4.7/0.5	4.0/0.1	1.1/0.0	0.4/0.0
Aug	6.3/0.2	4.7/0.1	1.8/0.0	0.9/0.0
Sep	3.0/0.0	2.6/0.0	1.2/0.0	0.6/0.0
Oct	5.3/0.2	7.3/0.3	2.1/0.0	1.1/0.0
Nov	22.4/19.8	23.0/15.1	11.8/5.2	7.8/3.0
Dec	30.8/20.9	32.8/24.0	19.6/8.4	14.3/4.3
Annual	13.7/1.9	13.1/1.1	6.9/0.1	4.5/0.0

<sup>a</sup>Average (first value) and median (second value) of the monthly and annual cloud coverage.

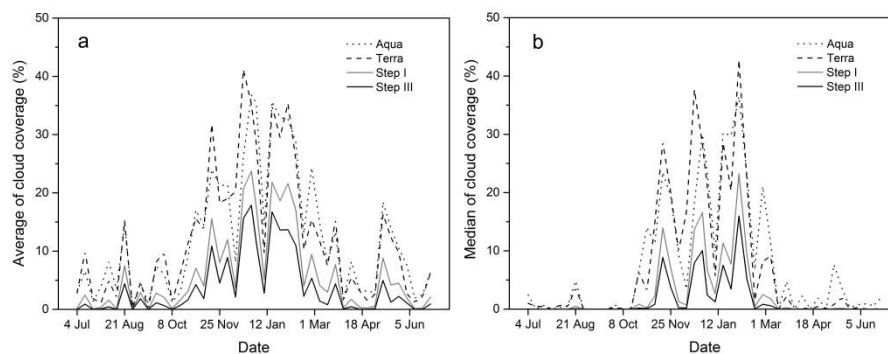


**Figure 2.3** Average (a) and median (b) of the 8-day cloud coverage over Rhineland-Palatinate (period 2002-2013) in the original Terra and Aqua images, as well as after step I and step III, respectively.

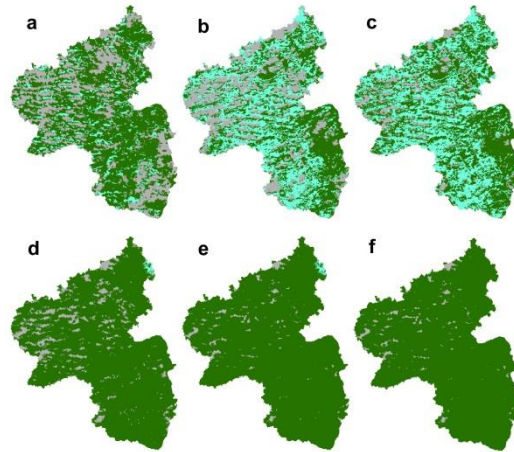


**Figure 2.4** Snow and cloud cover maps of original 8-day MODIS Terra and Aqua images and after implementation of the four steps. Maps are for the 8-day period from 29 September to 6 October 2008. (a) original MODIS Terra, (b) original MODIS Aqua, (c) after step I, (d) after step II, (e) after step III, (f) after step IV. Color legend: blue=snow, grey=cloud, and green=land.

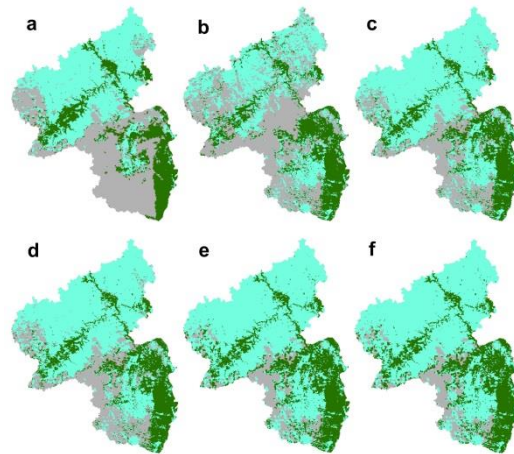


**Figure 2.5** Snow and cloud cover maps of original 8-day MODIS Terra and Aqua images and after implementation of the four steps. Maps are for the 8-day period from 10 February to 17 February 2013. (a) original MODIS Terra, (b) original MODIS Aqua, (c) after step I, (d) after step II, (e) after step III, (f) after step IV. Color legend: blue=snow, grey=cloud, and green=land.

Two examples of how the different steps of the methodology reduce cloud obstruction and improve information about snow cover extent are given in Figures 2.4 and 2.5. Figure 2.4 shows a typical situation during early autumn. In this example, the original Aqua and Terra images deliver a picture of relatively high cloud coverage and (assumed) scattered snow cover over the study region. After applying the different

steps of this methodology, cloud coverage was effectively reduced and the obviously false snow cover was completely removed. Figure 2.5 demonstrates a situation during winter in which a combination of snow and cloud cover dominates the original images. In this case, information on snow cover extent could be improved by minimizing cloud obstruction using steps I and III of this methodology.

**Table 2.4** Mean monthly and annual snow cover (% , period 2002-2013) in Rhineland-Palatinate from the original Aqua and Terra images and from the individual steps of the presented methodology<sup>a</sup>

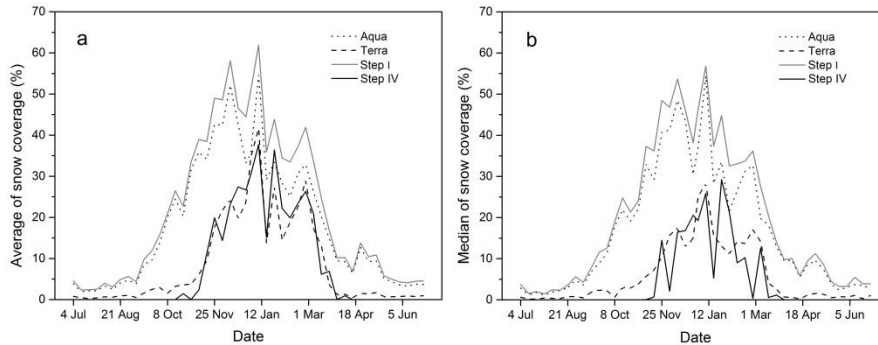
Month	Aqua	Terra	step I	step II	step III	step IV
Jan	37.2/37.0	28.5/14.7	47.2/43.8	44.1/43.7	48.3/50.2	31.7/24.4
Feb	29.8/25.9	21.8/10.1	37.5/28.9	35.4/27.3	39.0/38.5	24.2/12.5
Mar	20.6/16.5	13.3/2.9	25.2/18.5	23.2/14.1	25.7/19.4	12.6/0.0
Apr	9.7/8.2	1.2/0.7	10.5/8.8	7.9/7.6	9.2/8.1	0.2/0.0
May	6.9/5.7	1.1/0.8	7.9/6.5	2.5/0.2	2.9/0.6	0.0/0.0
Jun	3.4/3.3	0.8/0.5	4.1/3.7	0.0/0.0	0.4/0.0	0.0/0.0
Jul	2.9/2.2	0.5/0.4	3.3/2.5	0.0/0.0	0.2/0.0	0.0/0.0
Aug	3.1/2.5	0.7/0.5	3.8/2.8	0.0/0.0	0.4/0.0	0.0/0.0
Sep	6.3/5.4	1.3/1.1	7.5/6.0	0.4/0.0	1.1/0.0	0.0/0.0
Oct	21.5/16.9	3.0/2.2	23.3/19.2	13.2/5.4	15.4/9.3	0.3/0.0
Nov	33.2/29.3	8.2/5.2	36.9/33.6	29.3/29.5	32.0/31.6	7.0/0.0
Dec	38.8/39.9	23.0/16.1	47.7/49.6	45.6/47.3	49.8/50.4	25.9/15.8
Annual	18.1/9.8	8.6/1.7	21.6/11.9	17.1/3.0	19.1/7.4	8.5/0.0

<sup>a</sup>Average (first value) and median (second value) of the monthly and annual snow coverage.

### 2.5.2 Improved representation of snow cover

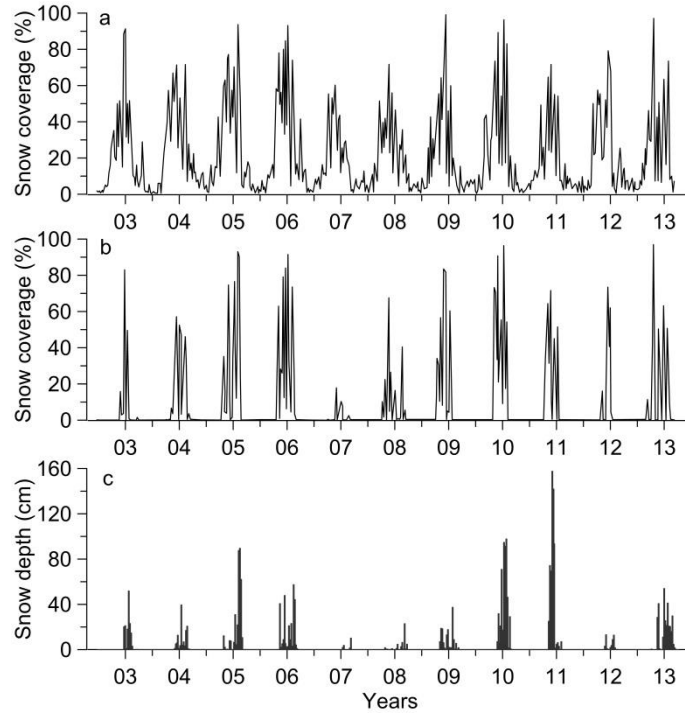
Table 2.4 presents a synopsis of monthly and annual snow cover from the original MODIS data and from the individual steps of the proposed methodology. Inspection of the data reveals that there is a clear overestimation of snow cover from the MODIS sensor residing aboard the Aqua platform, which reports non-negligible snow cover fractions throughout the year. It is clear that between April and October snow is absent in the study region or occurs only during very exceptional, short-term weather conditions. At first glance, the Terra-based images appear to deliver more realistic data; however, a certain, year-round fractional snow cover is reported here as well. Given that snow cover is usually absent between April and October, the mean misclassified snow coverage of Aqua and Terra data for that period is approximately 7.7% and 1.2%, respectively.

Table 2.4 shows that the mean annual snow coverage of Aqua data is nearly 10% higher than that of Terra. This difference is probably due to the replacement of MODIS band 6 through band 7 in the calculation of NDSI for the Aqua data (see Equation (2.1) in section 2.3.1). NDSI identifies snow based on the different reflectivities of the optical (band 4) and near-infrared spectrums (band 6 or band 7). But since cirrus clouds (i.e., ice clouds in the upper troposphere) have a similar spectral signature as snow, NDSI may mix up snow and cirrus, especially when band 6 is replaced by band 7 (in this case, NDSI is higher than that calculated from band 4 and band 6).



**Figure 2.6** Average (a) and median (b) of the 8-day snow coverage over Rhineland-Palatinate (period 2002-2013). Data are from the original Terra and Aqua images, and from the products following steps I and IV of the presented method.

When data from Aqua and Terra are merged (step I), an even higher overestimation of snow cover occurs (Table 2.4). This is unsurprising because the goal of step I is to reduce cloud obstruction, which has no direct effect on the improvement of snow cover information. However, after steps II and IV, a clear reduction in snow cover occurs, with practically snow-free conditions between April and October. Here, the PT filter plays a major role (see Figure 2.6). Although a first glance suggests that snow cover following the final step (i.e., step IV) is similar to that of the original Terra data, it is clear from Figure 2.6 that obvious April to October snow misclassifications were removed (compare also with the example given in Figure 2.4). At the same time, possible quantities of snow omitted during winter could be retrieved (compare with the example in Figure 2.5). Following step IV, the final snow products demonstrate that December, January and February show mean monthly snow coverages between 24.2 % and 31.7%, followed by March (12.6%) and November (7.0%). These values are in agreement with point information from individual stations (see the following section).



**Figure 2.7** Temporal variation in snow cover and snow depth over Rhineland-Palatinate during 2002-2013. (a) Snow cover of the combined Terra-Aqua 8-day product (step I); (b) snow cover after step IV; (c) 8-day accumulated snow depth calculated from observations at 60 meteorological stations (see Figure 2.1 for station distribution).

## 2.6 Validation

As a first test of the validity of the MODIS snow optimization method, the results of steps I and IV were compared with snow depth data recorded at 60 meteorological stations distributed over Rhineland-Palatinate (Figure 2.7). Because snow depth is the original data measured at the stations, the author did not convert it to snow duration; instead, it was aggregated to 8-day data in the same way as described for the daily MODIS data. In addition, daily snow depth was accumulated over the respective 8-day periods. It was supposed that the 60 stations, which are more or less evenly distributed across the study region (Figure 2.1), represent the spatial variability of snow information in a satisfactory way, especially when the information from the individual stations was aggregated to an average value as shown in Figure 2.7. The comparison between the different time series shows that MODIS data after step I of the procedure clearly overestimate snow duration. However, the temporal distribution of snow cover represented by the data generated after step IV is in good accordance with the occurrence of snow cover given by the observations. Further, Figure 2.7 clearly shows

the high temporal variability of snow cover duration and snow coverage in the study region, with snow-scarce winters (e.g., 2006/2007), winters with low snow depth but relatively high snow coverage (e.g., 2007/2008 and 2011/2012), and winters with high snow depth and high snow coverage (e.g., 2009/2010, 2010/2011).

As a further validation, the author applied three evaluation indicators to the modified MODIS snow cover maps following Parajka and Blöschl (2008a). Table 2.5 presents the confusion matrix between MODIS-derived snow cover and observed snow depth over Rhineland-Palatinate during the period 2002-2013. The data from the 60 meteorological stations (Figure 2.1) were compared with those 60 MODIS pixels in which the stations are located. If the measured snow depth for the pixel equaled or exceeded a threshold value  $\zeta$ , it was regarded as snow-covered; otherwise, it was categorized as "land" (i.e., snow free) (Parajka and Blöschl, 2008a). It was found that a threshold value that is too low (e.g., 1 cm) leads to many misclassifications because thin snow cover frequently disappears during the day (snow depth observations at DWD stations are carried out in the morning). A threshold value  $\zeta$  of 3 cm was found to provide the most accurate results.

**Table 2.5** Confusion matrix comparing observed snow depth with processed MODIS snow cover

		Observed Snow Depth	
		No Snow ( $< \zeta$ )	Snow ( $\geq \zeta$ )
MODIS	Land (snow free)	a	b
	Cloud	c	d
	Snow	e	f

Based on the confusion matrix given in Table 2.5, the three evaluation indicators are defined as follows (Parajka and Blöschl, 2008a):

$$\text{MODIS overestimation error: } MO = \frac{e}{a+b+c+d+e+f} \cdot 100 \quad (2.3)$$

$$\text{MODIS underestimation error: } MU = \frac{b}{a+b+c+d+e+f} \cdot 100 \quad (2.4)$$

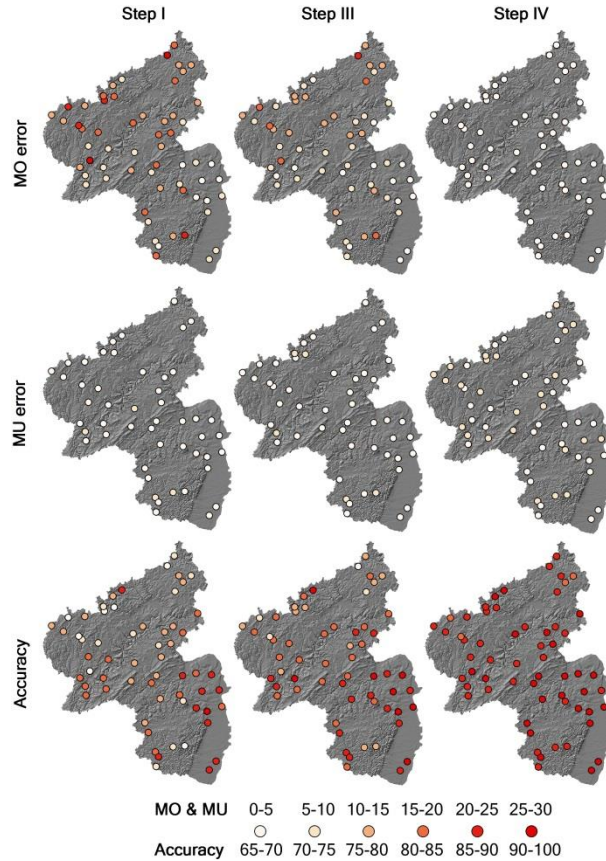
$$\text{MODIS overall accuracy: } k = \frac{a+f}{a+b+c+d+e+f} \cdot 100 \quad (2.5)$$

Figure 2.8 and Table 2.6 present the overestimation ( $MO$ ) error, the underestimation ( $MU$ ) error and the accuracy  $k$  of the improved MODIS snow data after step I, step III and step IV for the ensemble of 60 stations. It is clear that both meteorological filters effectively reduced the  $MO$  error of the MODIS snow data. Figure 2.8 presents the spatial distribution of the three validation indices over the study area. The data from

the 60 meteorological stations where snow depth is recorded were compared with those 60 MODIS pixels in which the stations are located. If the accumulated snow depth of an 8-day period exceeded 3 cm, this 8-day period was rated as snow-covered and compared with the respective 8-day period from the improved MODIS data. The commission (*MO*) error is suggested to be larger than the omission (*MU*) error, especially in the mountain regions of northwest Rhineland-Palatinate. In contrast, the lower Rhine Valley in the southeast showed lower *MO* and *MU* errors. This might indicate that heterogenous snow cover frequently occur in mountain regions because of the complex terrain with high variability in elevation, slope, and land use, leading to higher MODIS snow mapping errors. However, as shown in Figure 2.8, the *MO* error at each station dropped to below 5% after step IV. Accordingly the overall accuracy at the majority of the stations increased to above 85%. Furthermore, the *MU* error at each station did not exceed 10%. Table 2.6 shows that the mean *MO* error of the MODIS data declined from 11.0% ( $\zeta = 1$  cm) resp. 11.9% ( $\zeta = 3$  cm) after step I to 1.0% ( $\zeta = 1$  cm) resp. 1.5% ( $\zeta = 3$  cm) after step IV. Concurrently, the *MU* error rose slightly, from 4.9% ( $\zeta = 1$  cm) resp. 3.1% ( $\zeta = 3$  cm) after step I to 7.1% ( $\zeta = 1$  cm) resp. 4.8% ( $\zeta = 3$  cm) after step IV. During relatively warm days, a number of snow pixels might be rejected by the meteorological filters, leading to a small increase in the omission error. However, the high performance of the meteorological filters in reducing the *MO* error outweighed the increase of *MU* error.

**Table 2.6** The overall *MO* error (%), *MU* error (%) and accuracy (%) of the improved MODIS snow data after step I, step III and step IV and with snow depth thresholds  $\zeta$  of 1 cm and 3 cm (reference period 2002-2013).

Processing Steps		$\zeta = 1$ cm	$\zeta = 3$ cm
		%	%
step I	<i>MO</i> Error	11.0	11.9
	<i>MU</i> Error	4.9	3.1
	Accuracy <i>k</i>	77.1	78.0
step III	<i>MO</i> Error	7.9	8.9
	<i>MU</i> Error	5.3	3.4
	Accuracy <i>k</i>	82.1	83.0
step IV	<i>MO</i> Error	1.0	1.5
	<i>MU</i> Error	7.1	4.8
	Accuracy <i>k</i>	87.1	89.0



**Figure 2.8** Overestimation error ( $MO$  %), underestimation error ( $MU$  %) and accuracy (%) after step I, step III and step IV of the procedure to improve MODIS information. Results are given for all the 60 meteorological stations with a snow depth threshold  $\zeta$  of 3 cm.

During the four-step process, the overall accuracy  $k$  kept rising, from 77.1% ( $\zeta = 1$  cm) resp. 78.0% ( $\zeta = 3$  cm) after step I to 87.1% ( $\zeta = 1$  cm) resp. 89.0% ( $\zeta = 3$  cm) after step IV. Additionally, it should be noted that the mean accuracy  $k$  of the final snow maps approached 93.4% for  $\zeta = 3$  cm (91.5% for  $\zeta = 1$  cm) when cloud pixels were ignored (i.e., during cloud free periods;  $c$  and  $d$  in the denominator of Equation (2.5) are removed). Comparing the two error indicators ( $MO$  and  $MU$ ) with the threshold values  $\zeta$  of 1 cm and 3 cm, the threshold of 3 cm appears to be more reasonable. For  $\zeta = 3$  cm, the over- and underestimation errors of the final snow maps are of similar magnitude, which implies that the biases are small (Parajka and Blöschl, 2008a).

Figure 2.9 shows the mean interannual distribution of the  $MO$  and  $MU$  errors, as well as the accuracy  $k$  of the improved MODIS snow data with snow depth thresholds of 1 cm and 3 cm. The  $MO$  error remains high throughout the year when only step I is applied to improve the original MODIS data. This is especially true between October

and January, when the MO error after the implementation of step I exceeds 30%. A similar picture follows for MODIS data that have passed steps I-III, except that the MO error is then restricted to a period between mid-September and May and is absent (i.e., 0%) for the other months of an average year. A significant reduction of the MO error only took place after all the steps of this methodology were applied to MODIS data. Figure 2.9 shows that only small MO errors limited to December – February occur when all the steps are applied. This demonstrates that the PT filter (step IV) is the most important for minimizing the wintertime MO error.

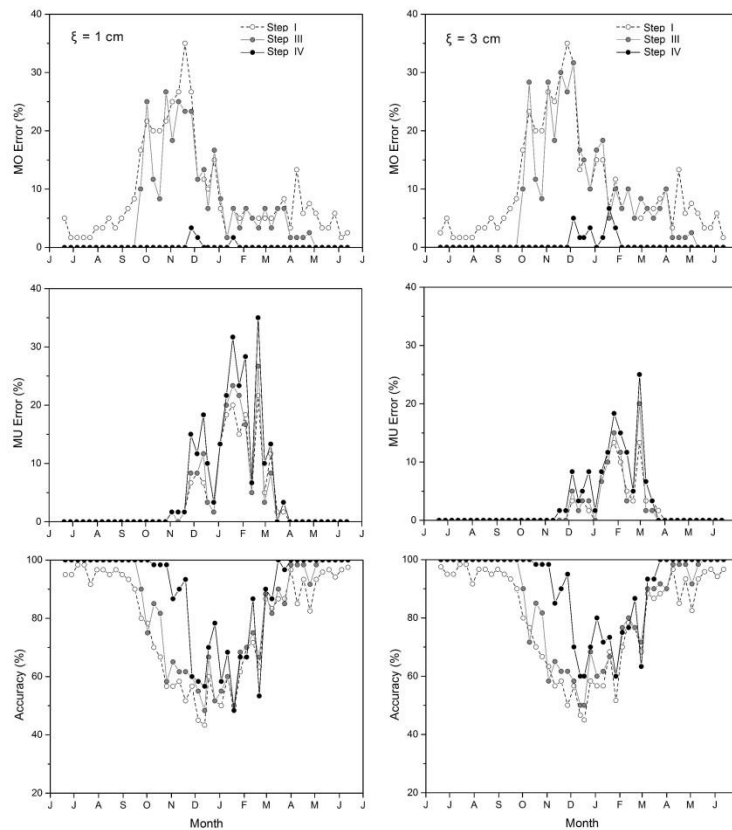


**Figure 2.9** Mean annual distribution of the median of the 8-day MODIS overestimation error (MO %), underestimation error (MU %) and accuracy (%) for the MODIS snow data after step I, step III and step IV of the proposed methodology. The left panels refer to a snow depth threshold  $\xi$  of 1 cm, the right panels to a threshold of 3 cm. Data refer to 60 stations distributed over Rhineland-Palatinate (reference period 2002-2013).

With respect to the MU error, Figure 2.9 confirms the findings discussed earlier in this chapter: The proposed methodology slightly increases the MU error. It is mostly restricted to a period between November and April, and it appears that the highest

error values are shifted towards late winter and early spring (February-March). Apart from the occurrence of a temporal snow cover in the morning, an underestimation of the snow cover might indicate a possible shortcoming of MODIS and/or the PT filter (step IV): During late winter and early spring, daily mean air temperature increasingly rises above the threshold of 0°C. However, the melting process requires a certain period until snow-free conditions are reached, especially when winter snow depth is high and no rainfall occurs. During the melting process, an increasingly patchy snow cover develops. At first, MODIS correctly classifies the respective area as snow, but the information regarding snow/no snow becomes increasingly uncertain in the late snow season. The PT filter described in section 2.4.4 excludes such situations. Thus, no snow cover is assumed when mean daily air temperature exceeds 0°C, which generally leads to an underestimation of snow cover. Although this effect is not significant in the study region, it might be a problem in higher elevation regions with deep snow cover. Therefore, the proposed two meteorological filters require improvement before they can be applied in high mountain regions or used as a global algorithm. However, developing regional filters is a possible approach to improve the standard MODIS snow cover products at basin scale.

Figure 2.9 gives also an impression of the mean inter-annual distribution of the accuracy  $k$ . Although the mean annual accuracy is high after step IV (Table 2.6), the accuracy clearly drops during wintertime and may reach values of 60% (with respect to a threshold  $\zeta$  of 3 cm). However, this methodology is able to restrict reduced accuracy to the (late) wintertime, with the lowest values occurring during January and March. This might occur for the same reason that there is a slight increase in the MU error in winter. Furthermore, the high cloud fraction in wintertime significantly influenced the performance of MODIS data in mapping snow cover. In general, a reduced accuracy with values of 60% or higher, limited to a period of three months, is acceptable with respect to the overall improvements achieved with the methodology presented in this chapter.

## 2.7 Spatio-temporal analysis of snow cover

### 2.7.1 Spatial variation of snow cover and snow duration

Since snow coverage and snow depth represents different characteristics of the snowpack, it is valuable to examine the individual properties of the two snow parameters in their spatial distribution, which can enhance our understanding of the relationships between snow and other environmental variables. Figure 2.10 shows the spatial distribution of MODIS snow coverage and in situ snow depth with elevation in the study area. These statistics were based on the MODIS 8-day snow products and in

situ observed snow depth data at 60 climate stations during the snow seasons of 2002-2013 (Figure 2.1). Two thresholds (snow coverage  $\geq 5\%$  or snow depth  $\geq 1\text{ cm}$ ) were set to determine whether the snow season had begun or ended, which meant the length of snow season at individual elevation zones was different. Figure 2.10a and 2.10b demonstrate the inter quartile ranges of snow coverage and snow depth during the snow season at different elevation zones. From lowland areas to the highlands, the median snow coverage increased from about 30% to 60% while the median snow depth slightly increased by about 1-2 cm, though the large values of snow depth showed a significant increase at high elevations. Figure 2.10c and 2.10d present the curve fittings of the mean values of the two snow parameters with elevation during the snow season. The two figures show that during the snow season the mean snow coverage increased from 38% to 63% with altitude while the mean snow depth rose approximately 5-6 cm. Moreover, there was typical power function relation between snow coverage and elevation in snow season, while it was exponential relation between snow depth and elevation. All the four regression equations passed the F-test ( $P < 0.01$ ).

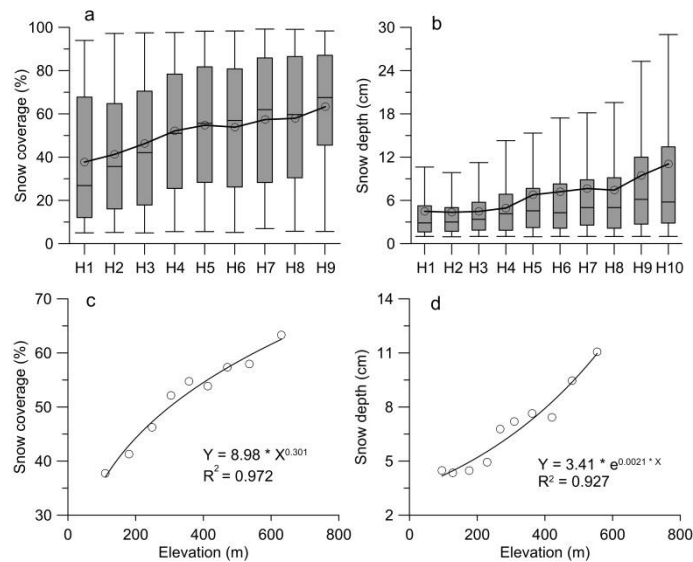


**Figure 2.10** Elevation dependent relationships for (a) Inter Quartile Range (IQR) of snow coverage derived from MODIS 8-day products, (b) Inter Quartile Range (IQR) of in situ snow depth, (c) mean snow coverage derived from MODIS 8-day products, (d) mean in situ snow depth over Rhineland-Palatinate during the snow seasons in the period of 2002-2013.

As is shown in Figure 2.10, the spatial variation of the two snow parameters with elevation was different. Snow coverage represents the presence or absence of snow over a region, while snow depth indicates the snow quantity. As an indicator of snow

occurrence, snow coverage is mainly related to air temperature, leading to a smooth increase of snow coverage with elevation (Figure 2.10a and c), because the restriction of temperature is weakened at highlands. However, snow depth also depends on precipitation, which results in the exponential relation between the mean snow depth and elevation (Figure 2.10d), indicating the influence of the obviously increased precipitation with elevation. To conclude, Figure 2.10 suggests that elevation plays an important role in affecting the spatial distribution of seasonal snow at regional scale, and the different spatial distribution patterns of snow coverage and snow depth might be generated by the changing spatial combination of precipitation and temperature.

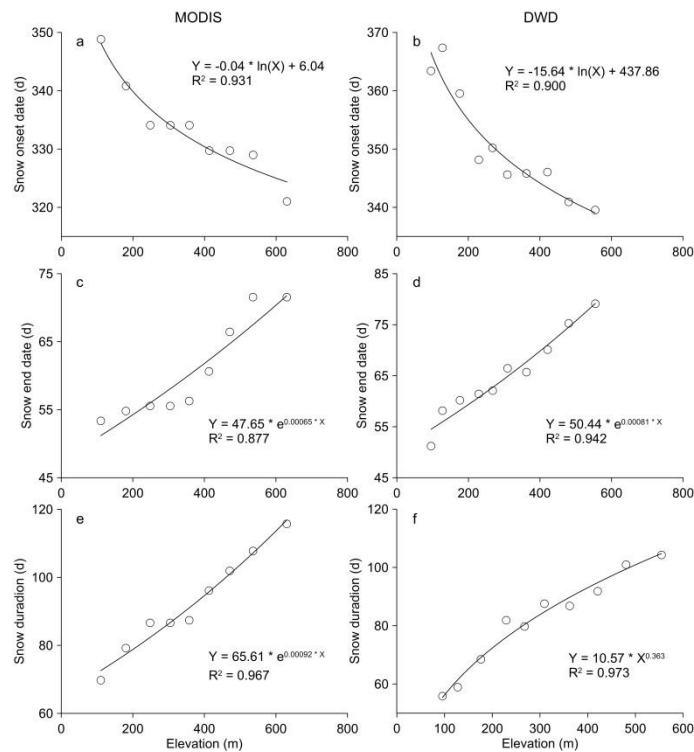


**Figure 2.11** Spatial distribution of (a, b) snow onset date, (c, d) snow end date, (e, f) snow duration at different altitudinal zones derived from MODIS 8-day snow cover products (left) and in situ snow depth data (right) in Rhineland-Palatinate during 2002-2013. Snow onset date and end date are given in Julian numbers.

Figure 2.11 presents the spatial distribution of mean annual snow onset date, end date and snow duration with elevation in the study area from 2002 to 2013. The results derived from MODIS 8-day snow products and ground observed snow data are plotted for the different elevation zones given in Table 2.2. All the fittings in Figure 2.11 passed the F-test ( $P < 0.01$ ). On average, the analysis demonstrated that the snow onset date began about 30 days earlier in the mountainous regions with respect to the

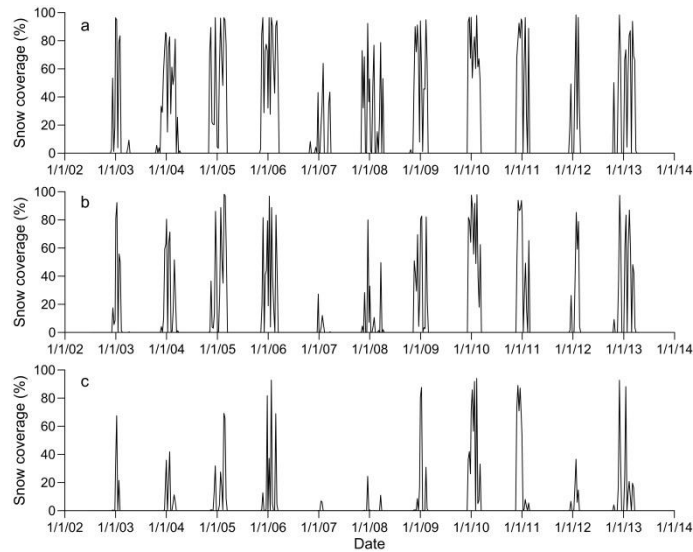
low-lying areas. At the same time, the snow end date is about 30 days later in the mountains. Accordingly, the mean annual snow duration increased about 50 days from the low elevations to the highlands. There was some disagreement between the results derived from the two data sources. This might be caused by the different analysis resp. observation methods. MODIS sensors collected remote-sensing images twice every day over a large area, while in situ snow depth was observed once every day at a point. In consequence, MODIS might capture more snow cover than ground observations. The results from the two kinds of data suggested that there was logarithmic relation between snow onset date and elevation (Figure 2.11a and 2.11b). The snow onset date indicates the first occurrence of snow, and thus it is more related to air temperature, instead of precipitation. Therefore, a turning point of elevation should exist, at which the low temperature for snowfall is satisfied in the early winter, and above which the rate of change of snow onset date with elevation declines. Figure 2.11c and 2.11d suggests that the snow end date had exponential relation with elevation, which is different from the relation between snow onset date and elevation. Snow end date represents the last presence of snow, which means the retreat of thick snow cover in high mountains ends later than the low regions, i.e., increasing precipitation with elevation might delay the snow end date in high mountainous regions. Besides, the different temperature gradients in the beginning and end of the snow seasons can also contribute to the varied spatial patterns of the snow onset and end date.

Figure 2.11e and 2.11f illustrate that the derived snow durations from MODIS data and in situ snow measurements had some difference as well. The former showed exponential relation between snow duration and elevation, while power function fitted the relation better for the latter. It might be led by the individual determination of the thresholds of snow coverage ( $\geq 5\%$ ) and snow depth ( $\geq 1$  cm) for defining the snow seasons. However, Figure 2.10 and 2.11 indicate that the increase of elevation generally accompanies the decrease of air temperature and increase of precipitation, resulting in more snow pack and longer snow duration. At the same time, the seasonal as well as spatial variations of temperature and precipitation obviously increase the spatial complexity of the snow duration parameters.

### **2.7.2 Temporal variation of snow cover and snow duration**

Figure 2.12 shows the temporal variation of snow coverage in three elevation zones of the study area. Increasing snow coverage with altitude is more obvious in relatively snow poor winters when snow coverage is low or even absent in low-lying areas. This is demonstrated by the winters 2006/2007, 2007/2008 and 2011/2012. In contrast, winters with cold spells extending into the lowlands show high snow coverage across

all elevation zones, such as winters 2005/2006 or 2012/2013. It should be noted that snow duration is definitely shorter in the lowlands, even during relatively cold winters. A very similar behavior occurs when the spatio-temporal distribution of snow depth is considered (Fig. 2.13). However, Figure 2.13 suggests that snow depth has higher difference at the three altitudes compared to snow coverage shown in Figure 2.12, indicating snow depth is more sensitive to elevation, which is supported by the results demonstrated in Figure 2.10. In other words, increased precipitation with elevation can contribute to the rise of snow depth (snow quantity), while snow coverage (snow occurrence) is more related to air temperature and less influenced by precipitation. Snow coverage tends to approach an upper limit at a moderate elevation, where the decreased air temperature satisfies the meteorological condition of snowfall.



**Figure 2.12** Temporal variation of MODIS snow coverage at the altitude of (a) 583-817 m, (b) 331-385 m, (c) < 145 m from 2002 to 2013.

The three snow parameters of snow onset date, end date and snow duration obtained from MODIS 8-day snow cover products and in situ snow data are shown in Figure 2.14. It illustrates that the two kinds of snow data fit each other very well in most years during 2002-2013, except in some specific years like 2006-2008. The reason might be there was particularly less snow both in the two winters, leading to more errors in determining snow onset and end date with the two different data sources (see Figure 2.12 and 2.13). Even though Figure 2.14 shows some inter-annual fluctuations of the snow onset date, end date and duration, neither significant uptrend nor downtrend was found during 2002-2013. Figure 2.14a and 2.14b show that snow onset date has an opposite inter-annual variation with snow end date. It means that if snow began earlier in one winter then it tended to end later, and vice versa.

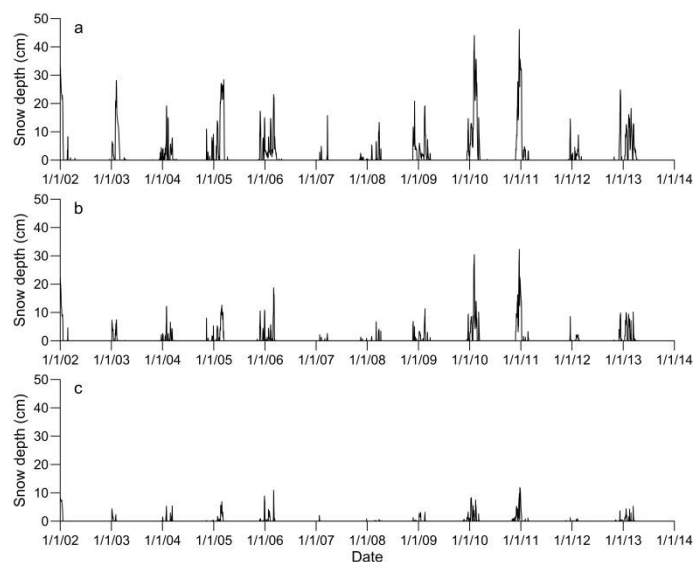


**Figure 2.13** Temporal variation of in situ snow depth at the altitude of (a) 510-650 m, (b) 320-390 m, (c) < 110 m from 2002 to 2013.

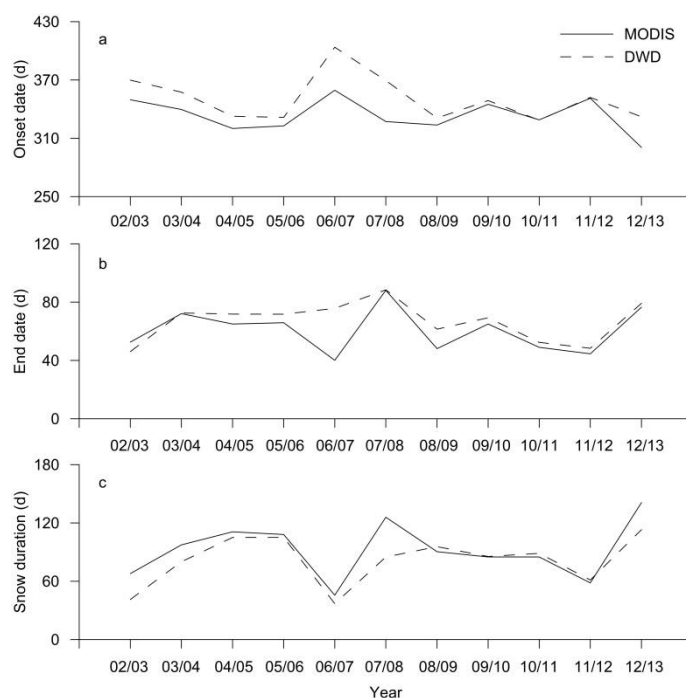


**Figure 2.14** Temporal variation of (a) snow onset date, (b) snow end date, (c) snow duration derived from MODIS 8-day snow products (solid line) and in situ snow depth data (dotted line) from 2002 to 2013.

Figure 2.15 demonstrates the overall snow cover variation in winters in Rhineland-Palatinate during 2002-2013. It is obvious that in highlands the number of years with

snow was higher, e.g. in the mountain regions of the Eifel, the Hunsrück and the Palatinate Forest, and vice versa. The spatial distribution of snow cover showed high consistency with elevation (Figure 2.1 and 2.15). In this region, the majority of the snow occurred in the three months of December to February. In addition, there were more snowfalls in two periods of from mid-December to the beginning of January and the end of January, while the latter period had the most snowfalls.

**Table 2.7** Correlations between the number of snow days and spatial factors.

Correlation	Control Variables	Lat.	Lon.	Aspect	Slope	Albedo	NDVI	Elev.
Pearson	-none-	0.196*	-0.412*	0.049*	0.155*	-0.248*	0.629*	0.876*
Partial	Elev.	0.013	0.065*	-0.014	0.061*	-0.275*	0.369*	

\*. Correlation is significant at 0.01 level.

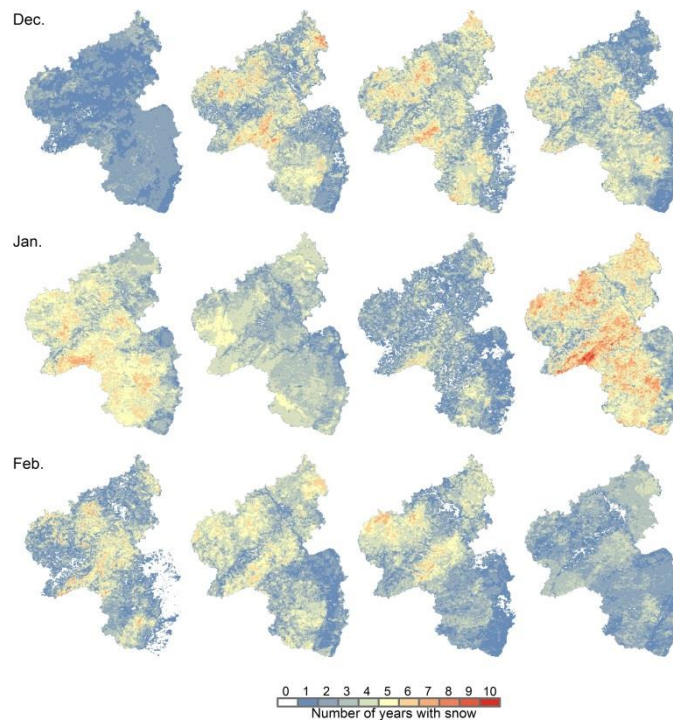


**Figure 2.15** Number of years with snow in the winters (Julian day 337 to 57, with 8-day interval) of 2002-2013 derived from MODIS 8-day snow cover products. Each month refers to four 8-day periods.

### **2.7.3 Influence of spatial factors on snow cover**

To investigate the relations of the number of snow days with various spatial factors, i.e., latitude, longitude, elevation, slope, NDVI, albedo and aspect, correlation analysis was conducted at 10,000 random points over Rhineland-Palatinate (Table 2.7). NDVI and albedo were supposed to be indexes of the regional vegetation and land use. The results show that elevation and NDVI are more related to the number of snow days, both of which have significant positive correlations with the number of snow days. Moreover, the correlations between the number of snow days and other spatial factors are relatively lower. To some extent, the different correlations represent various impacts of spatial factors on snow occurrence. Compared with the Pearson correlation, elevation was selected as a control variable in the partial correlation. Table 2.7 also shows the coefficients of partial correlation between the number of snow days and latitude, longitude, slope drop obviously, which indicates that the Pearson correlations between the number of snow days and the three spatial factors were adulterated with the influence of elevation. In general, slope and aspect are significant factors determining snow cover on the small scale, which was not reflected in the correlation analysis. The reason might be that MODIS snow products only have moderate spatial resolution of 500 m, and thus the topographical details are smoothed in the study region that has relatively low elevations. Moreover, the capability of 8-day MODIS snow maps in differentiating snow occurrence was also weakened by the declined temporal resolution. Since NDVI is closely related to altitudes because of the vertical zonation of vegetation, the relatively high Pearson correlation between NDVI and the number of snow days is partly a response to elevation change. It is supported by the decreased partial correlation between NDVI and the number of snow days (Table 2.7). However, both NDVI (vegetation) and albedo (land use) have particular influence on snow cover, e.g., affecting the snow accumulation and ablation through changing the local energy balance, even though elevation played the most important role in the spatial distribution of snowpack.

## **2.8 Discussion and conclusions**

The overall aim of this study was to contribute to the provision of more reliable time series of MODIS snow products and to therefore support a better assessment of the spatial and temporal distribution of snow on regional and continental scales. To do this, this study focused on reducing the overestimation error and increasing the overall accuracy of snow-related data from the MODIS sensors. The proposed methodology includes a four-step procedure that reduces the cloud obstruction and snow misclassification on MODIS images. In the case study, the 8-day MODIS Aqua and Terra snow products for the period 2002-2013 over Rhineland-Palatinate were applied.

This case study was chosen because snow distribution is highly variable in this region, and dense cloud cover is a common phenomenon. In addition, a sequence of mountain ranges, deep valleys and extended lowlands makes the topography complex, and thus is a further challenge for testing MODIS products. The highest elevation in Rhineland-Palatinate is only about 820 m and the regional climate is relatively moderate, which means snow cover cannot retain for a long time in winter. However, it is still quite necessary to study the temporal and spatial variety of the snow cover in these low mountain regions. As it is, the snowfalls can melt quickly and rain-on-snow events become an important generator of peak flow, which might lead to flood disasters (Floyd, et al., 2008). Flood occurs easily when a snow pack is inundated by a warm, moisture-laden front producing rapid melt coupled with large inputs of rainfall into the hydrologic system (Marks, et al., 1998). Therefore interpreting the spatio-temporal distribution characteristics of snow cover in low mountains and coupling it into hydrological models is of great significance. Full understanding of the hydrologic processes related to snowfalls offers support to water resources management.

The implementation of the various steps of this methodology showed that the percentage of pixels with cloud-obscured images could be significantly reduced. The combination of the MODIS images from Aqua and Terra (step I) and the use of neighborhood analysis (step III) led to a decline in the mean annual cloud cover from 13.1-13.7% to 4.5% only. Although this method does not completely remove cloud obstruction, it efficiently minimizes the perturbing effects of cloud cover. The approaches of Aqua-Terra combination and neighborhood analysis have been used by many researchers to reduce cloud obscuration from MODIS snow-cover images. Parajka and Blöschl (2008a) reduced the annual cloud coverage of the daily MODIS snow maps over Austria from 66.1% for Terra images and 70.1% for Aqua images to 55.0% for the composites, and they further reduced the cloud coverage to 46.3% by using neighborhood analysis. Tong et al. (2009) reported that the cloud coverage on MODIS 8-day snow products declined by 10% after the application of a spatial filter (neighborhood analysis) in a watershed of western Canada. As suggested by Parajka and Blöschl (2008a), there is a tradeoff between cloud coverage and mapping accuracy when the cloud pixels on MODIS snow products are reclassified. In high mountains where stable snow cover exists, utilizing the snow line method to further remove the cloud obstruction is a good solution (Gafurov and Bárdossy, 2009; Krajčí et al., 2014). However, this method implies shortcomings when it is applied for low mountain ranges where snow cover variability is high. Besides, extending the neighborhood analysis to a larger spatial window is a possible option for enhanced cloud removal. A cloud-gap filled daily MODIS snow cover product developed by Hall et al. (2010) will be available in Collection 6, which addresses the need to improve the frequency of mapping snow. In addition, the algorithm for processing Aqua images has been

updated and is nearly as accurate as the Terra algorithm in Collection 6 of MODIS snow products.

The two meteorological filters (steps II and IV) reduce the snow overestimation (commission) error, which is high for the original MODIS data. After application of the min. ground-T filter, the overall snow commission error was reduced from 11.0-11.9% to 7.9-8.9%. The PT filter further reduced the overestimation of snow cover to 1.0-1.5%, although at the cost of a slight increase in the snow underestimation (omission) error. Nonetheless, the omission error remains relatively low. There has been a large body of literature focusing on the reclassification of the cloud pixels on MODIS snow products (Gafurov and Bárdossy, 2009; Gao et al., 2010; Hall et al., 2010; López-Burgos et al., 2013; Parajka and Blöschl, 2008a; Xie et al., 2009), which can retrieve some omitted snow pixels and thus reduce the underestimation error. However, less attention was paid to the elimination of false snow detection (overestimation error), which is an obvious problem in many regions of the globe. López-Burgos et al. (2013) reduced the cloud obscuration of MODIS snow maps by 94% with a multistep method in the Salt River basin, but the commission error increased by 2%, compared to the original Terra images. Therefore, using meteorological data to relieve the overestimation of snow on MODIS images as presented in this study is a beneficial attempt. The validation of the MODIS snow maps indicates that the snow commission error peaks at the beginning of the winter, while the omission error frequently occurs toward the end of the snow season. The users may be able to further reduce both errors by optimizing the definition of snow-free and snow days. This could be done by a further improvement of the PT filter, especially when the method is applied to higher elevated mountain ranges or regions with a long-lasting and deep snow cover.

Following the four-step process, the overall accuracy of the final MODIS snow products was about 87.1-89.0%, and approached 91.5-93.4% for cloud-free snow maps. The analysis of the temporal variation of snow cover showed that the modified MODIS snow data have a clearly better agreement with observed data, and that the snow duration can be determined more accurately. A critical aspect in the validation procedure is the comparison of areal data (i.e., MODIS snow cover information for a 500 x 500 m grid cell) with point information (i.e., snow depth measured at a single location). It is well known that there is high small-scale spatial heterogeneity of snow depth and snow water equivalent. Measurements at one point are therefore not able to reproduce this heterogeneity. The availability of relatively dense and spatially distributed point snow data, however, made it possible to at least compare aggregated station data with the areal data from the improved MODIS products. Further, Figure 2.8 shows that a direct comparison between point information and areal data might also be useful, although an unquantifiable uncertainty remains.

The spatio-temporal variation of the snow cover in Rhineland-Palatinate from 2002-2013 was studied with the improved MODIS 8-day snow cover products and in situ snow depth measurements. The results showed that both the snow coverage and snow depth rose with elevation. Snow coverage had typical power function relation with elevation in snow season, while it was exponential relation between snow depth and elevation, indicating snow coverage mainly depended on air temperature but snow depth was also significantly influenced by the orographic effect of precipitation. Both MODIS data and in situ snow data suggested there was logarithmic relation between snow onset date and elevation, but exponential relation between snow end date and elevation, which might reflect the delayed snow ablation in high mountainous regions and different temperature gradients in the beginning and end of the snow seasons. All these results demonstrated that elevation plays a crucial role in the spatial distribution of snowpack on the regional scale. Comparing the individual spatial variation of different snow parameters is useful to interpret the relations between snowpack and other environmental variables. MODIS snow products and in situ snow depth data illustrated the similar temporal variation of the snow pack in the study area during 2002-2013. There was less snow in the winters of 2006-2008 and 2011-2012, while there was more snow in the years of 2004-2006, 2009-2011 and 2012-2013. Moreover, most snowfalls occurred at the end of January in this region according to the results derived from the MODIS snow cover products in the period 2002-2013.

The relations between spatial factors and snow cover were examined using correlation analysis. The results suggested that elevation was the most important factor in affecting the number of snow days. NDVI and albedo also showed some influence on the number of snow days. The other spatial factors of latitude, longitude and slope had low correlation with the number of snow days in Rhineland-Palatinate. The influence of slope on snowpack might be neglected because of the coarse spatial and temporal resolutions of MODIS 8-day snow products. At large scales, latitude and longitude have great impact on snow cover, but given the small spatial extension of Rhineland-Palatinate, only weak influence was detected.

## **Chapter 3**

### **Improvement and application of MODIS daily snow products**

#### **3.1 Introduction**

Snow cover maps are useful information for snow-related research, even though only the spatial extent of the snow cover is given. In chapter 2, a new algorithm has been developed to improve MODIS 8-day snow cover products, which achieved promise in cloud removal and rejection of false snow. However, a critical aspect of the methodology is that the MODIS snow product used in this study is maximum snow extent aggregated over 8 days. Auxiliary daily information used either in the methodology or for validation (e.g., precipitation or temperature) needs to be aggregated in the same way. The 8-day maximum snow extent may lead to an overestimation of snow duration, especially at low elevations where snow frequently disappears after a period of a few days. Overestimation might also occur at all elevations during relatively warm periods in which snow cover is irregular. Figure 2.12a shows that the snow cover continued for the whole winters and approached the coverage of nearly 100% in mountainous regions during the winters of 2004-2005 and 2005-2006, which obviously deviated from the normal reality in Rhineland-Palatinate. The major overestimation was generated by the algorithm that was used to produce MODIS 8-day snow maps with daily products. As maximum snow extent products, MODIS 8-day snow data accumulated the snow occurrence in each 8-day period, and thus they cannot distinguish the short snow events in the study region, where the snow cover has high variability. In addition, an underestimation of snow cover could also occur when MODIS 8-day snow maps are applied. For example, if some temporary snow cover was obscured by cloud followed by snow-free conditions during the same 8-day period, snow-free over the entire 8-day period would be reported with the obstructed snow being omitted. Therefore, MODIS daily snow products have the potential to reduce the snow over- and underestimation, with the snow cover variation over a large area being correctly represented. Nonetheless, the cloud obstruction on MODIS daily snow products is significantly higher than that on the 8-day products, especially for mountainous regions.

Parajka and Blöschl (2006) suggested that clouds obscured 63% of Austria on daily MODIS snow cover images. López-Burgos et al. (2013) reported that clouds covered 39% of the MODIS daily snow maps in a basin of central Arizona, USA, mostly during periods of active snowfall. Wang et al. (2009) indicated that the annual mean cloud blockage for MODIS Aqua and Terra daily snow data were 47% and 44% respectively in northern Xinjiang, China. Therefore, the applicability of MODIS daily snow cover products is significantly restricted by cloud obscuration.

Much research effort has been devoted to the task of cloud removal of daily MODIS snow data over the past ten years (Gafurov and Bárdossy, 2009; Hall et al., 2010; Krajčí et al., 2014; López-Burgos et al., 2013; Parajka and Blöschl, 2008a; Riggs and Hall, 2003; Wang et al., 2009; Xia et al., 2012; Xie et al., 2009). Cloud removal of remote sensing data is essentially an information reconstruction process, i.e., cloud reclassification for MODIS snow data. The published techniques for removing cloud pixels from MODIS snow cover products mainly includes combination of Aqua and Terra data, neighboring spatial combination, temporal combination, variational interpolation, snow season determination, snow transition elevation and locally weighted logistic regression (Gafurov and Bárdossy, 2009; Hall et al., 2010; López-Burgos et al., 2013; Parajka and Blöschl, 2008a; Xia et al., 2012). The idea of the former four approaches is to utilize the MODIS snow observations of another sensor, neighboring pixels, recent images, while the latter three methods consider the temporal and spatial variation of snow cover. The former four techniques hence have less effect for the regions regularly covered by massive clouds, because of the scarce reference information from MODIS data themselves. For the regions where snow cover has high spatial and temporal variability, the latter three solutions also fail to work. Riggs and Hall (2010) employed a decision tree technique to improve the MODIS snow mapping algorithms for snow/cloud discrimination, achieving up to 5% increase in mapped snow cover extent, but large cloud fractions still remained.

Besides, snow misclassification is another limitation on daily MODIS snow cover products, as same as 8-day MODIS snow data presented in chapter 2. Reclassification of cloud cover is also a process of retrieving omitted snow pixels, and thus it can contribute to the reduction of snow underestimation errors. As data noise, the committed snow can only be rejected in assistance with reference information. The previous studies rarely focused on relieving the snow misclassification errors of MODIS snow data. Thompson et al. (2015) employed a liberal cloud-masking algorithm for addressing snow/cloud confusion errors of MODIS snow data, which showed well performance. In chapter 2 (Dong and Menzel, 2016a), two meteorological filters have been used to reduce the commission errors of MODIS 8-day snow products. This study showed the potential of utilizing meteorological data to improve MODIS snow information. For example, the meteorological data of precipitation, temperature

and snow depth are valuable information that provides the possibility of snow presence over an area, which can be applied to reject false snow on MODIS daily snow data. Moreover, as another snow observation technique, the ground-based snow measurements can be used to extrapolate the cloud obscured snow cover and thus to remove the cloud obstruction on remotely sensed snow maps.

Based on the above notions, the aim of this study is therefore to further develop a methodology for reclassifying the cloud cover and reducing the misclassification error of daily MODIS snow cover products with the help of ground-based meteorological data. A five-step procedure for improving daily MODIS snow maps was introduced in this chapter, which showed high performance in a case study in southwestern Germany. In the new algorithm presented in this chapter, ground-based snow depth was involved in detecting the snowpack accumulated at the mountains when air temperature was high (e.g. snow ablation stage in spring), which could help generate more accurate cloud-free MODIS daily snow time series. Due to the complex topography and the highly inhomogeneous climate, snow cover in southwestern Germany has high temporal and spatial variability, and thus this region is very appropriate for validating the efficiency of the proposed methodology.

## **3.2 Study region and data**

### **3.2.1 Study area**

The study area is located in southwestern Germany (Figure 3.1), which is mainly occupied by the upper reaches of the Rhine River and the Danube River. As the watershed of the two rivers, the Black Forest, located at the southwest of the study area, is the highest region with elevations up to about 1493 m. The high plateau of the Swabian Alb, between the Black Forest and the Danube, has elevations between 600 and 1015 m a.s.l. The geomorphology of the northern part is mainly characterized by plains and some dotted low mountains and hills, such as the Eifel, the Westwald, the Hunsrück, the Taunus, the Palatinate Forest and the Odenwald, symmetrically distributed on the banks of the Rhine. The elevations of the northern area range between 10 and 817 m a.s.l.

As a transition zone, the whole study region is alternatively influenced by temperate maritime and continental climates, having warm summers and cool winters in the low elevations. The heterogeneous terrains increase the complexity of the regional climate with uneven distribution of water and heat. In the high mountains, snow frequently occurs from November to April, and stable snow cover could accumulate for a long time on the mountain tops, accounting for up to 37% of total precipitation (Peters and van Balen, 2007). In contrast, snow has a high variability in the warm and dry Rhine

Valley and the lower plains, which only have an annual precipitation of about 500-600 mm/yr while it can approach 2000 mm/yr in the Black Forest mountains (BMUNR, 2003). Potential evapotranspiration is about 600-700 mm/yr in the plains and 400-500 mm/yr over the mountain tops, respectively (BMUNR, 2003). Mean annual air temperature is about 6 °C at the high mountain ranges and exceeds 10 °C in the warm Rhine valleys. Cloud amount is regularly high through the winter, which seriously interferes with the remotely sensed observations of snow cover.

Most of the mountain ranges over the study area are covered with forest, mixed with some small-scale clearings for agriculture. From the high mountains in the south to the lower hills in the north, the forests switch from coniferous-dominance (pine, spruce, fir) to more shares of deciduous trees (beech, oak, larch, chestnut). The total forest coverage of the Black Forest and the Palatinate Forest exceed 70%. Agricultural lands are mostly distributed from the piedmont areas to the deep valleys. The complex topography and vegetation of this region lead to high temporal and spatial variability of the snow cover in winter.

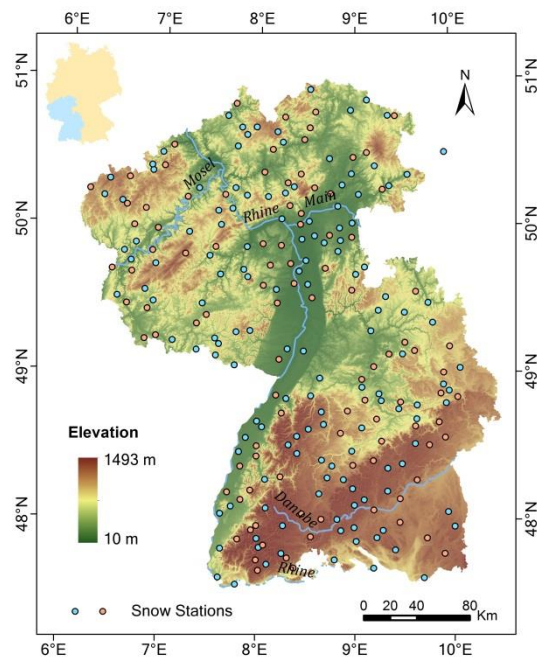


**Figure 3.1** Topography of the study area in southwestern Germany and locations of the snow measurement stations.

### 3.2.2 MODIS data

The MODIS snow data used in this study consist of the daily snow cover maps (MOD10A1 and MYD10A1) from 8 August 2002 to 30 May 2015. The Collection 5

(Riggs et al., 2006) MODIS standard snow products were applied and the snow maps of 20 days during this period were rejected because of the gaps of the MODIS Aqua or Terra data. Thus, a total of 9,318 MODIS snow cover images were downloaded through the Earth Observing System Data and Information System (EOSDIS, <https://earthdata.nasa.gov/>), which is operated by NASA's Earth Science Data Systems Program. The daily MODIS snow cover products have a spatial resolution of  $500 \times 500$  m. The two tiles of h18v03 and h18v04 were combined to cover the whole study area in southwestern Germany. The MODIS Reprojection Tool (MRT) was employed to execute the data format conversion (HDF to GeoTIFF), image-mosaic (h18v03 and h18v04) and reprojection (Sinusoidal to WGS84-UTM).

### **3.2.3 Meteorological data and DEM**

All the meteorological data used in this study were provided by the German Weather Service (DWD, [www.dwd.de](http://www.dwd.de)). The daily time series of precipitation (P) at 325 stations, air temperature (T) at 119 stations, snow depth (SD) at 242 stations (Figure 3.1) for the period from 8 August 2002 to 30 May 2015 were included. Among the snow depth measurements, the snow data from 142 random stations were applied in the improvement procedure of MODIS snow products and the data from the other 100 stations were utilized for validation purpose. The overall precipitation and air temperature data, and the snow depth data from 142 stations were interpolated to grids using the Kriging method with the same cell size of the MODIS data. The gridded meteorological data were then applied to generate meteorological filters, which were involved in the processing of MODIS snow maps.

The Shuttle Radar Topography Mission (SRTM) data was used in this study as digital elevation model (DEM) to execute the topographical correction of temperature grids. It can be obtained free of charge through Consultative Group for International Agricultural Research-Consortium for Spatial Information (CGIAR-CSI, <http://srtm.csi.cgiar.org/>). The SRTM data has a spatial resolution of  $90 \times 90$  m, and it was resampled to the same cell size as the temperature grids.

## **3.3 Methodology**

The processing of MODIS snow products in this study was focusing on three aspects, including removal and reclassification of cloud contamination, retrieval of omitted snow information, and rejection of misclassified snow cover. Based on previous studies, a five-step procedure (Figure 3.2) has been developed to improve the MODIS snow cover maps. The individual steps of the method are presented in the following sections.

### 3.3.1 Aqua/Terra Combination

The Aqua and Terra satellites have distinct viewing and cloud cover conditions because of their different orbits, which provides opportunity for users to reduce cloud obstruction and to retrieve some omitted snow cover. The cloud pixels within the non-coincidence region of Aqua and Terra images can be replaced with snow or land on the composites. The combination process was only carried out at cloud pixels, and it could not achieve an obvious effect in the heavily cloudy days. The Aqua/Terra combination has been introduced by Parajka and Blöschl (2008a).

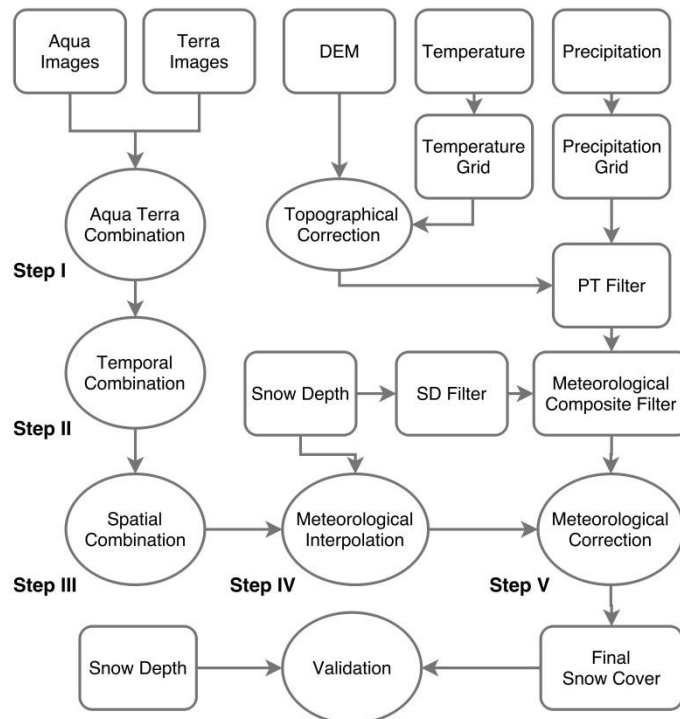


Figure 3.2 Flow chart of MODIS snow data processing.

### 3.3.2 Temporal Combination

The temporal combination of cloud covered pixels has the similar idea as the Aqua/Terra combination. Since the MODIS data has a high temporal resolution of one day, the data gaps in snow maps can be filled based on the most-recent cloud-free observations. The temporal combination has a principal assumption that the snow conditions in the study area remain constant (no snowfall or ablation) during the gap-filling period. Parajka and Blöschl (2008a) significantly reduced the cloud coverage of MODIS snow data over Austria with 7-day temporal combination at the expense of a slight decrease in accuracy. Thus, the above assumption has good reliability in high

mountains and cold regions, but it is not true in those regions with warm winters, such as the Rhine Valley in this study area, where the snowpack can disappear within one or two days. Consequently, only the one-day temporal window ( $\pm 1$  day) was selected to execute the temporal combination in this chapter, even though the cloud removal efficiency was weakened. The detailed procedure for temporal combination can be found in previous studies (Parajka and Blöschl, 2008a; Gafurov and Bárdossy, 2009).

### **3.3.3 Spatial Combination**

Reclassifying the cloud pixels with spatial combination is supported by the Spatial Similarity Theory. In this step, the eight pixels surrounding each cloud pixel ( $3 \times 3$  spatial window) were examined, and the cloud pixel in the center was defined as the type that was in the majority among the surrounding eight pixels. In previous studies, snow transition elevation (Gafurov and Bárdossy, 2009) and aspect information (López-Burgos et al., 2009) were also involved into the neighboring pixel analysis. However, it has limitations in this study area, which has relatively low elevations and high snow variability, and thus topographical information was not included in the spatial combination in this study.

### **3.3.4 Meteorological Interpolation**

After the above three steps, a large number of cloud pixels still remain in MODIS snow cover products. As ground-based snow measurements, the snow depth data derived from meteorological stations have the potential to interpolate the data gaps. Gafurov et al. (2015) reconstructed the snow cover with in situ observations and MODIS snow products based on a conditional probability method in a catchment of Central Asia. In this study, this method was applied to interpolate the residual cloud pixels on the MODIS snow maps. The snow depth data from 142 stations over southwestern Germany were selected to implement the meteorological interpolation. All the cloud pixels in MODIS snow cover products were removed in this step. The detailed procedure is described as follows:

In the first step, the conditional probability (CP) of one pixel covered by snow (land) given that one station records snow depth  $\geq k$  ( $< k$ ) at the same time is calculated.  $k$  is the threshold of observed snow depth to define a station is covered by snow. It is assumed that slight snow cover less than  $k$  melts quickly or forms patchy snowpack and cannot be observed by MODIS. In this study, the threshold of 3 cm was chosen because of the regular warm winters in this study area. The conditional probabilities were calculated with the following equations (Gafurov et al., 2015):

$$P^s(S_{x,y}|S_n) = \frac{\sum (1 - ABS(S_{x,y,t} - S_{n,t}))}{N_{x,y}} \quad (3.1)$$

$$\forall S_{n,t} = 1,$$

$$P^l(S_{x,y}|S_n) = \frac{\sum (1 - ABS(S_{x,y,t} - S_{n,t}))}{N_{x,y}} \quad (3.2)$$

$$\forall S_{n,t} = 0.$$

where  $P^s(S_{x,y}|S_n)$  and  $P^l(S_{x,y}|S_n)$  are the CPs of a pixel with coordinates  $x, y$  to be observed as snow (land) given that the station  $n$  also records snow (land) at the same time.  $S_{x,y,t}$  and  $S_{n,t}$  are binary variables indicating the presence ( $S = 1$ ) or absence ( $S = 0$ ) of snow at pixel  $x, y$  of MODIS snow data and meteorological station  $n$  for day  $t$ , respectively.  $N_{x,y}$  is the number of days in which station  $n$  shows snow ( $S = 1$ ) or land ( $S = 0$ ) among the cloud-free days of MODIS data at pixel  $x, y$  over the study period 2002-2015.  $P^s(S_{x,y}|S_n)$  and  $P^l(S_{x,y}|S_n)$  range between 0 and 1.  $P^s(S_{x,y}|S_n) = 1$  ( $P^l(S_{x,y}|S_n) = 1$ ) means pixel  $x, y$  on MODIS data was invariably snow (land) during cloud-free days when the snow depth at station  $n \geq 3$  cm ( $< 3$  cm), i.e., MODIS has completely consistent observations of snow cover at pixel  $x, y$  with station  $n$  in cloud-free days of this period. Conversely,  $P^s(S_{x,y}|S_n) = 0$  ( $P^l(S_{x,y}|S_n) = 0$ ) indicates that pixel  $x, y$  on MODIS data was constantly land (snow) during cloud-free days when the snow depth at station  $n \geq 3$  cm ( $< 3$  cm), i.e., MODIS has entirely opposite observations at a pixel to the measurement of a station. The snow and land CP values for each pixel ( $687 \times 828$  pixels) to each station (142 stations) were calculated to generate two judgement matrices. Then the cloud pixels were reclassified as follows:

$$S_{x,y,t} = 1 \quad \text{if } (P^s(S_{x,y}|S_n = 1) \text{ and } S_{n,t} = 1), \quad (3.3)$$

$$S_{x,y,t} = 0 \quad \text{if } (P^l(S_{x,y}|S_n = 1) \text{ and } S_{n,t} = 0). \quad (3.4)$$

In some extreme cases, the conditions of Equation (3.3) and (3.4) might be both satisfied; those cloud pixels would be valued as snow, which means snow has higher priority than snow-free. This step could interpolate a part of cloud pixels on MODIS snow maps, and the remained cloud pixels were further reclassified completely in the next procedure.

For the cloud pixels on which the CPs  $< 1$ , their conditional probabilities have distinct confidence levels because of their different sample numbers ( $N_{x,y}$ ), i.e., each pixel has different cloud-free days and snow days during the study period. When the judgements from various stations conflict with each other, the confidence levels of the

different CP values should be considered. Therefore, the lower bound 95% confidence interval (CI) of each CP for snow was computed as follows:

$$CI_{(P^s(S_{x,y}|S_n))} = P^s(S_{x,y}|S_n) - 1.96 \sqrt{\frac{P^s(S_{x,y}|S_n)(1 - P^s(S_{x,y}|S_n))}{N_{x,y}}} \quad (3.5)$$

where  $CI_{(P^s(S_{x,y}|S_n))}$  is the lower bound of 95% CI of CP for snow condition both observed at pixel  $x,y$  and station  $n$ . Then the residual cloud pixels were reclassified according to the levels of the maximum lower bound CI of CP for snow, which can be described in the following equation:

$$S_{x,y,t} = 1 \quad \text{if } \max(CI_{(P^s(S_{x,y}|S_n))}) \geq 0.5, \quad n \in 1:142 \quad (3.6)$$

$$S_{x,y,t} = 0 \quad \text{if } \max(CI_{(P^s(S_{x,y}|S_n))}) < 0.5, \quad n \in 1:142 \quad (3.7)$$

It means one undefined cloud pixel is determined as snow when at least one station judges that the possibility for this pixel having snow is higher than or equal to 50%, and the credibility is more than 95%. In the study of Gafurov et al. (2015), the maximum lower bound CI of CP for snow was compared with that for land, and the cloud pixels were valued as snow if  $\max(CI_{(P^s(S_{x,y}|S_n))}) > \max(CI_{(P^l(S_{x,y}|S_n))})$ ; otherwise the pixels were changed to land. This criterion was initially tried, but most of the undefined cloud pixels were found to be classified as land. The reason is that the number of snow days is far less than that of snow-free days in this study area, and thus the CP and lower bound CI for snow are prone to be lower than those for land. This criterion can lead to obvious underestimation errors of snow. Therefore, Equation (3.6) and (3.7) were chosen to interpolate the remained cloud pixels over this area. However, this modification finally increased the overestimation errors of snow, which will be discussed in the section 3.5 of this thesis. As suggested by Dong and Menzel (2016a), the underestimation error of snow is difficult to reduce because it is spatial information loss while the overestimated snow can be rejected as redundant information in assistance with meteorological data. For this reason, the following meteorological correction was utilized to reduce the misclassified snow pixels on MODIS snow data.

### 3.3.5 Meteorological Correction

Among the measurements of environmental variables at meteorological stations, precipitation (P) and air temperature (T) are important reference information for snow occurrence, and snow depth (SD) is direct indication of snow cover presence. Thus, the

above three meteorological data were selected to generate snow cover filters. Precipitation and air temperature were combined to produce PT filters as described in Table 3.1. Snow depth was used to produce SD filters as shown in Table 3.2. All the in situ precipitation, air temperature and snow depth data were firstly interpolated to grids using ordinary Kriging. Topographical correction was carried out to improve the temperature grids in assistance with DEM and daily temperature gradient derived from meteorological observations. The topographical correction acted as a scale transformation step for converting point-based temperature data to areal scale. The detailed correction procedure has been introduced by Dong and Menzel (2016a). Due to the complex spatial patterns of precipitation and snow depth in the heterogeneous terrains, the upscaling of the two variables were not involved in this study. Finally meteorological composite (MC) filters were computed by adding PT filters and SD filters.

PT (or SD) filter = 2 means the ground surface has high possibility of being covered by snow, while PT (or SD) filter = 1 and = 0 indicate the possibilities of snow observations on MODIS data are medium and low, respectively. However, there are some differences between PT and SD filters, i.e., the former indicating the possibility of fresh snow while the latter demonstrating the possibility of remained snow cover over a region. After PT filter and SD filter being added together, the generated MC filter ranges between 0 and 4, which combines the possibility of fresh and old snow cover. Then, the snow pixels were reclassified to land when MC filters  $\leq 1$ . Thus, the detrimental impact on detection of snow cover over mountainous areas in spring and summer can be avoided, i.e., the residual snow cover before ablation at high elevations was reserved on the MODIS snow maps. This step showed high performance in removing the misclassified snow and improving the data quality of MODIS snow cover products.

**Table 3.1** Criterion of PT filters.

	$T < 0\text{ }^{\circ}\text{C}$	$0\text{ }^{\circ}\text{C} \leq T < 3\text{ }^{\circ}\text{C}$	$T > 3\text{ }^{\circ}\text{C}$
$P > 2\text{ mm}$	2	1	0
$P \leq 2\text{ mm}$	0	0	0

**Table 3.2** Criterion of SD filters.

$SD \geq 3\text{ cm}$	$0\text{ cm} < SD \leq 3\text{ cm}$	$SD = 0\text{ cm}$
2	1	0

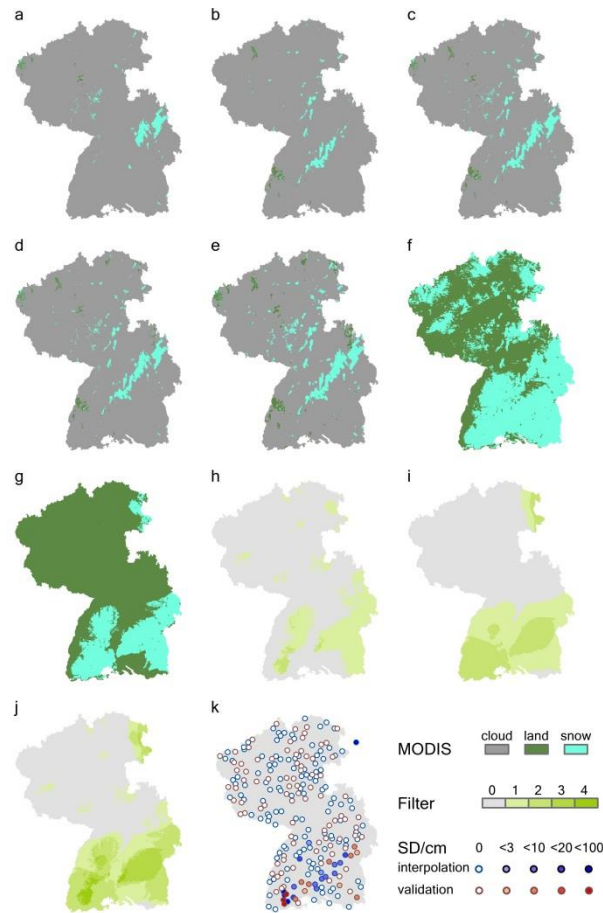


**Figure 3.3** Snow and cloud cover maps of original MODIS images and after implementation of the five steps (a-g), meteorological filters (h-j) and in situ snow depth measurements (k) for 9 January 2012. (a) original MODIS Aqua; (b) original MODIS Terra; (c) after step I; (d) after step II; (e) after step III; (f) after step IV; (g) after step V; (h) PT filter; (i) SD filter; (j) MC filter; (k) snow depth data from both the stations for meteorological interpolation (blue) and validation (red).

## 3.4 Results

### 3.4.1 Reduction of cloud contamination

The above presented step I-IV can contribute to cloud removal of MODIS snow data. Figure 3.3 shows an example of the original MODIS Aqua and Terra snow images and those improved by individual steps on 9 January 2012 in southwestern Germany. It is suggested that the original MODIS data have very high cloud fractions, but all the cloud pixels have been removed from step I to step IV, and step IV played a crucial

role in the cloud-gap-filling. It also demonstrates that heavily cloudy weather can continue for several days in winters in the study area, which limits the efficiency of Aqua/Terra combination (step I), temporal combination (step II) and spatial combination (step III) in eliminating cloud contamination of MODIS data. It can be inferred that even extending the temporal and spatial windows in step II and III cannot achieve an apparent effect.

Figure 3.4 illustrates the monthly variations of cloud coverage of the original MODIS data and those after step I-III. It indicates that Terra images were prone to have less cloud obstruction than Aqua images. Temporal combination (step II) and spatial combination (step III) showed lower performance in removing cloud pixels in winter half-year (October to March) than in summer half-year (April to September), which was led by the long persistence of cloudy weather conditions during the snow season. Accordingly, meteorological interpolation (step IV) has more value than the previous steps in reducing cloud contamination of MODIS snow products during the snow season, and all the residual cloud pixels can be removed after step IV.

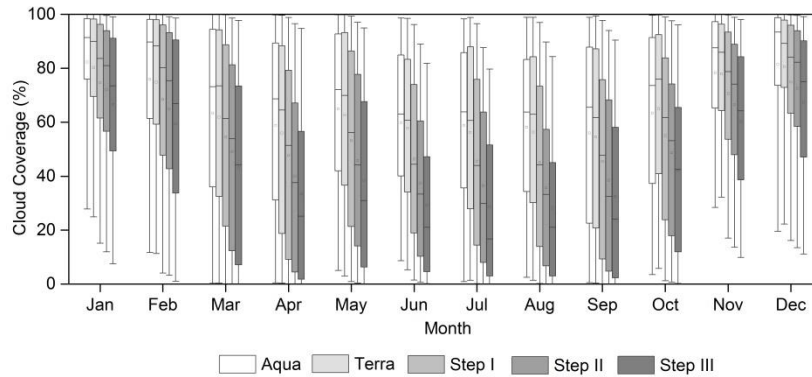


**Figure 3.4** Monthly medians and Inter Quartile Range (IQR) of cloud coverage of the original MODIS Aqua and Terra images and after implementation of the first three steps. The remained cloud cover was completely removed in step IV.

### 3.4.2 Improvement of snow cover mapping

Improving the snow representation of MODIS data consists of two objectives, i.e., retrieval of omitted snow pixels and rejection of false snow. Figure 3.3a-f demonstrate that the snow cover obstructed by cloud was reconstructed step by step. It also suggests that available information from MODIS snow data themselves is relatively limited during heavily cloudy days (Figure 3.3c-e). However, meteorological observations showed high potential in repairing the incomplete remotely sensed snow data (Figure 3.3f); nevertheless, some misclassified snow pixels were also mixed into the snow maps in the process of meteorological interpolation. The last step of

meteorological correction (Figure 3.3g) was utilized to eliminate both the newly generated and originally existed false snow. Figure 3.3h-j show the PT filter, SD filter and MC filter used in this step, respectively. The environmental information of precipitation, air temperature and snow depth were examined to correct the remotely sensed snow maps. Figure 3.3k illustrates the in situ snow depth measurements and suggests that the final MODIS snow cover map (Figure 3.3g) had high consistency with the ground observations.

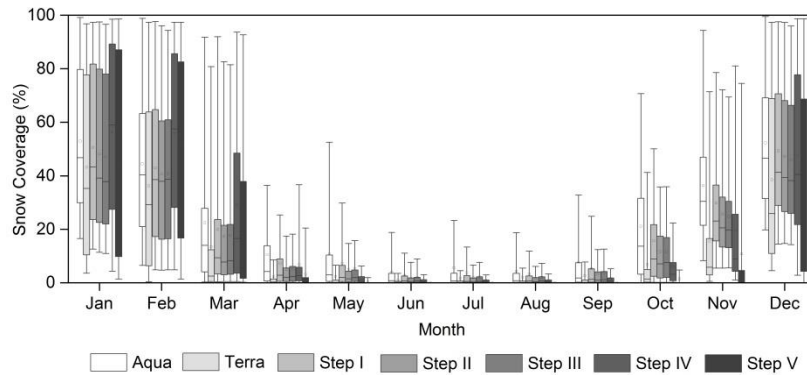


**Figure 3.5** Monthly medians and Inter Quartile Range (IQR) of snow coverage of the original MODIS Aqua and Terra images and after implementation of the five steps.

The monthly snow coverage of the original MODIS Aqua and Terra images and after implementation of the five individual steps is shown in Figure 3.5. MODIS Aqua data present higher snow fractions as compared with Terra data. The snow coverage did not vary remarkably in the processes of Aqua/Terra combination (step I), temporal combination (step II) and spatial combination (step III). Meteorological interpolation (step IV) considerably increased the snow coverage during the snow season (December to March) and reduced it during the non-snow season (April to November), which means even though step IV caused more commission errors of snow in winter, but it also lessened the commission errors in the other seasons. Besides, Figure 3.5 suggests that meteorological correction (step V) reduced the snow coverage of the snow maps again, indicating the decline of overestimation errors of snow, and the false snow during non-snow season (April to October) was nearly rejected completely.

Figure 3.6 shows the daily time series of snow coverage derived from both the combined Aqua/Terra images and the final snow maps after the five-step procedure, as well as the mean snow depth observed by all the in situ stations in the period 2002-2015 over southwestern Germany. Figure 3.6a indicates that the original MODIS snow maps significantly overestimated the snow cover in southwest Germany, especially at the beginning and end of the snow seasons. Figure 3.6b and 3.6c illustrate that the

snow coverage derived from the final MODIS snow products possessed higher concordance with the snow depth observations, which shows more clearly in those winters that had two snowfall peaks, such as 2006/2007, 2007/2008, 2012/2013 and 2013/2014.

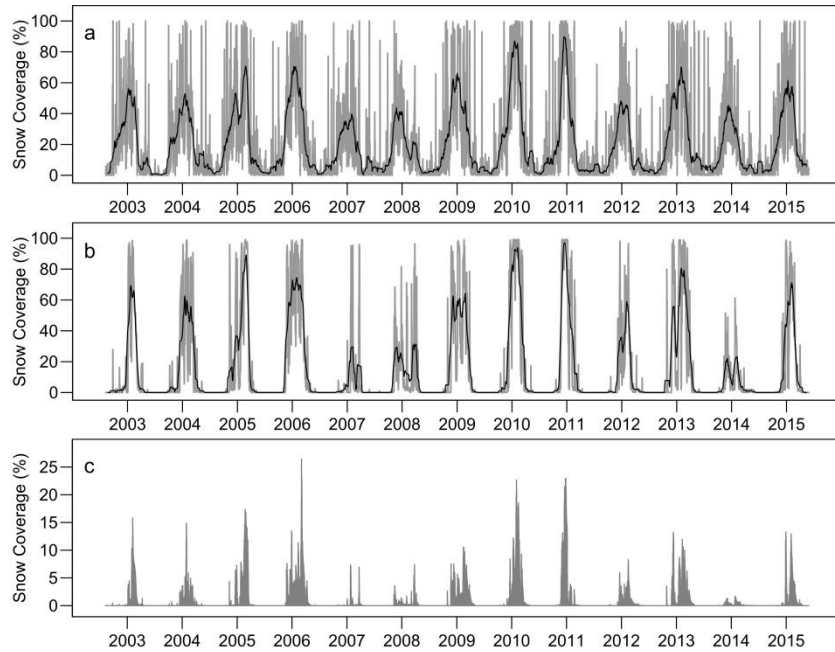


**Figure 3.6** Temporal variation in snow coverage and snow depth over southwestern Germany during 2002-2015. (a) snow cover of the combined Aqua-Terra products (step I); (b) snow cover after step V; (c) daily mean snow depth calculated from observations at all the 242 snow stations (see Figure 3.1 for station locations). The grey lines in (a) and (b) indicate the daily values while the black lines depict the 31-day moving average.

**Table 3.3** Confusion matrix comparing observed snow depth with MODIS snow cover.

		Observed Snow Depth	
		Snow ( $\geq 3$ cm)	No Snow ( $< 3$ cm)
MODIS	Snow	a	b
	Land (snow free)	c	d

### 3.5 Validation

To evaluate the accuracy and errors of the original and improved MODIS snow cover products, the validation indices recommended by Wilks (2006) were employed, which are defined based on the confusion matrix given in Table 3.3.

The four types of validation results mean  $a$  = number of hits,  $b$  = number of false alarms,  $c$  = number of misses,  $d$  = number of correct rejections. This study again select 3 cm as the snow depth threshold to determine whether a station is covered by snow, as the same threshold as used in meteorological interpolation (step IV). The five evaluation indicators are calculated as follows (Wilks, 2006):

$$PC = \frac{a + d}{a + b + c + d}, \quad (3.8)$$

$$TS = \frac{a}{a + b + c}, \quad (3.9)$$

$$B = \frac{a + b}{a + c}, \quad (3.10)$$

$$FAR = \frac{b}{a + b}, \quad (3.11)$$

$$H = \frac{a}{a + c}. \quad (3.12)$$

where  $PC$  is the proportion correct, representing the overall accuracy of MODIS in mapping the extent of snow cover and land;  $TS$  is the threat score, which is an alternative to  $PC$  when the event to be forecast (i.e., snow in this study) occurs substantially less frequently than the nonoccurrence (i.e., snow-free in this study);  $B$  is the bias, indicating the ratio of MODIS observed snow events to those recorded by the stations.  $FAR$  is called the false alarm ratio, which shows the proportion of overestimated snow events among all the MODIS snow observations.  $H$  is the hit rate, which means the proportion of MODIS observed snow events among all the snow events recorded by the in situ stations. Accordingly, an absolutely accurate estimator of MODIS data will achieve  $PC = 1$  ( $b = c = 0$ ),  $TS = 1$  ( $b = c = 0$ ),  $B = 1$  ( $b = c = 0$ ),  $FAR = 0$  ( $b = 0$ ), and  $H = 1$  ( $c = 0$ ); conversely, an entirely inaccurate observation of MODIS will show  $PC = 0$  ( $a = d = 0$ ),  $TS = 0$  ( $a = 0$ ),  $B = 0$  ( $a = b = 0$ ) or  $\infty$  ( $a = c = 0$ ),  $FAR = 1$  ( $a = 0$ ), and  $H = 0$  ( $a = 0$ ). Since there are many differences between remote sensing and ground-based snow measurements, complete concordance between the two snow data sets is impossible. MODIS snow products are areal data while station measurements are point data, and they have different observation time that may result in data disagreement because of temporary snowpack during the warm winters of the study

area. However, the five indices can provide some information about the relative data quality of the snow maps to be assessed against in situ snow observations.

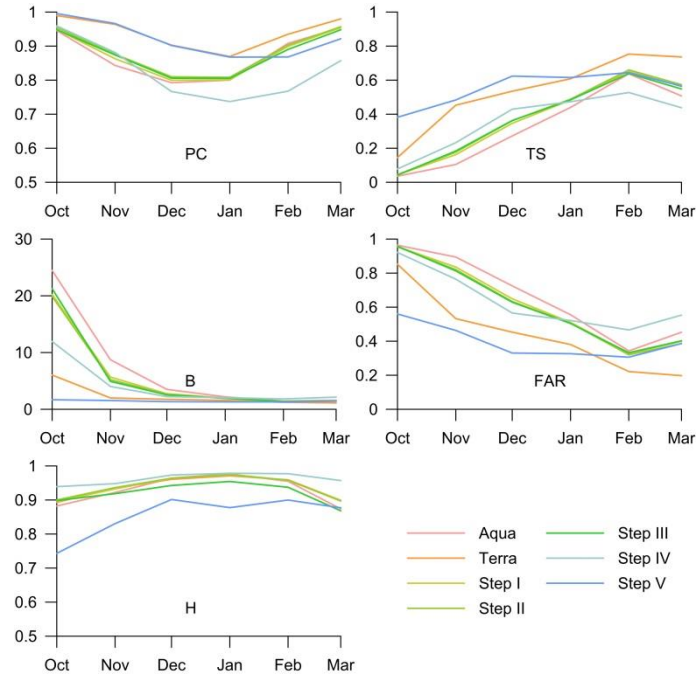


**Figure 3.7** Validation indices for the original MODIS snow cover images and individual results after the five processing steps during the snow season of the period 2002-2015.

Figure 3.7 presents the monthly variation of the five evaluation indicators for the original MODIS snow maps and after the five individual steps. It suggests that MODIS Terra data performed better than Aqua data, i.e., Terra data had higher *PC*, *TS* and *H*, lower *FAR* and bias (*B* close to 1). It might be caused by that MODIS band 7 instead of band 6 was used to calculate the normalized difference snow index (NDSI) and thus execute the snow classification of Aqua data, because the Aqua MODIS instrument shows mostly non-functional detectors in band 6. However, MODIS snow product Collection 6 developed by Hall et al. (2010) will be available in a short time, in which the algorithm for processing Aqua images has been updated and shows the same accuracy as Terra snow data. The validation indices of the snow images after step I-III varied close to those of Aqua data, indicating the snow mapping errors of Aqua data were transmitted to the followed snow images after the combination of Aqua/Terra data. After meteorological interpolation (step IV), the overall accuracy (*PC*) further declined; the indices of *TS* and *FAR* became better (increased *TS* and decreased *FAR*) in the first half of the snow season (October to December), but worse in the latter half of the snow season (January to March). At the same time, the bias (*B*) and hit rate (*H*)

for the snow maps after step IV were improved (decreased  $B$  and increased  $H$ ) substantially, compared to previous steps. Moreover, the hit rate ( $H$ ) rose to the maximum (close to 1) among all the snow maps, indicating the lowest underestimation errors of snow. The last step, meteorological correction redressed the overestimation errors generated in step IV, i.e.,  $TS$  increased and  $FAR$  decreased significantly, and derived higher overall accuracy ( $PC$ ) of about 92% during the snow season. In contrast, the original MODIS Aqua and Terra data showed overall accuracy of 87% and 94% respectively during the cloud-free days of the snow season (Figure 3.7). The annual mean overall accuracy ( $PC$ ) of the snow maps after step V achieved 96%, compared to 93% and 97% for original Aqua and Terra images. Besides, the snow mapping bias ( $B$ ) of the final snow cover images dropped to the minimum level (close to 1) after step V; nevertheless the hit rate ( $H$ ) also declined obviously, especially in October and November. The decline of  $H$  might be led by the rigorous rejections of meteorological composite filters, i.e., some real snow pixels were removed as well.

It has been tried to change the threshold of MC filters from 1 to 0, which meant only the snow pixels that have a respective MC filter = 0 were removed; then the mean hit rate ( $H$ ) of the final snow maps rose up to 0.95 during the snow season, but the mean false alarm ratio ( $FAR$ ) increased to 0.55 as well. In addition, changing the validation threshold of snow depth from 3 cm to 0 cm could reduce the mean  $FAR$  to 0.29 and the  $TS$  also had an increase, but the mean  $H$  declined to 0.76 during the snow season. Therefore, the evaluation indicators are very sensitive to the threshold adjustments of MC filter and validation snow depth. The MC filter is thus a "double-edged sword", i.e., strict meteorological filters can eliminate most of the false snow but some real snow is rejected as well, and loose filters can retain more snow covers but the commission error will increase. However, Figure 3.7 demonstrates that the validation indices of the final MODIS snow maps had an overall improvement, compared to the original images and those after step I-IV, indicating better performance in the representation of snow cover. Furthermore, the cloud cover with high fractions in the snow data was completely reclassified, resulting in cloud-free daily snow cover products, which have higher availability in hydrological applications.

The spatial distributions of the five evaluation indicators for the final MODIS snow cover products are given in Figure 3.8, showing that the high mountain regions (such as the Black Forest) have lower overall accuracy ( $PC$ ) compared to the northern low elevations. The deep Rhine Valley in the center has lowest  $TS$  values, indicating relatively inferior performance in recording snow cover. The Black Forest in the southwest has greater values of  $B$ ,  $FAR$  and  $H$ , meaning more snow-observation bias and overestimation errors, but lower underestimation errors. The Swabian Alb mountains in the southeast and the adjacent regions have high threat score ( $TS$ ), low bias ( $B$ ) and false alarm ratio ( $FAR$ ), and relatively high hit rate ( $H$ ), becoming the

region where MODIS achieved the best observations in this study area. The northern part of this region has more spatial heterogeneity in the five validation indices because of the complex terrains and the high variability of snow.

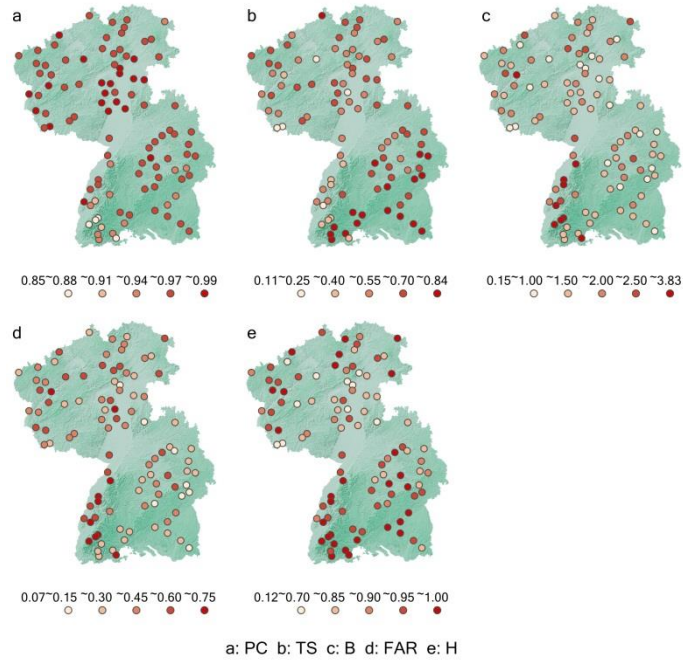


**Figure 3.8** Spatial distribution of the validation indices for the final MODIS snow maps after step V over southwestern Germany in the period 2002-2015.

### 3.6 Snow cover in southwestern Germany

After the five-step procedure, the improved MODIS snow data can be used to analyze the temporal and spatial distribution of snow cover during the period of 2002-2015 over southwestern Germany. Figure 3.9 gives the daily snow coverage variation for the snow seasons from 2002 to 2015 in this study area. It shows that the snow cover in the study region had great temporal variability with marked annual changes both in snow coverage and snowfall frequency, which is illustrated more clearly in Figure 3.6b-c. For example, the winters of 2007/2008 and 2013/2014 had both low snow coverage and snow depth; the winters of 2003/2004 and 2008/2009 had high snow coverage but low snow depth; the winters of 2005/2006 and 2009/2010 had both high snow coverage and snow depth; though the winters of 2005/2006 and 2010/2011 both had high snow coverage and snow depth, but they had very different snow duration.

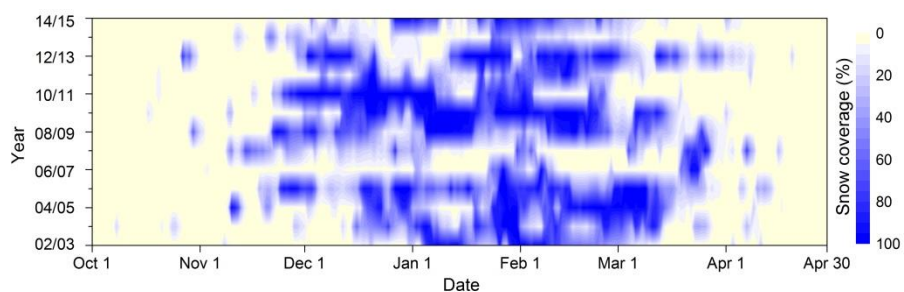


**Figure 3.9** Temporal variation of the snow coverage derived from the final MODIS snow-cover time series after step V over southwestern Germany in the period 2002-2015.

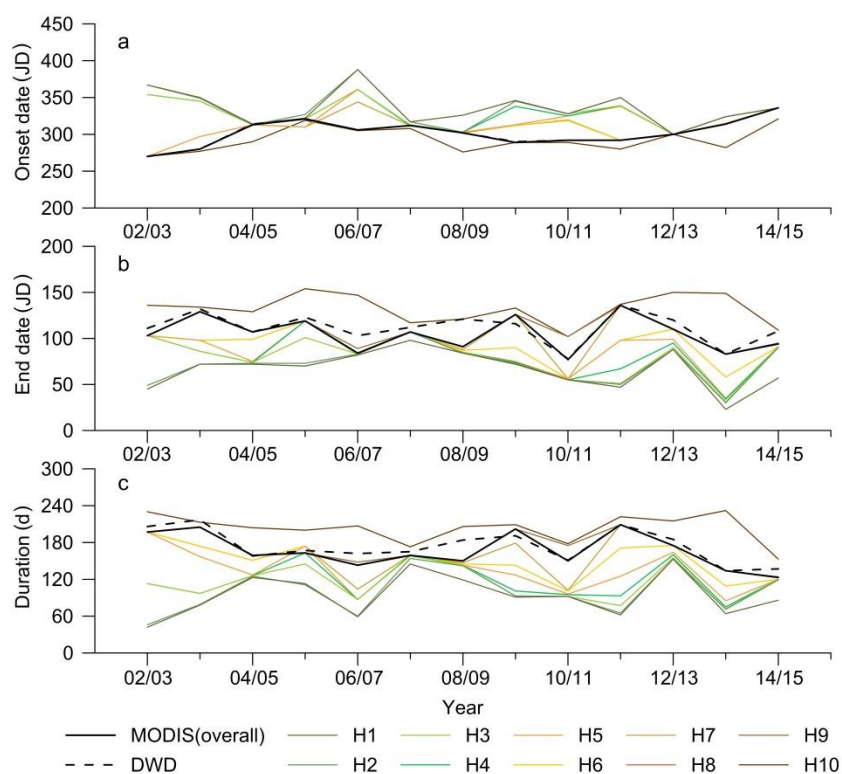


**Figure 3.10** Snow onset dates (a), end dates (b) and duration days (c) derived from the whole MODIS snow maps after step V and at 10 elevation zones and from DWD snow depth observations over southwestern Germany in the period 2002-2015. Onset and end dates are given in Julian date. The information of the elevation zones labeled H1-H10 is shown in Table 3.4.

Besides the quantitative parameters (snow coverage, snow depth, snow water equivalent) of snowpack, the periodical characteristics, such as onset date, end date and snow duration, are also important to decipher the temporal variation of snow.

Figure 3.9 suggests that the continuous snowfall period during the past 13 snow seasons had the trend of moving forward, i.e., shifting from mid-December through mid-March before 2006, to early December through early March after 2007, though the trend was not significant. Figure 3.10 shows the snow onset and end date as well as snow duration derived from the improved MODIS snow maps and in situ stations during the period of 2002-2015, and the parameters at the ten elevation zones (Table 3.4) are also plotted. Snow onset date was prone to move backward during the past 13 winters, i.e., snowfall occurred later. The snow end date and duration of the whole study region did not present apparent trends, but larger variation ranges than snow onset date. However, Figure 3.10b and c illustrate that snow end date at low elevations (H1, H2, 10-222 m a.s.l.) had a backward trend before 2008 and a forward trend after then, and meanwhile the respective snow duration was increasing before 2008 and decreased afterwards. Comparing the snow periodical parameters derived from the final MODIS snow data and the ground observations, they have high consistency with each other except for some disagreement for snow end date and duration (Figure 3.10). The reason is that snowfall usually occurs suddenly over large scales at the beginning of a snow season, marking the snow onset in a region, while the snow retreat always continues for a long time, leading to great snow cover heterogeneity at different elevation zones. Therefore, the snow end date and duration statistics from various elevations and multi data sources generally have more inconsistency (Figure 3.10b-c).

**Table 3.4** Parameters of the ten elevation zones.

Elevation Zones	Elevation Range (m)	Mean Elevation (m)	Median Elevation (m)	Area (km <sup>2</sup> )
H1	10 - 148	114	114	7106
H2	149 - 222	187	189	7191
H3	223 - 277	251	251	7181
H4	278 - 324	301	301	7077
H5	325 - 373	348	348	7131
H6	374 - 428	401	401	7055
H7	429 - 485	457	456	7104
H8	486 - 569	523	521	7036
H9	570 - 688	627	626	7016
H10	689 - 1491	813	778	7010

Figure 3.11 demonstrates the monthly maps of the snow occurrence days during the past 13 winters derived from the final MODIS snow cover products, indicating the frequency of snow presence in individual winter months and at different elevations. February is shown to have the maximum snow occurrence, with more than 200 days in

sum covered by snow in the southern part (the Black Forest and the Swabian Alb) of the study area. However, the south Black Forest had the most snow events in January, with the largest area having more than 300 snow days. December and March had many snow occurrences (120-300 days) as well, but mostly concentrated in the Black Forest and a limited region of the Swabian Alb. There were only scarce snow events from October to November, with less than 120 days having snow records even in the high mountains, and most of the regions only observed less than 20 snow days in the two months over the past 13 years. The warm Rhine Valley is suggested to have the fewest snow presence through the whole winter. The northern part of the southwestern Germany has obviously less snow covered days than the south, and the lower elevations might be the main reason.

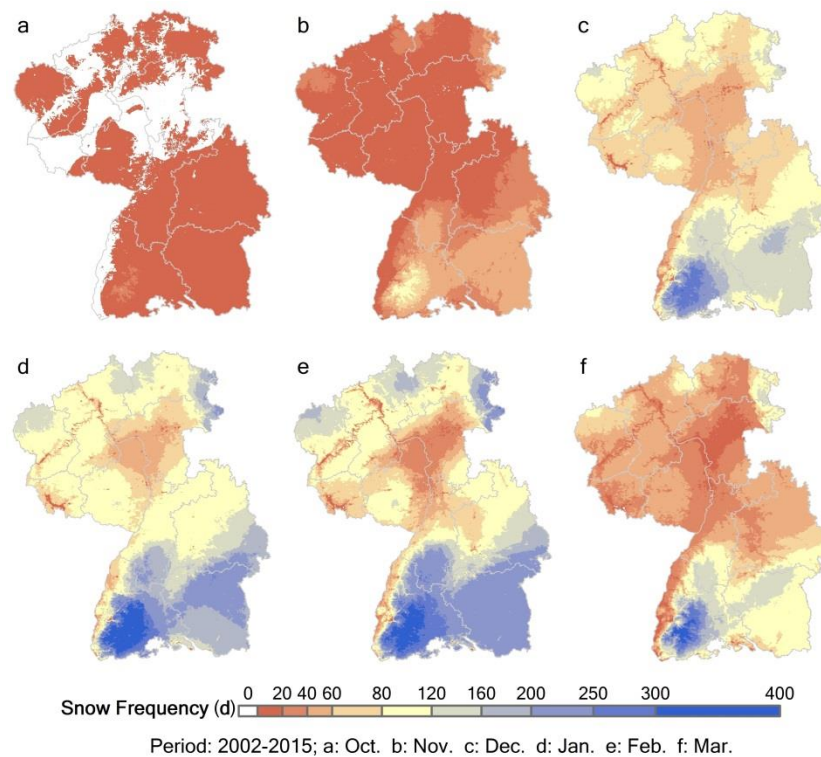


**Figure 3.11** The overall monthly snow occurrence days during the snow season derived from the final MODIS snow cover images after step V over southwestern Germany in the period 2002-2015.

### 3.7 Discussion and conclusions

Based on previous studies, this chapter has developed a five-step procedure to improve the snow cover representation of MODIS data. This study aimed at the three major issues of MODIS snow cover products, i.e., cloud obscuration, underestimation

as well as overestimation of snow. Among the proposed five processing steps, Aqua/Terra combination (step I), temporal combination (step II), spatial combination (step III) and meteorological interpolation (step IV) contributed to the cloud reduction, and meteorological interpolation showed the highest efficiency and reclassified all the remained cloud pixels. At the same time, step I to IV were utilized to retrieve cloud obstructed snow as well, and step IV (meteorological interpolation) again played the crucial role to reduce the omission error of snow by reclassifying the cloud pixels with high fractions in MODIS data. However, significantly overestimated snow was found in original MODIS snow products, and some false snow was also generated during step I-IV. Thus, step V (meteorological correction) was employed to reject the misclassified snow, which showed superior performance in achieving this objective.

To evaluate the accuracy and errors of the snow maps after individual steps and the original MODIS snow cover products, five indices were applied in this study to validate the snow maps against in situ observations. Compared to the original MODIS snow data and those after implementation of the first four steps, the final snow maps showed obvious improvement in the overall accuracy (*PC*), snow detection accuracy (*TS*), observation bias (*B*) and overestimation (*FAR*), at the expense of slightly increased underestimation (*H*). Since the snow images after step IV had the lowest underestimation error (highest *H*), the relatively rigorous meteorological filters used in step V might reject some real snow pixels. However, liberal filters can retain more misclassified snow, and thus increase the overestimation error. Therefore, the threshold of meteorological filters should be determined carefully in accordance with specific environments.

The validation suggested there was some disagreement between the MODIS snow cover products and ground observations. Though the observation errors of MODIS data can partially cause the data inconsistency, the essential distinction between remote sensing and ground measurements is also an important reason. Firstly, the two data sources have distinct observation time, i.e., MODIS sensors (installed on Aqua and Terra, respectively) collect images twice a day while snow depth is measured once a day by a meteorological station. As the temporary snow cover melts quickly in the regions where the winters have relatively high temperature, the time shifts between the two snow measurement techniques result in divergence of observations, and the mixed precipitation (rain and snow) will exacerbate this situation. Secondly, the different observation range between MODIS and snow stations can also lead to data disagreement. Ground observations have high accuracy on point scale, but each station only represents the snow conditions in a very limited area. Moreover, most of the meteorological stations are located at cities, i.e., the observations are largely influenced by human activities. However, each MODIS pixel aggregates the spectral features over

a region of  $500 \times 500$  m. Thus, remote sensing data have higher accuracy on large scales.

Even though remotely sensed snow data have apparent advantages compared to in situ observations in large-scale hydrological studies, the accuracy and integrity of the former are weakened by the weather conditions (e.g., cloud) and imperfect global classification algorithm, and thus the respective improvements are required at regional scales. This study is an attempt to improve the accuracy and integrity of MODIS snow information in accordance with meteorological observations, e.g., the meteorological interpolation (step IV) and meteorological correction (step V) utilized the ground observations of precipitation, air temperature and snow depth. The meteorological interpolation obviously improved the integrity (reclassifying cloud) of MODIS data while the meteorological correction (rejecting false snow) significantly increased the accuracy, both of which showed high performance. However, data accuracy may be decreased sometimes in pursuit of data integrity. For instance, the combination of meteorological interpolation and meteorological correction in this study largely increased the integrity and reduced the overestimation error of MODIS snow data, but the strict meteorological composite filters slightly increased the underestimation error. Since the accuracy and integrity are both important properties for a data set, it is valuable to greatly improve the data integrity at the expense of a little accuracy. Therefore, the fusion of meteorological and remotely sensed snow data is a useful option to enhance the availability of MODIS snow products both on spatial and temporal scales.

Gafurov et al. (2015) reconstructed the snow cover in a data-sparse basin of Central Asia using conditional probability interpolation based on in situ observations and MODIS snow data; even though the interpolated snow maps showed lower accuracy (83-86%) than original MODIS snow products (92%), this study provided a novel approach to combine in situ and remotely sensed snow observations. Based on their idea, this study attempted to only interpolate the cloud obscured snow on MODIS snow images with ground-based snow measurements, and a set of meteorological filters were employed to correct the snow overestimation. Finally, the updated cloud-free MODIS snow cover products achieved equivalent accuracy as the original MODIS snow data and lower overestimation errors. Liang et al. (2008b) produced cloud-free snow maps by combining MODIS snow cover images and AMSR-E snow water equivalent data in north Xinjiang in China, which showed the snow accuracy of 75%, compared to 34% of original MODIS Terra data. Gao et al. (2010) conducted a similar study in Alaska, USA, which suggested the snow accuracy increased from 31% (MODIS Aqua) and 45% (MODIS Terra) to 86% (combined MODIS and AMSR-E). Both the two above researches present great significance in integrating the advantages of the high spatial resolution of optical data (MODIS) and cloud transparency of passive

microwave data (AMSR-E) (Liang et al. 2008b; Gao et al. 2010). However, they did not pay attention to reducing the overestimation errors of the combined snow cover products; otherwise the accuracy can be further improved. Thus, it is valuable to firstly reclassify the cloud pixels of MODIS snow products according to microwave snow data and then to reject the misclassified snow pixels on the snow maps based on in situ snow observations in the future work, which provides another approach to generate new cloud-free snow cover maps with high quality. In addition, analyzing the sensitivity of the accuracy and errors of the improved MODIS snow data in response to the thresholds of the meteorological filters in different terrains and climate regions is another work which will be conducted in the future.

## Chapter 4

### Simulation of snow cover with TRAIN model

#### 4.1 Introduction

Snow interacts strongly with the global climate system, both influencing and forming as a result of this system (Pomeroy and Brun, 2001). Snow researches in mountain regions attract more attention (e.g. Andreadis et al., 2009; Essery et al., 2013; Molotch et al., 2009; Morán-Tejeda et al., 2013; Painter et al., 2007), not only because of the complex snow processes (e.g. canopy interception) but also the large spatial and temporal variability of snow cover in the heterogeneous terrains. Due to the sparse monitoring network in mountainous areas, hydrological modeling and remote sensing provide more options on this research issue. The relatively short-term observation periods of satellite imagery limit the availability of remote sensing technique in snow studies. Hydrological models are thus frequently utilized to investigate snow processes and the snow cover variations both in spatial and temporal dimensions (e.g. Grusson et al., 2015; Molotch, 2009; Musselman et al., 2012; Pomeroy et al., 1998; Shamir and Georgakakos, 2006), as well as the links between snowpack and climate change (e.g. Brown and Mote, 2009; Brutel-Vuilmet et al., 2013; McCabe and Wolock, 2010).

An intensely warming trend has become the most notable characteristic of the climate change both on the global and regional scales, while the precipitation trends are more complicated in different regions of the globe. As snow cover essentially has high sensitivity to changes in air temperature and precipitation, it is of great significance to detect the trends of snow cover under a changing climate and to decipher the relationship between snow and environmental variables, especially in mountain regions where snow related disasters (e.g. flood and drought) frequently occur. For this purpose, using a hydrological model to simulate the long-term change of snow cover is more appropriate than the other techniques. In this study, a distributed hydrological model TRAIN (Menzel et al., 2009; Wimmer et al., 2009) was applied to simulate the snow water equivalent variation in a central European low mountain region (Rhineland-Palatinate, Germany) during the past decades.

Since there are still a large number of uncertainties existed both in the structures and the observation data which are used as model input, employing hydrological models to estimate snow cover properties at a regional scale, particularly snow water

equivalent (SWE), but also snow covered area (SCA), remains a challenge (Dressler et al., 2006). Therefore, as a kind of areal snow observations, remotely sensed snow cover maps are useful in validating and calibrating snow hydrological models. Parajka and Blöschl (2008b) utilized MODIS snow cover products to calibrate a conceptual hydrological model, and it was suggested that the simulations of snow cover and runoff were both improved to some extent, with the snow cover overestimation and underestimation errors decreased from 7.1% to 5.6% and from 4.7% to 4.1% respectively, and the runoff model efficiency increased slightly from 0.67 to 0.70. Andreadis and Lettenmaier (2006) used an ensemble Kalman filter (EnKF) to assimilate remotely sensed MODIS SCA and AMSR-E SWE products into the variable infiltration capacity (VIC) macroscale hydrologic model, and it was concluded that the predictions of snow cover extent showed better agreement with ground measurements while the SWE simulations were not encouraging because of the large errors in the AMSR-E SWE product. Molotch and Margulis (2008) combined the SCA data from multi-sensors (Landsat ETM+, MODIS and AVHRR) into a spatially distributed snowmelt model to reconstruct SWE, but the model performance deteriorated when MODIS and AVHRR SCA data were used, and they emphasized the significance of reducing the errors of remotely sensed snow data prior to applying them in hydrological modeling. As compared to other remotely sensed snow observations (e.g. NOAA AVHRR and Landsat TM/ETM+), MODIS snow products have obvious advantages in reconciling spatial resolution (500 m) and temporal resolution (daily), and thus they are more appropriate to be used for validating and calibrating snow simulations. However, the availability of MODIS snow data is restrained by the high cloud fractions and misclassification errors. In consequence, improving the data quality of MODIS snow cover products is of great significance, otherwise the snow mapping errors and the cloud blockage would interfere with their applications in hydrological simulations. In chapter 3 (Dong and Menzel, 2016b), snow depth measurements were used to interpolate the cloud gaps of daily MODIS snow data, and a meteorological composite filter which combines ground-based temperature, precipitation and snow depth was involved in the removal of false snow; finally, more accurate and cloud-free MODIS daily snow cover products were generated using this method. In this study, the improve MODIS daily snow cover maps were employed to evaluate the snow cover simulations by TRAIN model.

This chapter is organized as follows. The data section introduces the applied MODIS snow cover products as well as the climatic and hydrologic data used in this study. The method section provides an overview of the study area, the TRAIN model, model evaluation indices and the approaches for analyzing the trends and relations of the environmental variables. Then the simulations of snow cover were presented in the result section. Finally, the snow cover trends and the relations with air temperature

and precipitation during the period 1961-2008 in Rhineland-Palatinate were demonstrated. This chapter concludes with discussion on the significance of improving the data quality of satellite-based snow records prior to using them for hydrological modeling purpose.

## **4.2 Data**

### **4.2.1 MODIS snow cover products**

MODIS snow cover products (Hall et al., 2002; Hall and Riggs, 2007) have been widely used for hydrological, climatological and modeling applications (e.g., Déry et al., 2005; Gillan et al., 2010; Hall et al., 2012; Kostadinov and Lookingbill, 2015). The daily MODIS snow cover products (MOD10A1 and MYD10A1, Collection 5) (Riggs et al., 2006) during the period of 1 September 2002 to 31 December 2008 were used in this study. The two tiles of h18v03 and h18v04 were combined to cover the study region Rhineland-Palatinate in southwestern Germany. Thus a total of 4592 daily MODIS snow cover maps were downloaded from the NASA's Earth Observing System Data and Information System (NASA/EOSDIS, <https://earthdata.nasa.gov>). The preprocessing procedures such as the format conversion (HDF to GeoTIFF), image-mosaic (h18v03 and h18v04) and reprojection (Sinusoidal to WGS84-UTM) were conducted using the MODIS Reprojection Tool (MRT).

Since the MODIS snow data in the study area have severe cloud obstructions, all the daily MODIS snow cover maps were firstly improved with a cloud reclassification algorithm, which has been presented in chapter 3 in detail. This algorithm consists of five processing steps, i.e., Aqua/Terra combination, temporal combination, spatial combination, meteorological interpolation and meteorological correction. The kernel procedure of this algorithm is reclassifying the cloud pixels in accordance with ground-based snow measurements using conditional probability interpolation. Moreover, the meteorologic observations, such as precipitation, air temperature and snow depth, are utilized to generate filters for removing the overestimated snow on MODIS snow cover images. The updated cloud-free snow cover products showed significantly higher performance than the original MODIS data (Dong and Menzel, 2016b), which are more appropriate to be used for evaluating the snow simulations by TRAIN model.

### **4.2.2 Climatic and hydrologic data**

The climatic and hydrologic data were applied for three purposes in this study. Firstly, the daily gridded data sets of precipitation, radiation, air temperature, relative humidity, and wind speed during the period of 1 January 1961 to 31 December 2008

were used to drive the hydrological model TRAIN for snow simulations. The data grids (1 km × 1 km) were interpolated using the Kriging method (Hinterding, 2003), and were provided by LUWG, the state agency for the environment and water management in Rhineland-Palatinate. Secondly, precipitation, air temperature and snow depth observations from the meteorological stations were used to produce the improved cloud-free MODIS snow cover maps. The daily time series of precipitation at 144 stations, air temperature at 58 stations and snow depth at 60 stations in Rhineland-Palatinate for the period from 1 September 2002 to 31 December 2008 were derived from the website of the German Weather Service (DWD, [www.dwd.de](http://www.dwd.de)). Thirdly, the gridded monthly air temperature and precipitation data (1 km × 1 km) from January 1961 to December 2008 were also downloaded from the DWD website, which were then used to analyze the climate change background of the snow cover dynamics during the past decades.

## 4.3 Method

### 4.3.1 Study area

This study was also conducted in Rhineland-Palatinate (Figure 4.1, 49.0-51.0° N, 6.1-8.5° E). Detailed information about the study area is presented in section 2.2 of chapter 2.

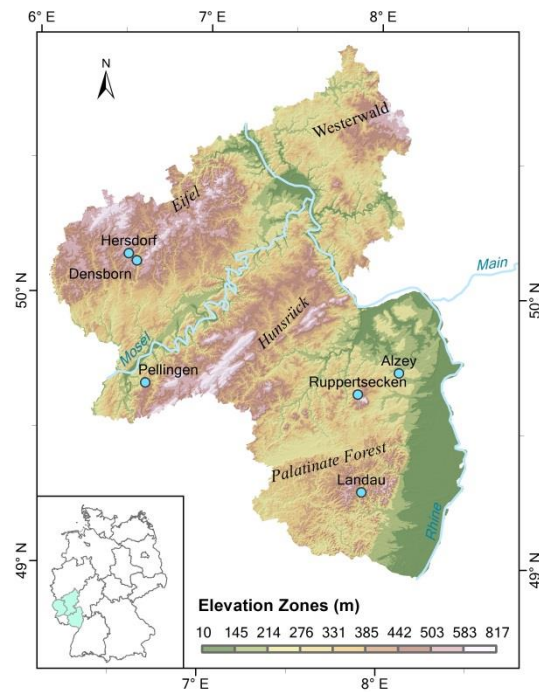


**Figure 4.1** Topography of the study region Rhineland-Palatinate in southwestern Germany. Blue dots shows six snow measurement stations.

### 4.3.2 Hydrological Model

The TRAIN model is a distributed physically-based hydrological model, which has a snow module for the simulations of snow water equivalent (SWE) and snow interception (Menzel et al., 2009). TRAIN is a one-dimensional model that can simulate the water-energy balance at the interface of soil, vegetation and atmosphere with a spatial resolution of 1 km × 1 km (Wimmer et al., 2009). It has been utilized to simulate the water balance or project the hydrological responses to different climate change scenarios in various climatic zones and terrains, e.g. Germany (Menzel, 1999), Switzerland (Menzel and Lang, 2005; Menzel, 2007), Mongolia (Wimmer et al., 2009) and the Mediterranean area (Menzel et al., 2009; Törnros and Menzel, 2014). The gridded model input includes the time series of precipitation, radiation, air temperature, relative humidity, and wind speed as well as the information regarding land use and soil parameters. Snow water equivalent is modeled as a fraction of total precipitation depending on air temperature. An upper threshold and lower threshold of air temperature are used to determine complete rainfalls and snowfalls, while the fraction of snowfall decreases linearly in between (Wimmer et al., 2009). The processes of snowmelt and sublimation are quantified by the degree-day approach (Dyck and Peschke, 1995) and the Penman-Monteith equation (Monteith, 1965). The detailed descriptions of the model structure and parameterization of the snow module have been presented by Menzel and Lang (2005) and Wimmer et al. (2009).

As the snow conditions derived from TRAIN model are snow water equivalent (SWE, mm), a threshold of 2 mm was set to convert the simulations of SWE to snow cover extent, which means those grids that having more than 2 mm SWE were determined as snow covered and the others were snow-free. Then the modeled snow cover extent by TRAIN was validated using MODIS snow cover maps.

### 4.3.3 Model evaluation

The simulated snow covered area (SCA, %) by TRAIN model was validated using four summary statistics: mean absolute error (MAE), Nash-Sutcliffe efficiency scores (NSE), Bias and correlation coefficient (R). The four evaluation indices were computed by comparing the simulated SCA (%) from TRAIN and observed SCA (%) from MODIS snow products at nine elevation zones (Figure 4.1). The calculation can be demonstrated by the following four equations (Franz and Karsten, 2013):

$$MAE = \frac{1}{T} \sum_{t=1}^T \frac{1}{N} \sum_{n=1}^N |S_{n,t} - O_{n,t}| \quad (4.1)$$

$$NSE = \frac{1}{T} \sum_{t=1}^T \left[ 1 - \frac{\sum_{n=1}^N (S_{n,t} - O_{n,t})^2}{\sum_{n=1}^N (S_{n,t} - \bar{S}_n)^2} \right] \quad (4.2)$$

$$Bias = \frac{1}{T} \sum_{t=1}^T \frac{1}{N} \sum_{n=1}^N (S_{n,t} - O_{n,t}) \quad (4.3)$$

$$R = \frac{1}{T} \sum_{t=1}^T \left[ \frac{\sum_{n=1}^N (S_{n,t} - \bar{S})(O_{n,t} - \bar{O})}{\sqrt{\sum_{n=1}^N (S_{n,t} - \bar{S})^2} \sqrt{\sum_{n=1}^N (O_{n,t} - \bar{O})^2}} \right] \quad (4.4)$$

where  $S_{n,t}$  is the simulated SCA at time step  $t$  in the elevation zone  $n$ ;  $O_{n,t}$  is the observed SCA at time step  $t$  in the elevation zone  $n$ ;  $N$  is the number of elevation zones;  $T$  is the total number of time steps. As an error index, lower MAE indicates higher capability in modeling. The NSE values between 0.5 and 1.0 suggest optimal model performance, values from 0.0 to 0.5 indicating some model accuracy, while the NSE values less than 0.0 demonstrate poor model performance. Bias values close to zero and R values close to one can be derived for favorable hydrological simulations.

In this study, the modeled and observed SCA both have a daily time step. Only the simulations during the snow season (November to April) were evaluated, otherwise the large quantity of verifications during snow-free days would indicate overestimated performance of the hydrological model. Since the improved cloud-free MODIS snow cover maps were only available from 2002 and the SWE over Rhineland-Palatinate was simulated using TRAIN for the period of 1961-2008, only the modeled SCA during the snow seasons of 2002-2008 (1 November 2002–30 April 2008) were validated.

#### 4.3.4 Trend and correlation analysis

The Mann-Kendall (MK) trend test for periodic data (Hirsch and Slack, 1984; Hirsch et al., 1982; Kendall, 1975; Mann, 1945) and Theil-Sen estimator (i.e. Sen's slope) (Gilbert, 1987; Sen, 1968) were employed in this study to detect the long-term trends of the simulated snow water equivalent (SWE) as well as the trends of air temperature (T) and precipitation (P) during the period 1961-2008. The trends of the mean daily SWE, mean T, (mean) monthly P during the snow seasons (December to March) and in the four individual months were examined with the two methods, and the values of the trend tests were represented by Kendall's tau ( $\tau$ ) coefficient and Sen's slope (S). As a nonparametric test, Mann-Kendall trend test is less sensitive to extreme values, and there is no requirement for the trend to be linear or nonlinear, while Theil-Sen estimator is an approach specifically for linear regression that chooses the median slope among all fitting lines through pairs of two-dimensional sample points (Tahir et al., 2015). However, as Yue et al. (2002) have reported, statistically significant serial

correlation frequently exists in hydrological time series, which increases the probability that the MK test detects a significant trend. Therefore, the pre-whitening method proposed by Yue et al. (2002) was followed to remove the autocorrelation of the SWE, T and P time series, prior to the Mann-Kendall trend tests and Theil-Sen slope estimates.

To analyze the relationship between SWE and the two climatic variables of T and P, the Pearson correlation (Rodgers and Nicewander, 1988), Spearman rank order correlation (Spearman, 1904) and Kendall's rank correlation (Kendall, 1975; Kendall and Gibbons, 1990) tests were conducted based on the monthly standardized anomalies of the three variables during the snow seasons (December to March) of 1961-2008. All the trends and correlation coefficients presented in this study were tested at the significance levels of 1%, 5% and 10%.

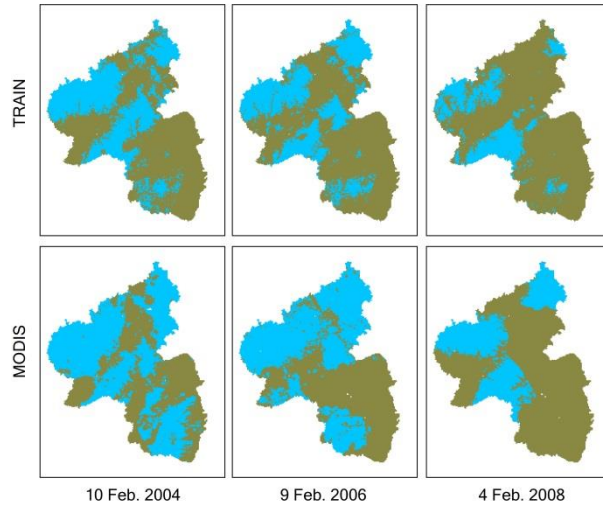
## **4.4 Results**

### **4.4.1 Simulation of snow covered area (SCA)**

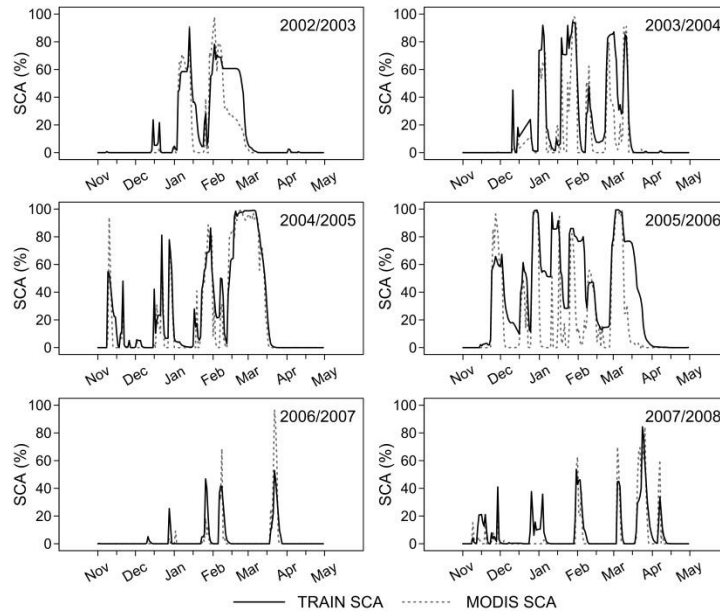
As demonstrated above in section 4.3.2, a threshold of 2 mm was applied to transform the simulated SWE by TRAIN model to snow cover extent. Figure 4.2 shows the comparisons of the modeled and observed snow cover by TRAIN and MODIS at the similar time in the winters of 2004, 2006 and 2008 in Rhineland-Palatinate. It illustrates that TRAIN model has relatively good performance in simulating the snow cover in this study area, though slight underestimation is suggested as compared to MODIS snow cover maps. Both the modeled and observed snow cover was mainly distributed in the mountainous regions, such as the Eifel Mountain in the northwest, the Hunsrück Mountain in the center and the Westerwald Mountain in the northeast.

Figure 4.3 depicts the daily time series of the simulated and observed snow covered area (SCA) by TRAIN and MODIS in the six snow seasons from 2002 to 2008. The comparisons suggest that TRAIN model could reconstruct the snow cover very well in most of the time, and the simulations had high consistency with the remotely sensed snow information from MODIS. All the recorded snowfall events during the six snow seasons were captured by TRAIN model. However, the modeled SCA was prone to be higher than MODIS SCA at the ablation phases of some snow events, e.g. February 2003 and March 2006. Raleigh et al. (2013) validated the MODIS snow cover products in a forest covered region using a ground-based monitoring network, and they concluded that MODIS data showed an underestimation bias of snow due to canopy obstruction in forests, though NDVI information has been involved into the snow mapping algorithm of MODIS snow products. About 42% of the study region is covered by forests, and this ratio is even higher in the highlands where snow more

frequently occurs. During the snow ablation phases, the intercepted snow on canopies unloads prior to the snowmelt on the ground because of the declined solar radiation in forests, but the remained snowpack under canopies is difficult to be detected by satellites. Thus, there are some uncertainties in judging whether TRAIN model has snow overestimation in the snow ablation phases. More in situ monitoring of snow processes, especially in the forest sites, is needed in the future.



**Figure 4.2** Snow cover simulations by TRAIN model and MODIS snow maps in Rhineland-Palatinate for 10 February 2004, 9 February 2006 and 4 February 2008.



**Figure 4.3** Simulated SCA by TRAIN model and observed MODIS SCA in Rhineland-Palatinate during the six snow seasons from 2002 to 2008.

To quantitatively assess the capability of TRAIN model in simulating snow cover, four evaluation indices of MAE, NSE, Bias and R as presented in section 4.3.3 were utilized to compare the simulated and observed SCA during the period 2002-2008. The four indices were calculated based on the SCA values derived from TRAIN model and MODIS snow products for each month from November to April and for the entire snow season. The results are demonstrated in Table 4.1, which indicates that the modeled SCA has overall MAE of 9.28%, NSE of 0.48, Bias of 5.92% and correlation coefficient (R) of 0.79 during the whole snow season (November to April), suggesting satisfactory performance in modeling the snow cover extent in the study area. However, the simulations from December to January showed lower accuracy as indicated by the smaller NSE values. The inconsistency between simulated and observed SCA in some snow ablation periods is an important reason. Table 4.1 illustrates that the modeled SCA has positive Bias values, especially in January and February. As discussed above, the bias might be partly led by the snow underestimation of MODIS in forest regions during the snow ablation processes.

**Table 4.1** Evaluation indices of mean absolute error (MAE), Nash-Sutcliffe efficiency scores (NSE), Bias and Correlation Coefficient (R) for simulated snow covered area (SCA) by TRAIN model verified using MODIS snow cover maps for the whole snow seasons and for individual months from November to April during the period of 2002-2008.

Month	MAE (%)	NSE	Bias (%)	R
Nov.-Apr.	9.28	0.48	5.92	0.79
Nov.	4.35	0.75	1.65	0.86
Dec.	8.05	0.26	6.13	0.86
Jan.	17.05	0.18	12.25	0.61
Feb.	15.56	0.23	10.01	0.80
Mar.	11.07	0.51	6.26	0.81
Apr.	0.67	0.94	-0.01	0.71

Besides the evaluation of snow cover simulations in temporal dimension, it is also important to know the model performance in spatial dimension. Nine elevation zones were defined in the study area according to the altitudes (Figure 4.1). Table 4.2 shows the four evaluation indices of the simulated SCA at each elevation zone, and the parameters of the nine elevation zone are also demonstrated. Table 4.2 illustrates that TRAIN model showed the best performance at the medium elevations (H4-H7) according to the higher Nash-Sutcliffe efficiency scores (NSE). MAE and Bias values suggest that the overestimation errors of modeled SCA tended to increase from medium elevations to the highlands (H5-H9). It might be partly related to the higher

underestimation error of MODIS snow products in the forest covered mountain regions. In addition, a fixed threshold of 2 mm was used in this study to convert the simulated SWE to snow covered area (SCA), which was easier to be achieved at higher elevations where snow accumulated more. Therefore, the relatively smaller SWE threshold for determining snow cover extent in the mountainous regions might be another reason for the positive Bias of modeled SCA at high elevations (e.g. H7-H9). The correlation coefficient (R) at H9 elevation zone was lowest (0.62), which might be also led by the obviously lesser area (435 km<sup>2</sup>) compared to the other elevation zones.

**Table 4.2** Evaluation indices of mean absolute error (MAE), Nash-Sutcliffe efficiency scores (NSE), Bias and Correlation Coefficient (R) for simulated snow covered area (SCA) by TRAIN model verified using MODIS snow cover maps for the 9 elevation zones over Rhineland-Palatinate during the period of 2002-2008. The elevation ranges and area of the 9 elevation zones are also listed.

Elevation zones	Range (m a.s.l.)	Area (km <sup>2</sup> )	MAE (%)	NSE	Bias (%)	R
H1	53-145	2527	4.70	0.42	-0.47	0.71
H2	145-214	2015	5.24	0.52	-0.48	0.76
H3	214-276	2691	6.18	0.58	0.30	0.79
H4	276-331	3136	6.75	0.63	1.86	0.79
H5	331-385	2921	7.64	0.63	3.88	0.76
H6	385-442	2630	8.81	0.62	6.55	0.72
H7	442-503	2198	10.57	0.62	9.11	0.72
H8	503-583	1318	13.55	0.55	12.78	0.73
H9	583-817	435	20.06	0.30	19.80	0.62

#### 4.4.2 Simulation of snow water equivalent (SWE)

Due to the lack of snow water equivalent observations at meteorological stations, the SWE simulations were validated with station-based snow depth measurements. The snow depth data from six representative stations were used to compare with the modeled SWE during the two winters of 2003/2004 and 2004/2005 (station locations are given in Figure 4.1), and the comparisons are shown in Figure 4.4 and 4.5. The winter 2003/2004 had fewer snowfalls while the winter 2004/2005 recorded positive anomaly of snow depth. Since the SWE was simulated by TRAIN model at grids with a cell size of 1 km × 1 km while snow depth was observed at station points, the daily SWE simulations were averaged over a 3 × 3 grid extent where a station was located, and then the mean SWE over the 3 km × 3 km region was compared with the snow depth observations. Figure 4.4 and 4.5 illustrate that the temporal dynamics of the modeled SWE by TRAIN fitted very well with snow depth observations during most of the

snowfall events at the six stations. Moreover, most of the temporary slight snow events were also successfully reconstructed by TRAIN model, e.g. at the beginning of the two snow seasons. However, some disagreements still exist, e.g., modeled SWE showed delayed snow ablation at the end of March 2005 at Densborn and Pellingen stations (Figure 4.5).

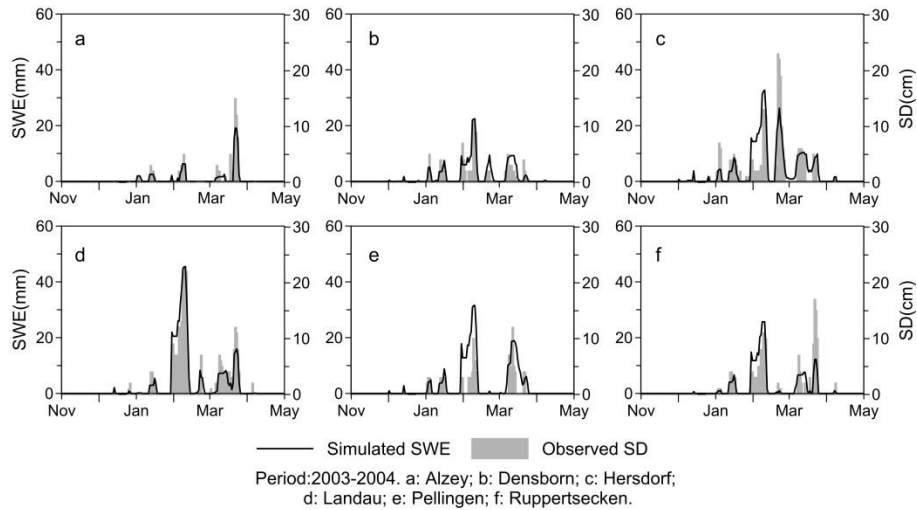


**Figure 4.4** Simulated SWE by TRAIN model and observed snow depth (SD) at six in situ stations during the snow season of 2003/2004.

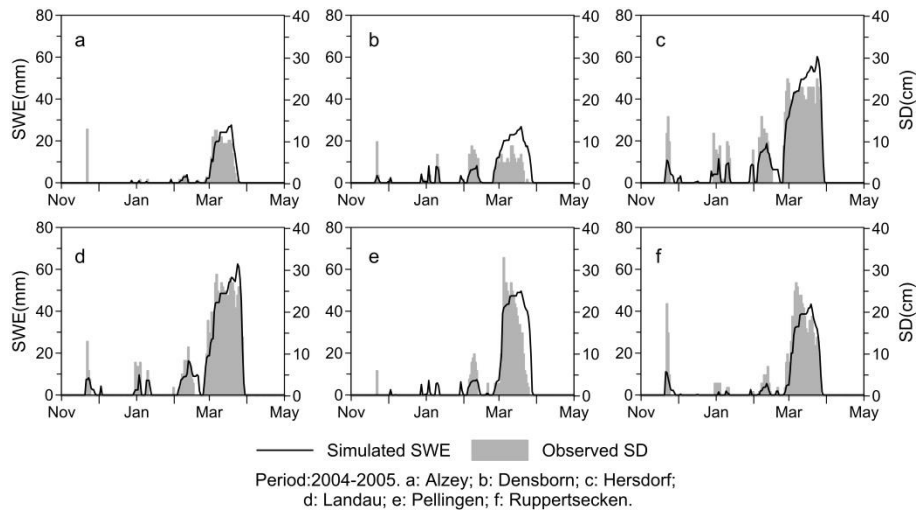


**Figure 4.5** Same as Figure 4.4, but for the snow season of 2004/2005.

It should be noted that there are also significant uncertainties in comparing SWE with snow depth and in comparing areal simulations with point observations. For example, snow density has high variability during the snow recession period in spring.

Alternate snow melting and freezing can result in obviously declined snow depth, but only a slight decrease of snow water equivalent. Moreover, due to the high heterogeneity of the terrains and land use, the snow depth observations at meteorological stations sometimes have limited representative range, especially because of the influence of human activities on the local climate of cities where most of the meteorological stations are located.

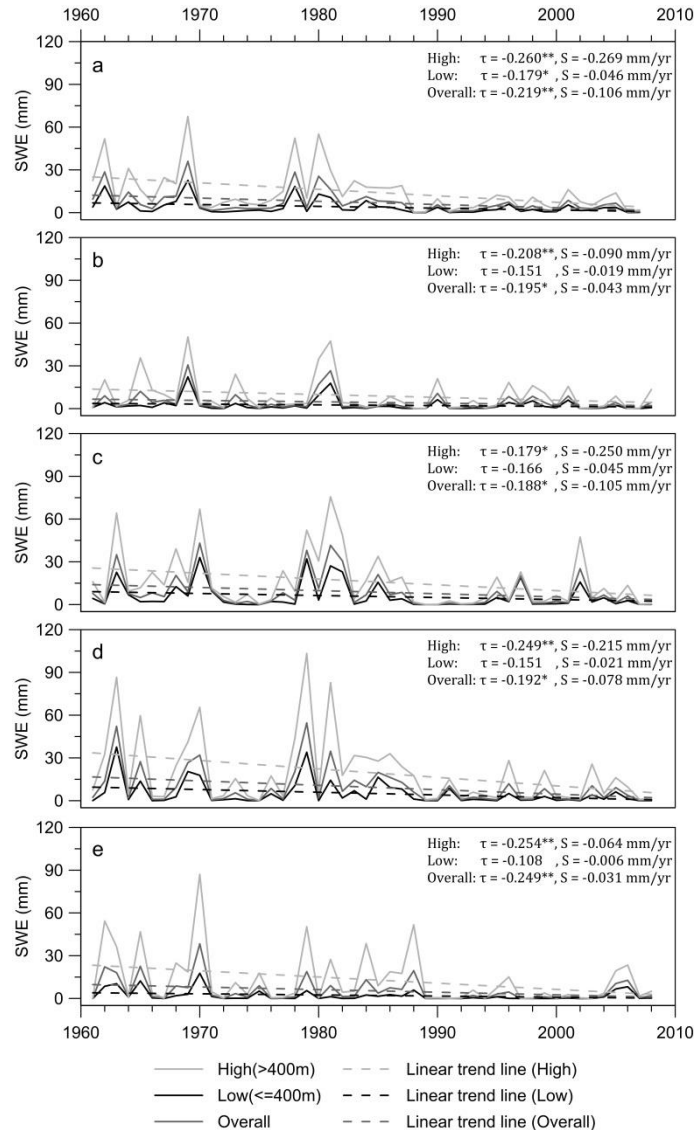


**Figure 4.6** Trends of simulated mean daily SWE by TRAIN model in high (> 400 m a.s.l.) and low ( $\leq$  400 m a.s.l.) elevations as well as the overall Rhineland-Palatinate for the whole snow seasons (a) (December to March) and individual months of December (b), January (c), February (d) and March (e) during 1961-2008. Trends were analyzed using a linear trend line equation, Mann-Kendall's

trend test " $\tau$ " and Sen's slope estimator "S". Significant Mann-Kendall trends are indicated by \*\* ( $P < 0.05$ ) and \* ( $P < 0.10$ ).

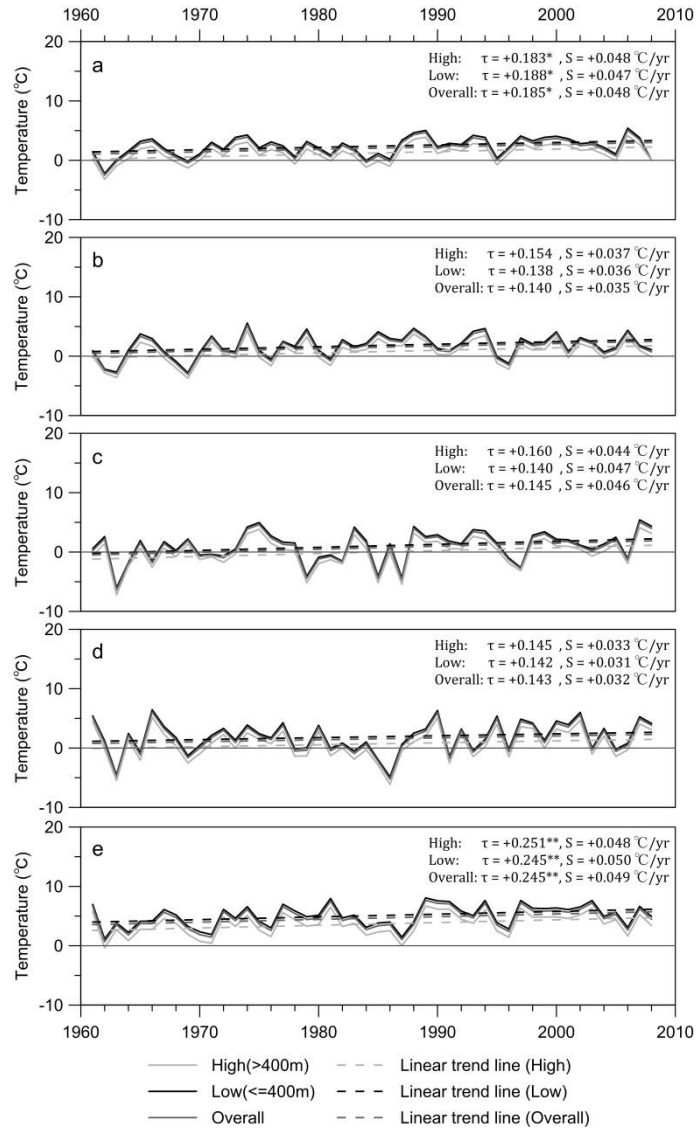
## **4.5 Snow cover trends under a changing climate**

### **4.5.1 Trend analysis of snow water equivalent and climate variables**

According to the above evaluation of the modeled SCA and SWE, both the temporal and spatial dynamics of the snow cover could be well reconstructed by TRAIN model. To decipher the long-term behavior of the snow cover and the corresponding climate change background, Mann-Kendall (MK) trend test and Theil-Sen estimator were utilized to detect the trends in the gridded time series of the simulated SWE as well as the recorded air temperature and precipitation during the snow seasons of 1961-2008. The trends were also estimated individually at the high ( $> 400$  m a.s.l.) and low ( $\leq 400$  m a.s.l.) elevations and in each month of the major snow season (December to March). The Mann-Kendall trends were tested at the significance levels of 5% and 10%.

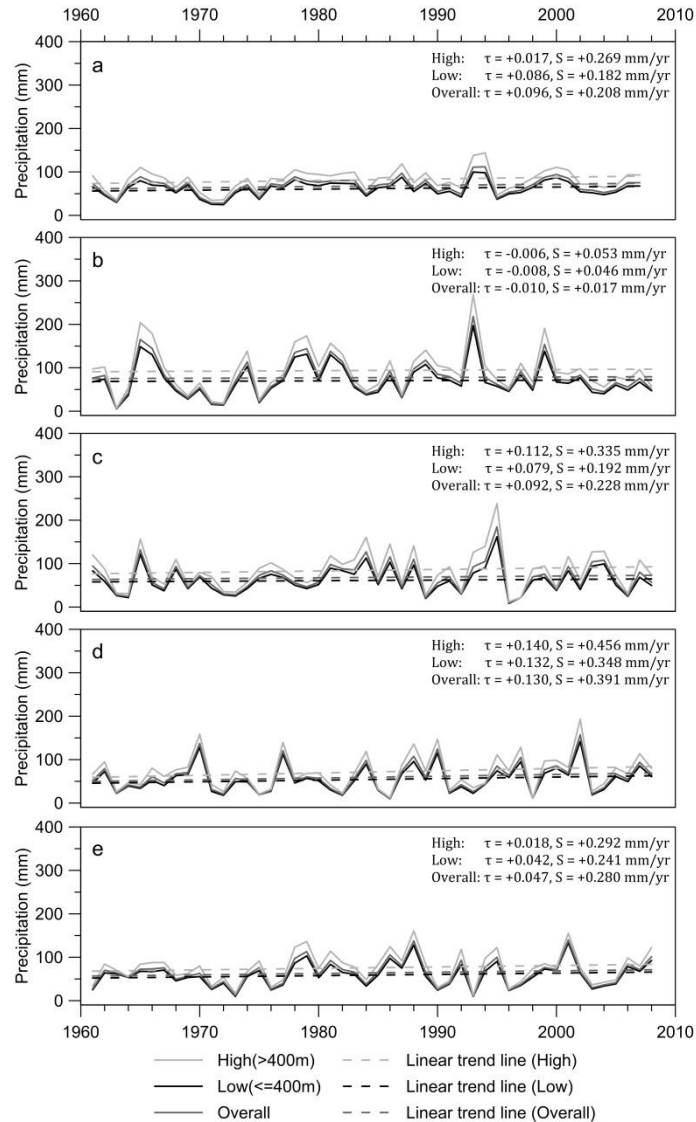
Figure 4.6-4.8 shows the trend tests of the mean daily SWE, mean air temperature and monthly total precipitation, respectively. Mann-Kendall trend tests suggest that snow water equivalent has endured significant decrease at the high elevations ( $> 400$  m a.s.l.) in each month of the main snow season (December to March), with Kendall's tau ( $\tau$ ) coefficients ranging from -0.179 to -0.254 in individual months. SWE decline was most remarkable in March, because both the high elevations ( $\tau = -0.254$ ) and the whole Rhineland-Palatinate ( $\tau = -0.249$ ) reached the smallest MK's  $\tau$  values, compared to those in the other months. A relatively slight decreasing trend of SWE was found in January with the Kendall's tau ( $\tau$ ) coefficients closer to zero both for the high elevations ( $\tau = -0.179$ ) and for the whole region ( $\tau = -0.188$ ). The MK trends were not significant for the low elevations ( $\leq 400$  m a.s.l.) in individual months except for the whole snow season ( $\tau = -0.179$ ). Theil-Sen estimator indicates the largest decreased net value of SWE occurred at the high elevations in January, with a Sen's slope of -0.250 mm/yr, which can be traced back to the high snow accumulation in January.

Finally Kendall's tau ( $\tau$ ) coefficients of -0.260 and -0.219 and Sen's slope of -0.269 mm/yr and -0.106 mm/yr were found for the high elevations and the whole study region respectively during the snow seasons of 1961-2008, indicating significant SWE decreasing trend in Rhineland-Palatinate, especially for the mountains. In addition, the SWE time series shown in Figure 4.6 also illustrate that the fluctuating ranges of SWE have obviously declined since the end of 1980s, which might reveals a reaction to the changing climate.



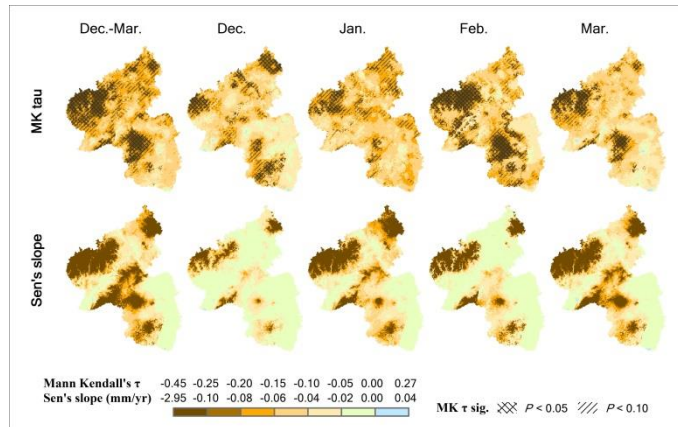
**Figure 4.7** Same as Figure 4.6, but for recorded mean air temperature.

Figure 4.7 demonstrates the recorded time series and trend test results for air temperature during the snow seasons of 1961-2008. A sharp increasing trend of temperature in March was found according to the significant Kendall's tau ( $\tau$ ) coefficients (+0.245 to +0.251,  $P \leq 0.05$ ) and highest Sen's slopes (+0.048 to +0.050 °C/yr). For the other months from December to February, the positive MK trends were not significant, though high Sen's slopes (+0.031 to +0.047 °C/yr) were also observed, which was an unexpected result. Due to the rapid warming trend in March, a significant ( $P < 0.10$ ) Kendall's tau ( $\tau$ ) coefficient of +0.185 and a Sen's slope (S) of +0.048 °C/yr were found for the entire Rhineland-Palatinate during the snow season, indicating significant increasing trend of air temperature.



**Figure 4.8** Same as Figure 4.6, but for recorded mean monthly total precipitation during each snow season (a) and in individual months from December to March (b-e). All the Mann-Kendall trends of precipitation are not significant ( $P > 0.10$ )

The trend analysis results for precipitation are given in Figure 4.8, which illustrates that the mean monthly precipitation during the whole snow season had a slight increasing trend with Kendall's  $\tau = +0.096$  and Sen's slope  $S = +0.208$  mm/yr, though the trend is not significant. In addition, the MK trends in the individual months of the snow season are not significant as well. However, the largest Kendall's tau ( $\tau$ ) coefficient and highest Sen's slope ( $S$ ) were observed in February, suggesting a wetter climate trend.



**Figure 4.9** Distribution of the trends of the simulated mean daily SWE during the snow season and in individual months from December to March. Trends were indicated with Mann-Kendall's " $\tau$ " and Sen's slope "S". Significant Mann-Kendall trends are indicated by crossed lines ( $P < 0.05$ ) and skew lines ( $P < 0.10$ ).

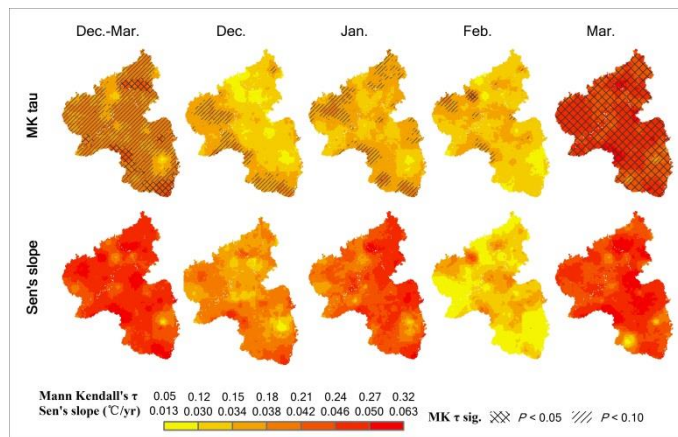


**Figure 4.10** Same as Figure 4.9, but for recorded mean air temperature.

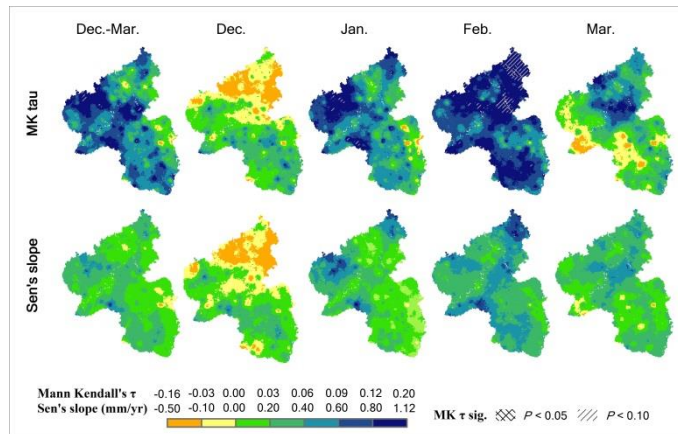


**Figure 4.11** Same as Figure 4.9, but for recorded mean monthly total precipitation during the snow season and in individual months from December to March.

#### **4.5.2 Seasonal and spatial dynamics of the long-term trends**

To further extract the spatial distribution of the changing trends of the three environmental variables, grid-based Mann-Kendall (MK) trend test and Theil-Sen estimator were also performed for each month of the main snow season (December to March), the results of which are depicted in Figure 4.9-4.11. Figure 4.9 suggests that the significant and highest decreasing MK trends are mainly concentrated in the mountainous regions, such as the Eifel, Westerwald and Hunsrück. The Sen's slope of SWE more clearly shows that the above three mountains had the most obvious declining trends during 1961-2008. Moreover, the mean daily SWE in February and March showed more significant decreasing trends according to MK trend test, while an apparent decline of SWE was also found in January according to Theil-Sen estimator, due to the higher SWE values in January. Regarding the SWE during the whole snow season, most of the study area, especially in the mountainous regions in the center and northwest, was subject to a snow cover retreat in this period (Figure 4.9).

Figure 4.10 demonstrates that the air temperature trend during the past five decades was mainly characterized by the intense warming in March, with significant Kendall's tau ( $\tau$ ) coefficients of more than +0.21 ( $P < 0.05$ ) and Sen's slope higher than 0.042 °C/yr in most area. In addition, some significant ( $P < 0.10$ ) increase of temperature also occurred in the mountains from December to February, with Kendall's tau ( $\tau$ ) coefficients lower than +0.21, which corresponds to the decreased SWE in the highlands (Figure 4.6 and 4.9). However, Figure 4.6 and 4.9 suggest that the SWE in February had a remarkable decline as well, with identical minus MK  $\tau$  values at the high elevations (-0.249 for February and -0.254 for March) and the MK trends even have a larger significant area in February, though Figure 4.10 shows the temperature increase in February was far less than that in March. This phenomenon might be related to the precipitation increase in February (Figure 4.11), which is more obvious than the other months. Figure 4.12 illustrates the spatial distribution of the air temperature, precipitation and SWE, indicating that the air temperature in Rhineland-Palatinate ranges around 0 °C during the snow season, with relatively high precipitation of 50-100 mm per month, even higher in the mountain regions. The wet and temperate winters in the study area lead to the frequent alternation of snowfall and rainfall as well as the mixture of the both. Increased precipitation in the form of rainfalls would restrain the presence and duration of snow cover. Therefore, the more obvious increasing trend of precipitation is extrapolated to be an important trigger factor of the declined SWE in February. Moreover, the slightly decreased precipitation in December and March at the highlands might be involved in reducing the synchronous snow accumulation (Figure 4.11).

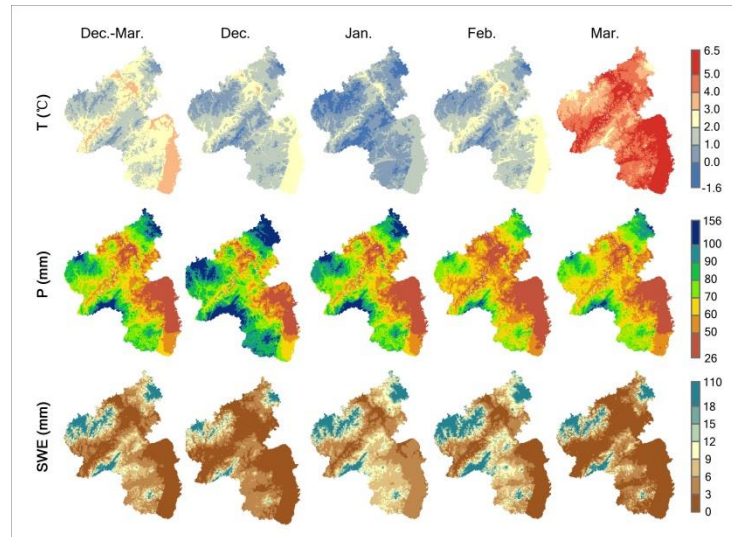


**Figure 4.12** Spatial distribution of the recorded mean air temperature, (mean) monthly total precipitation and simulated mean daily SWE for the whole snow season as well as individual months from December to March over Rhineland-Palatinate. Values are averaged in the period of 1961-2008.

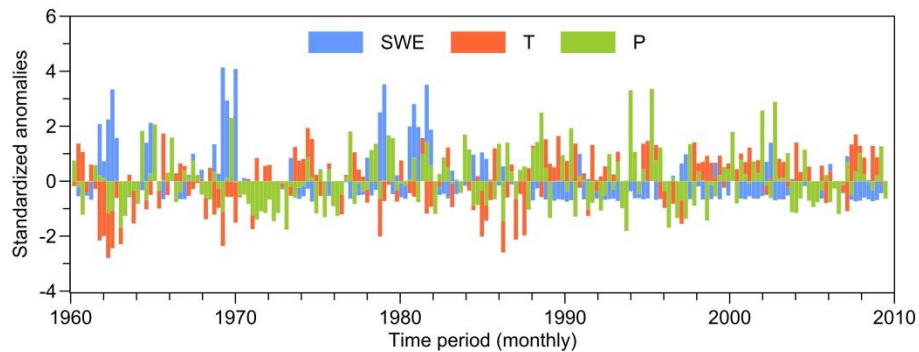


**Figure 4.13** Temporal dynamics of the monthly standardized anomalies of mean daily SWE, mean air temperature and monthly total precipitation during the snow seasons (December to March) of 1961-2008 in Rhineland-Palatinate.

#### 4.5.3 Correlation between SWE and climate variables

The monthly standardized anomalies of SWE, T and P during 1961-2008 are demonstrated in Figure 4.13, which provides information of the temporal dynamics of the three environmental variables. It can be seen that positive SWE anomalies generally occurred together with negative anomalies of air temperature while precipitation did not show apparent influence. Moreover, the coefficients of variation (CV) of SWE and temperature significantly declined after the end of 1980s. Positive anomalies of temperature became the dominant situation during the last two decades

while negative anomalies of SWE frequently occurred at the same time, which was obviously different from the period before the end of 1980s.

Correlation analysis was conducted to assess the individual roles of air temperature and precipitation in affecting snow cover. The coefficients of Pearson correlation, Spearman rank order correlation and Kendall's rank correlation of SWE with temperature and precipitation are given in Table 4.3. Table 4.3 indicated significant negative correlations ( $P < 0.01$ ) between SWE and temperature during the snow season and in each month. The three kinds of correlation coefficients between SWE and temperature all achieved the minimum values in February, suggesting that the snow cover was most sensitive to air temperature in February. Therefore, even slightly increased temperature in February could also lead to a decline of the synchronous SWE. Though the correlations between SWE and precipitation are not significant (Table 4.3), the negative correlation coefficients between the two variables in February indicate that precipitation increase could reduce the snow cover, which coincides with the discussions above in section 4.5.2. This emphasizes the fact that the snow cover in February was most sensitive to a changing climate compared to the other months, i.e., a warmer and wetter climate inhibited the presence of snow cover in February.

**Table 4.3** Correlation coefficients (Pearson, Spearman and Kendall) of mean daily SWE with mean air temperature and monthly total precipitation during the whole snow season and in individual months from December to March. The correlations were analyzed based on the monthly standardized anomalies of the three variables.

Correlation	Dec.-Mar.		December		January		February		March	
	T	P	T	P	T	P	T	P	T	P
Pearson	-0.58*	-0.05	-0.47*	0.10	-0.65*	-0.03	-0.69*	-0.11	-0.51*	0.23
Spearman	-0.69*	-0.05	-0.42*	0.17	-0.77*	0.00	-0.84*	-0.16	-0.69*	0.23
Kendall	-0.50*	-0.03	-0.29*	0.10	-0.57*	0.01	-0.63*	-0.11	-0.53*	0.16

\* Correlation is significant at the 0.01 level (2-tailed).

## 4.6 Discussion and conclusions

In this study, corrected cloud-free MODIS snow products were applied to evaluate the snow cover simulations derived from a distributed hydrological model (TRAIN), indicating an improvement of the availability of remotely sensed snow information in validating snow models compared to the original MODIS snow images which have high cloud obstruction and misclassification errors. Then the indices of mean absolute error (MAE), Nash-Sutcliffe efficiency scores (NSE), Bias and Correlation Coefficient (R) were employed to evaluate the simulated SCA at nine elevation zones and in each month of the snow season in accordance with the remotely sensed snow maps. Besides,

in situ snow depth observations were also utilized to validate the snow water equivalent simulations at point scale. The evaluation of the modeled SCA and SWE both suggest well performance of the TRAIN model in reconstructing the seasonal snow cover in this selected central European low mountain region, even though high variability of snowpack is shown because of its temperate and wet winters. However, overestimated snow simulations were demonstrated as well in some periods, especially at the ablation stage, which might be partly caused by the snow underestimation of MODIS snow data in forested sites at the snow melting phases and the representative deficiency of snow measurements at meteorological stations.

The variation trends of modeled snow water equivalent (SWE) as well as recorded air temperature and precipitation were detected using Mann-Kendall (MK) test and Theil-Sen estimator for the period from 1961 to 2008. Significant decreasing trends of SWE at highlands in each month of the snow season (December to March) were suggested, and the SWE declines were more obvious in February and March. The temperature trend analysis showed a significant intense warming trend over the whole Rhineland-Palatinate in March, while relatively slight increasing trends of air temperature were only found in the high elevations for the other winter months. The trend tests illustrated an overall increasing trend of precipitation, which was more apparent in February, but most of the precipitation trends did not pass the significance tests. Correlation analysis indicated that snow cover had closer relations with air temperature compared to precipitation, which means precipitation is not a limit factor for the snow presence in this region. The snow cover in Rhineland-Palatinate was suggested to be most sensitive to the temperature changes in February. Moreover, the variation ranges of SWE and temperature both displayed significant declines after the end of 1980s, and positive anomalies of temperature more occurred at the same time while SWE showed an inverse change.

As areal snow information, remotely sensed snow records demonstrated obvious advantages over station-based snow observations in evaluating snow simulations. However, MODIS snow products only provide the snow covered area and cannot validate the modeled snow water equivalent. Though there are also a number of satellite-based SWE products, e.g. AMSR-E and SSM/I, they are not included in this study because of the large errors in the SWE remote sensing data, especially in mountain regions. Assimilating remotely sensed SWE observations into hydrological models is a helpful technique to improve the model performance, while the data quality can significantly influence the efficiency of the data assimilation, as suggested by Andreadis and Lettenmaier (2006). Some researchers have contributed great efforts to airborne laser altimetry (LiDAR) of snow cover (e.g. Deems et al. 2013; Kirchner et al., 2014), which has the capability to collect SWE information in high precision and accuracy. The airborne-based snow measurements have great potential in improving

the snow modeling at regional scales, either by providing better calibration datasets or by involving a data assimilation scheme.



## Chapter 5

### Monitoring of snow processes with time-lapse photography

#### 5.1 Introduction

Snow is an important component of the hydrologic cycle in different scales. In high latitudes, precipitation is stored in the snowpack over the winter, and released to the rivers quickly in spring, which can lead to flood damage (Koivusalo and Kokkonen, 2002). Snow accumulation and ablation processes in mountainous regions are complicated by the heterogeneity of the vegetation and topography. As forest cover increases, snow accumulation on the ground is reduced by canopy interception which is not only an important process for rainfall events but also for snowfalls (Essery et al., 2003). As solid precipitation, snow is prone to be intercepted more than rain in forests. Up to 60% of cumulative snowfall may be intercepted by the boreal forest in winter while over 30% of the annual snowfall returns to the atmosphere through sublimation (Pomeroy and Schmidt, 1993). Compared to the snow on the ground, sublimation is enhanced by the larger ratio of surface area to mass for the snow in canopies, and by the intercepted snow's more exposure to wind (Schmidt and Gluns, 1991). Forest cover can also influence the snow melting by altering the energy balance of the microclimate. Woo and Giesbrecht (2000) suggested that longwave radiation is enhanced under trees relative to the clearings, allowing to higher melting rates. It was supported by Bewley et al. (2010), who reported that increases in incoming longwave radiation beneath shrubs could outweigh the decreases in shortwave radiation due to shading, giving greater net radiation at snow surfaces below shrubs than for the exposed snow.

Due to the vertical precipitation gradient, elevation has an influence on the magnitude of snowfall events (D'Eon, 2004). Besides, lower temperatures at higher elevations are expected to retard the snow melting rates. Pomeroy et al. (1997) have reported that high wind is another important factor affecting snow redistribution since it can reduce the interception efficiency and release some intercepted snow to the clearings. Therefore, in montane forest environments, snow process characteristics and snow cover properties are of high complexity. To strengthen our ability in describing the interaction between forest structure and snow accumulation and ablation, it is necessary to identify the additional factors which explain the spatial and temporal distribution patterns of snow (Varhola et al., 2010). Detailed and continuous monitoring of snow processes is crucial for this purpose.

Snow characteristics have traditionally been measured either at meteorological stations or by snow course campaigns at irregular intervals in space and time (Parajka et al., 2012a). The traditional snow surveys can provide accurate information about the snow cover at point-scale. However, the low observation frequency limits their availability. In addition, the sparse network of climate stations sometimes cannot fulfil the requirements of specific snow research. Remote sensing techniques have been widely used in snow monitoring these years, such as optical and microwave monitoring based on satellites, as well as aerial photography (König and Sturm, 1998; Hall et al., 2002; Kelly et al., 2003; Hüsler et al., 2014). As areal data, remote sensing can monitor the snow cover over a large spatial scale; nevertheless, remotely sensed data has inferior accuracy at point-scale and lower temporal resolution, daily data at most. Besides, remote sensing cannot obtain some special snow parameters, such as snow canopy interception. Automatic weather station (AWS) is another method, which has high accuracy and is possible to be installed in unattended mountainous regions. Various sensors are responsible for the observations of different snow parameters. For example, integrated ultrasonic sensor and force transducer can collect snow depth and intercepted snow mass data, respectively (Hedstrom and Pomeroy, 1998; Liu et al., 2015). However, AWS is generally costly and malfunction often occurs because of the complex sensor system. Time-lapse photography has been proved to be an available solution to continuously monitor the snow processes in mountainous forest environments. Bründl (1997) used a video camera to record the deflection of the tree branches with snow load at two sites in the Swiss Alps in snow season, and then he estimated the intercepted snow mass with Young modulus. Leo (2010) calculated the snow covered area fraction based on the digital camera images taken in a Norwegian peninsula, and the seasonal variability of the snow cover was analyzed. Parajka et al. (2012a) obtained the snow depths and snow cover patterns with digital cameras at three sites in the eastern Austrian Alps, and an automatic procedure for snow depth readings from digital pictures was developed. Garvelmann et al. (2013) carried out a continuous observation of snow processes with a camera network in the Black Forest of Germany, and the time series of snow depth as well as snow interception were extracted from the camera images.

In this study, the above snow monitoring approach of time-lapse photography has been improved. Acquiring the snow interception information from the digital images is based on the classification of snow. The snow classification method plays the decisive role in the quantification of the intercepted snow amount. This study compared the performance of six thresholding classifiers frequently used in extracting targets from complex background, i.e., MaxEntropy (Kapur et al., 1985), Huang (Huang and Wang, 1995), IsoData (Ridler and Calvard, 1978), Li (Li and Tam, 1998), MinError (Kittler and Illingworth, 1986), Otsu (Otsu, 1979). In this study, MaxEntropy

classifier was proved to be in a superior as compared to the others in determining snow interception levels. Moreover, digital single-lens reflex (DSLR) cameras instead of compact cameras were applied to execute the observations, which have better operational reliability and image quality. Based on the measurements by digital cameras and automatic weather stations at several sites in southwestern Germany, this chapter also shows some results about the influence of meteorologic conditions, elevations and forest cover on snow accumulation, melting and interception processes.

## **5.2 Methodology**

### **5.2.1 Study area**

This study was also conducted in the topographically heterogeneous Upper Rhine Region, situated at the French-German border (Figure 5.1). It is composed of the Upper Rhine Graben in the center and several mountains on the shoulders, such as the Black Forest mountains in the east, the Palatinate Forest and the Vosges mountains in the west. The Rhine River flows along the central axis of the Upper Rhine Graben, which contains Tertiary marls and clays, covered by Quaternary alluvium deposited by the Rhine River and forming the alluvial aquifer; the mountains on the graben shoulders are constituted of much older materials such as crystalline, metamorphic and ancient sedimentary rocks (Peters and van Balen, 2007). The area of the Upper Rhine catchment is 62,967 km<sup>2</sup>, including the catchments of the Neckar and Main Rivers. Elevations range from 1493 m a.s.l. (Black Forest) to 88 m a.s.l. (Bingen) (Uehlinger et al., 2008).

Climate conditions have high heterogeneity because of the complex and varied terrains over the Upper Rhine Region. The orographic effect of mountain ranges or uplands results in large contrasts of precipitation patterns, with annual values ranging from 500 mm/yr in the Rhine basin to 2000 mm/yr in the Black Forest mountains (BMUNR, 2003). Snowfall accounts for approximately 3% of total precipitation in the plain, and up to 37% over the mountain ranges (Peters and van Balen, 2007). Mean annual snow duration ranges between less than 20 days at the lowest elevations to up to 80 days in the mountains. Therefore, snow accumulation and melting processes in the montane forests significantly influence the dynamics of river flows in this region. Moreover, potential evapotranspiration at the mountain tops (around 400-500 mm/yr) is lower than in the plain (around 600-700 mm/yr, BMUNR, 2003). Consequently, the rivers originated from the mountainous areas carry a large proportion of the snowmelt water involved in the hydrosystem budget and thus contribute to the recharge of the Rhine alluvial aquifer (Peters and van Balen, 2007). Mean annual air temperature is about 6°C at the highest Black Forest and exceeds 10°C in the warm Rhine valleys.

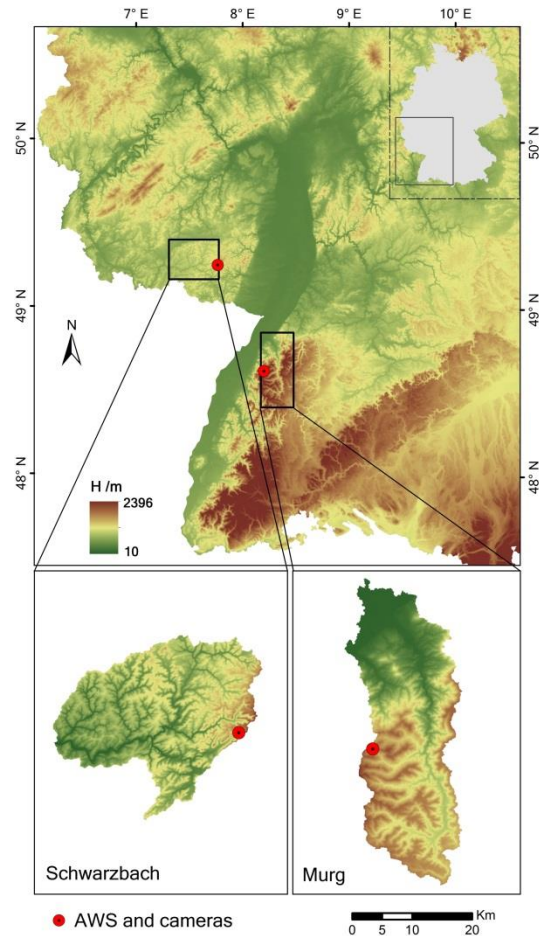


**Figure 5.1** The two study catchments of Schwarzbach and Murg in the Palatinate Forest and Black Forest respectively. Red dots refer to the locations of automatic weather stations and cameras in the Hertenkopf site (Schwarzbach catchment) and Hundseck site (Murg catchment).

The snow process monitoring was accomplished in two small catchments Schwarzbach and Murg, located at the Palatinate Forest and the Black Forest respectively. About 82% of the Palatinate Forest is covered by mixed woodland, with deciduous trees (beech, oak, larch, chestnut) accounting for around 48% and coniferous trees (pine, spruce, fir) taking up to 50%. The forests in the Black Forest consist of about 80% coniferous (spruce, fir, pine) and about 20% deciduous (beech, birch, oak), with a total forest coverage of about 70% (Garvelmann et al., 2013).

### 5.2.2 Observation setup

In order to conduct a continuous snow process monitoring in the montane forests of the study area, four digital cameras were installed at the Schwarzbach (Hertenkopf site,

Palatinate Forest) and Murg (Hundseck site, Black Forest) catchments. One camera in Hortenkopf was fixed up in a beech forest (49.273°N, 7.807°E, 537 m) and another one faced an oak forest (49.275°N, 7.802°E, 520 m). Both the two cameras in Hundseck focused on a spruce forest in the Black Forest, and one was installed on a mountaintop (Hundseck high, 48.643°N, 8.228°E, 950 m) while the other one was near the base of the mountain (Hundseck low, 48.644°N, 8.233°E, 867 m). Seven snow stakes painted in black and red scales were set up in the camera views to determine the snow depths. Each one of them had a height of 1.7-1.8 m. One stake at the Hundseck high site stood in open field and the others were positioned beneath canopies. The cameras in the Hortenkopf site were installed in the winters of 2013/2014 and 2014/2015 while those in the Hundseck site were installed in the winter 2014/2015. Since only a few light snowfalls occurred in the Palatinate Forest during the winter 2013/2014 and the camera in the beech forest (Hortenkopf site) stopped working for a period in the winter 2014/2015, these photos were rejected to use in this study. The arrangements of the other three cameras are shown in Figure 5.2.

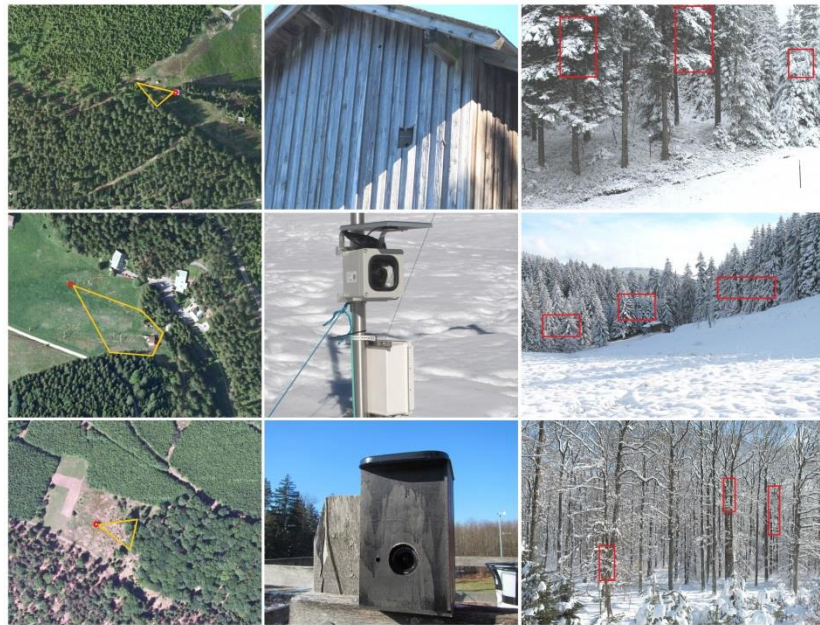


**Figure 5.2** Locations and views of the digital cameras at three sites: Hundseck high (top), Hundseck low (middle), Hortenkopf (bottom). Red bounding boxes refer to the regions of interest (ROI) for determining snow interception.

In addition to the camera network, meteorologic elements such as snow depth, air temperature, humidity, global radiation, wind speed and wind direction were also observed with automatic weather stations (AWS). Moreover, manual snow surveys per week were conducted at the Hundseck site during the winter 2014/2015. The manual

measurements included snow depth and snow water equivalents both on an open meadow and under the spruce forest.

### 5.2.3 Digital camera

Digital camera is the major component for automatic time-lapse photography. A timer remote control and continuous power-supply as well as a water-proof container are required, besides the camera. In this study, Canon EOS 1100D (Rebel T3) DSLR cameras (Figure 5.3, Table 5.1) were used to monitor the snow processes. Digital single-lens reflex (DSLR) cameras have obvious advantages than compact cameras in time-lapse photography. Firstly, DSLR cameras have much larger sensors and relatively large lenses, making it possible to receive more light even in dark environment. Thus DSLR cameras have superior performance in monitoring snowfall in abominable weather conditions. Besides, DSLR cameras consume less power and have a larger battery capacity than compact cameras, and accordingly they can keep working for a longer time, especially in low-temperature environments. In addition, DSLR cameras provide more flexible self-setting functions, such as aperture, shutter speed, photosensitivity and focal distance, allowing them to adapt various shooting environments and objectives.

**Table 5.1** Parameters of the Canon cameras.

Model	Specifications
Effective pixel	12,2 million
Maximum resolution	4.272 x 2.848
Sensor type	CMOS
Sensor size	22,2 x 14,7 mm
File format	JPEG
Zoom	18-55 mm
Lens aperture	F3.5-F5.6
Shutter speed	30-1/4000 s
Sensitivity equivalent	ISO 100-6400
Timer remote control	Pixel TC-252/DigiSnap 2700 (hourly)
Storage	SDHC-16GB
Battery	2 x LP-E10 (1900 mAh)/ 18 Ah with solar panel
Water-proof box	Wooden/Fiberglass

Each Canon EOS 1100D camera (Figure 5.3) was connected with a timer remote control, which triggered the camera per hour to take a photo. Because the daytime in winter in the study area was short, only the photos from 8:00 a.m. to 17:00 p.m. (7:00 a.m. to 18:00 p.m. in February) were possible to be obtained. Battery grip and solar panel were applied to extend the power supply of the cameras. All the cameras were put into

water proof boxes and then mounted to towers, trees or automatic weather station (Figure 5.2). The detailed specific settings of the time-lapse photography system are listed in Table 5.1.



**Figure 5.3** Camera Canon EOS 1100D and the timer remote control used in this study.

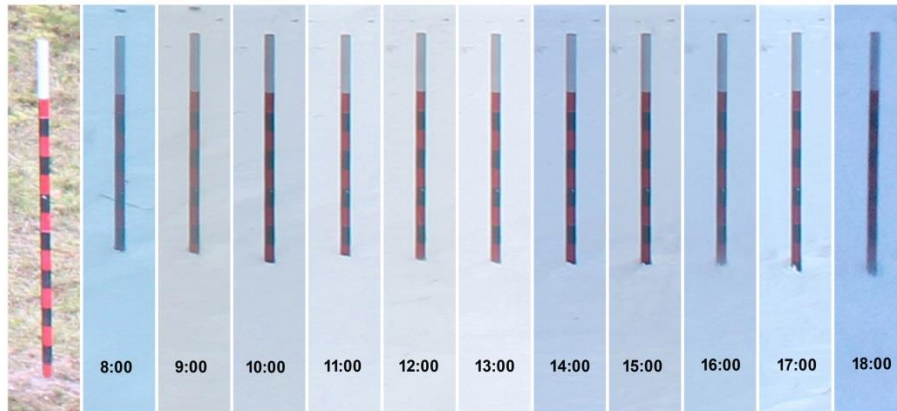


**Figure 5.4** Hourly photos of a snow stake at Hundseck site (high, open) on 6 Feb. 2015. The left panel refers to the stake without snow.

#### 5.2.4 Image analysis

The photos recorded by the Canon EOS 1100D cameras were JPEG images. In the camera views, the snow stakes and the snowpack in canopies provided the information of snow depth (Figure 5.4) and snow interception (Figure 5.5). Since large quantities of images were obtained during the observation period, efficient image analysis should be applied to extract the above snow parameters. As shown in Figure 5.4, snowpack was in sharp contrast to the snow stakes. Hence if the snow stakes were

clipped out from the pictures, then their brightness dynamics would demonstrate the snow surface on the ground and give out the snow depths. A semi-automatic procedure was developed to execute this task. Firstly, the pictures taken in poor visibility conditions (night, dense fog, and snowstorm) were discarded manually. Then a batch routine of Photoshop was used to extract a measure line with three pixel width from each snow stake on each picture. After that all the measure lines were imported to ArcGIS and converted to ASCII files, which contained the brightness values of the snow stakes. Then the snow surfaces were detected based on the abrupt increase of brightness compared to the exposed snow stakes. The pixel lengths of all the snow stakes above snow surfaces were extracted accordingly. Since the snow stakes had painted scales, their original lengths without snow as well as the relations between pixel length and real length could be determined. Finally, the snow depth of each measure line was calculated out and the time series of snow depth both in clearings and beneath canopies were obtained. To validate the snow depths derived from the semi-automatic routine, a number of manually interpreted snow depths based on the readings of the snow stake scales on the digital pictures were also obtained.

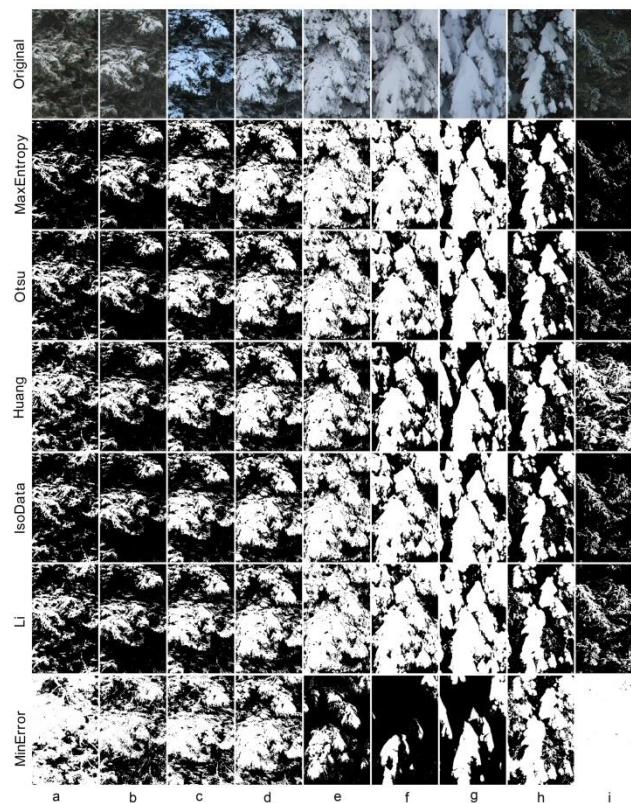


**Figure 5.5** Snow interception as observed by time-lapse photography (top panel) and corresponding binary photos derived from distinct classification methods.

For the calculation of snow interception in the forest canopies based on the digital images, a snow interception index should be firstly defined, because the real intercepted snow mass cannot be measured through photography. However, the time-lapse pictures could intuitively present the interception levels at a different time (Figure 5.5). A snow interception index,  $SII$ , was defined as,

$$SII = \frac{1}{n} \sum_{i=1}^n \left( \frac{S_i}{P_i} \right) = \frac{\sum_{i=1}^n S_i}{\sum_{i=1}^n P_i} \quad (5.1)$$

where  $n$  is the number of the regions of interest (ROI) for determining the snow interception index ( $SII$ ).  $S_i$  is the snow pixel number in the foreground of one ROI and  $P_i$  is the total pixel number of the corresponding ROI.  $SII$  varies from 0 (no snow) to 1 (intense snow) and can be expressed as a percentage. The positions of the ROIs should be kept consist in all the images to comparably assess the temporal variation of snow interception. Furthermore, it is of great importance to select an appropriate classification method to distinguish the snow pixels in the foreground and background of the ROIs, which can significantly influence the final  $SII$  values. Generally, binary classification is applied because of the higher brightness of snow pixels than the background (Leo, 2010; Garvelmann et al., 2013). The available binary classification should satisfy two criteria. Firstly, it can adapt to varying illumination conditions, i.e. it has stable classification performance when the contrast has large dynamics. The thresholds for differentiating snow and canopy could adjust themselves to changes in illumination. Fixed thresholds or those which cannot fit well with the brightness variation of the snow pixels in the digital pictures are not recommended. Secondly, the appropriate classification could sensitively reflect the snow interception dynamics in canopies. It means only the foreground snow should be included to characterize the canopy interception, otherwise the superposed snow in the background would lead to high  $SII$  values even after light snow.

In this study, six commonly used binary methods were compared for accurately quantifying the snow interception levels on the time-lapse images, i.e., MaxEntropy, Huang, IsoData, Li, MinError and Otsu. The binary processing was executed in Image J software (Collins, 2007), which is generally employed to interpret medical images. The binary pictures for nine example digital images through the six binary classifications are illustrated in Figure 5.5, and the original images are also shown for reference. The nine images demonstrate the representative snow interception dynamics in canopies in winter, and both the snow accumulation and ablation phases are included. Figure 5.5 illustrates that MaxEntropy classifier has a better performance than the others in reflecting the snow interception variation. A common shortage for the other binary methods is showing more snow pixels in low snow interception

situations (Image a, b, i in Figure 5.5). In other words, the binary thresholds for the other five methods could not accurately vary along the snow interception dynamics. Table 5.2 and Figure 5.6a show the thresholds of the six binary methods in classifying the nine digital pictures. MaxEntropy classification determined relatively higher thresholds for image a, b and i than the others, which means the other methods classified more pixels as snow, leading to greater *SII* values. Especially, the computed *SII* values for image b with the other five binary methods are higher than those for image a (Table 5.2), which is against the truth derived from the original images (Figure 5.5). In addition, MinError failed to demonstrate the snow interception conditions when there was a large amount of snowpack in canopies and it only showed some shadows (Image e, f, g in Figure 5.5). Figure 5.6b plotted the referential snow brightness dynamics in a clearing of image a-i, which shows that the self-adaptation thresholds of MaxEntropy in Figure 5.6a fit better with the illumination dynamics. Therefore, MaxEntropy binary classification was selected in this study to process all the ROI images, and the snow interception indices (*SII*) were calculated with Equation (5.1).

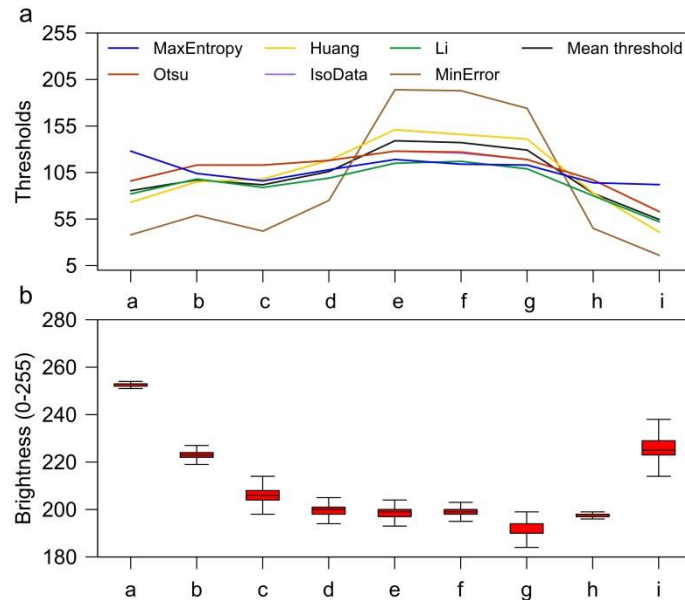


**Figure 5.6** Thresholds of individual binary classification methods (a) and the median as well as Inter Quartile Range (IQR) of the referential snow brightness in open field.

**Table 5.2** Thresholds of different binary classifications for the pictures in Figure 5.5, and the corresponding *SII* are listed in the parentheses.

	MaxEntropy	Huang	IsoData	Li	MinError	Otsu	Mean
a	128 (11.7)	73 (33.8)	96 (21.5)	82 (28.1)	38 (77.0)	96 (21.5)	85.5
b	104 (21.3)	95 (23.8)	113 (19.2)	98 (22.9)	59 (48.8)	113 (19.2)	97.0
c	96 (35.4)	98 (35)	113 (32.3)	89 (36.8)	42 (55.9)	113 (32.3)	91.8
d	108 (46.6)	118 (44.2)	118 (44.2)	99 (48.9)	75 (56.5)	118 (44.2)	106.0
e	119 (69.9)	151 (55.3)	128 (66.4)	115 (71.4)	194 (24.6)	128 (66.4)	139.2
f	114 (73.4)	146 (55.7)	126 (67.7)	117 (71.9)	193 (12.1)	127 (67.2)	137.2
g	113 (71.8)	141 (58.1)	119 (69.5)	109 (73.3)	174 (30.2)	119 (69.5)	129.2
h	94 (42.6)	83 (45.3)	97 (41.9)	80 (46.1)	45 (60.1)	97 (41.9)	82.7
i	92 (3.6)	41 (37.5)	63 (10.6)	52 (18.8)	16 (99.6)	63 (10.6)	54.5

## 5.3 Results

### 5.3.1 Snow depth and validation

The snow depths derived from the digital images by the semi-automatic routine are shown in Figure 5.7 and 5.8, and the results from hand-operated readings as well as station-based measurements are also plotted for comparison purpose. Figure 5.9 demonstrates the regression models of the automatic and manual snow depth values, which shows that the RMSE ranged from 1.14 cm to 1.95 cm. The three figures illustrate that the semi-automatically obtained snow depths from the digital pictures had high consistency with the manual results and the observations by a climate station. Therefore, time-lapse photography proved to be an appropriate approach to monitor snow depth dynamics in mountainous and unattended environments. In addition, it has higher observation frequency than traditional manual measurements in climate stations, and it has lower cost than the observations by automatic ultrasonic sensors.

The snow depth variations shown in Figure 5.7 and 5.8 suggest that there were two main peaks during the winter 2014/2015 in the two locations of the Palatinate Forest and the Black Forest. The first peak occurred at the end of December 2014, and the second peak, as the largest peak, occurred in the beginning of February 2015, both of which corresponded to a frequently snowed period. Besides, the snow depths at the Hortenkopf site (Palatinate Forest) were smaller than those at the Hundseck site (Black Forest), and the snow season of the former ended about one month earlier than the latter. The lower elevations in the Palatinate Forest might be an important reason. Figure 5.7c shows that the snow depths in the clearing were always higher than those beneath canopies, but at the end of the snow season the snowpack in forest seemed to

melt more quickly than that in the open site. The differing energy balance and/or wind-blow-snow might play some roles in this special recession process.

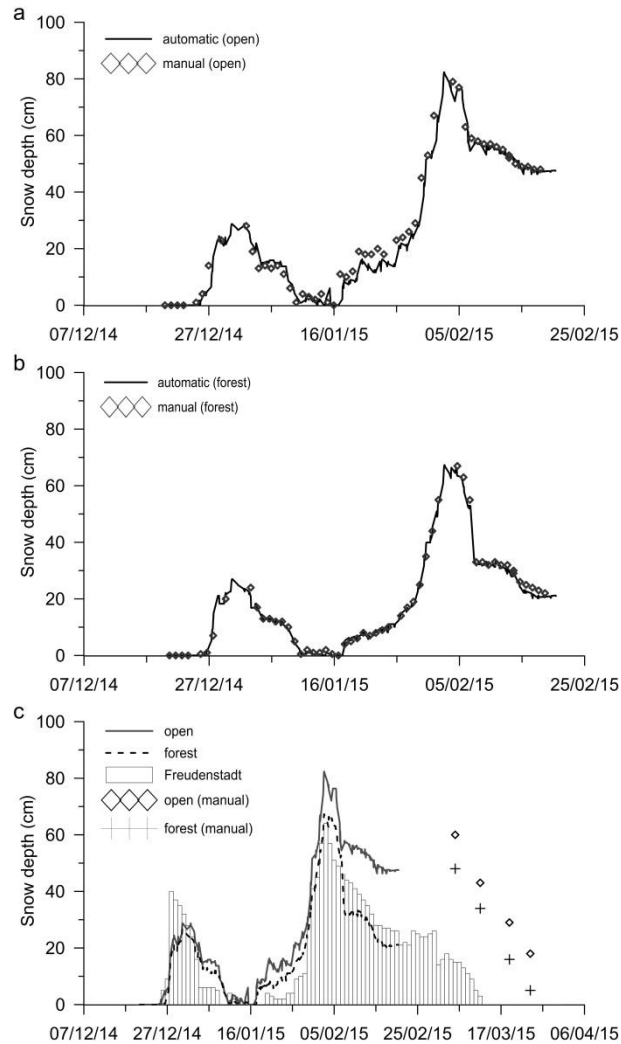


**Figure 5.7** Digital-image based snow depths derived from a semi-automatic procedure at Hundseck open site (a) and forest site (b), and from manually interpreted results for the snow season 2014/2015. (c) Comparison of snow depths from digital images with the station-based measurements in Freudenstadt (48.455°N, 8.410°E, 797 m), and the scattered plots refer to the medians of manually measured snow depths in weekly snow surveys.

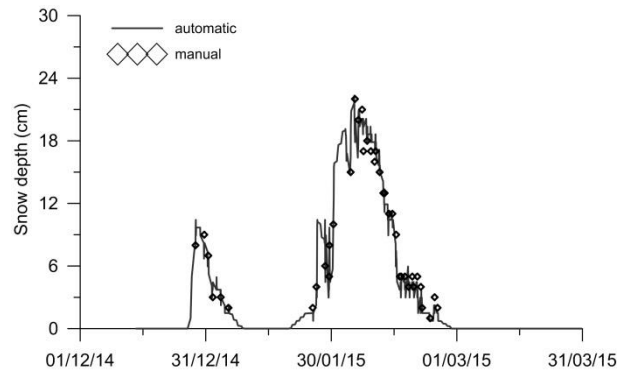


Figure 5.8 Same as Figure 5.7, but for results at Hortenkopf forest site.

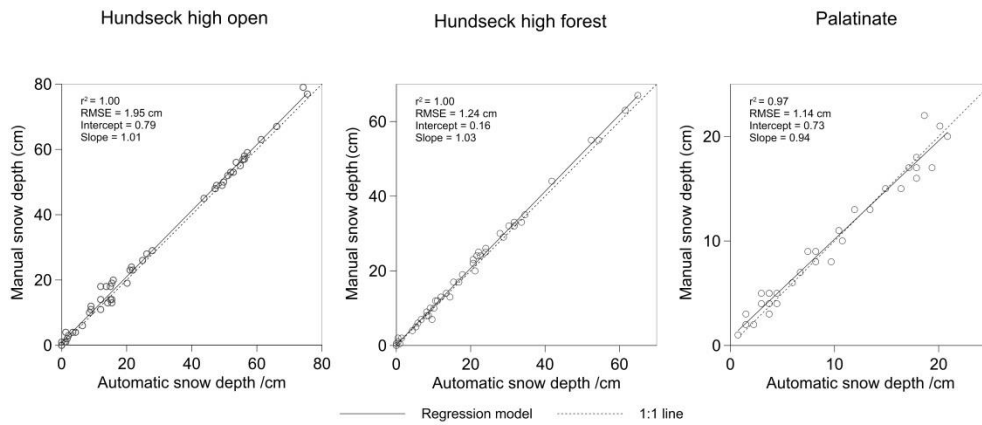


Figure 5.9 Automatically versus manually interpreted snow depths at Hundseck open site (a), Hundseck forest site (b) and Hortenkopf forest site (c).

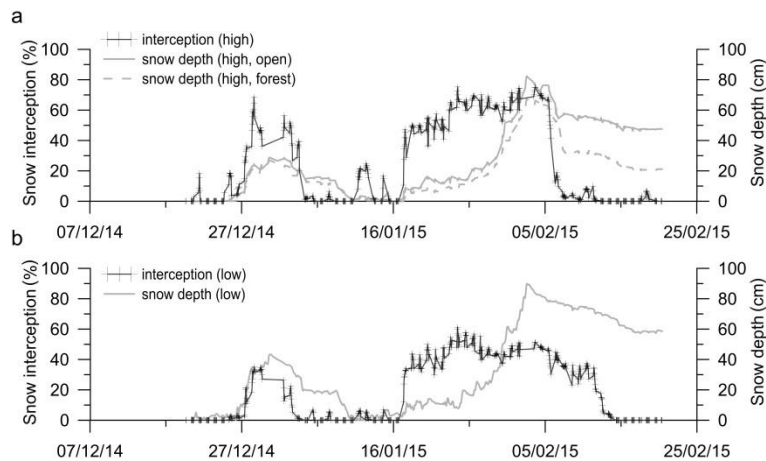
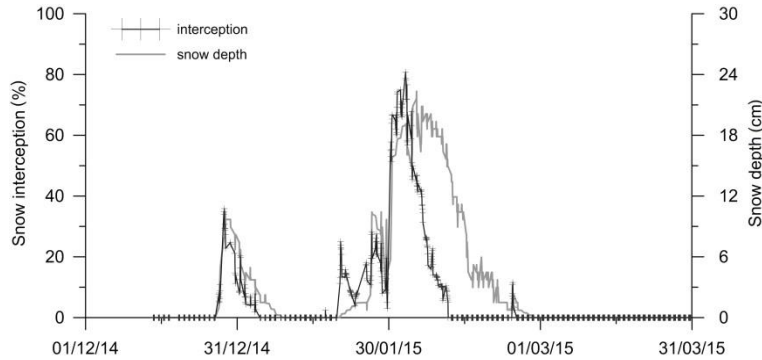


Figure 5.10 Snow interception (SII) dynamics at Hundseck high site (a) and Hundseck low site (b) in the winter 2014/2015. Cross plots refer to the acquired

digital images with time-lapse photography. Snow depths are shown for comparison.



**Figure 5.11** Same as Figure 5.10, but for the results at Hortenkopf forest site.

### 5.3.2 Snow canopy interception

Figure 5.10 and 5.11 demonstrate the snow interception dynamics obtained from images taken by the digital cameras, and the time series of snow depth are also plotted for comparison. Both the snow interception in the Hundseck site and the Hortenkopf site had two high-value phases in this winter, corresponding to the two periods with repeated snowfalls, even though the temporal variations of snow interception were obviously different to those of snow depths. The two figures suggest that snow interception responded to snowfalls more sensitively than snow depth. In the snow accumulation stage, snow interception rose quickly to a high level, and approached a high limit of about 60% on condition of frequent snowfalls. In the following snow accumulation processes in the cold winter, the snow interception could keep at a stable level, close to the maximum snow load of the canopies. However, once the snow depths began decreasing, which meant the recession of the snowpack under high temperature, the snow interception dropped off quickly, and the entire snow unloading could be finished in one week. Therefore, the fluctuations of snow interception were more steeply and frequently than that of snow depth. Both Figure 5.10 and 5.11 suggest that even a light snowfall could lead a significant rise of snow interception. Because in a dense montane forest environment, snow is initially intercepted in the canopies and then accumulate in the ground, but the intercepted snow depletes earlier than the snow upon the ground under the influence of wind and solar irradiation.

Figure 5.11 shows that the snow interception in the oak forest of the Hortenkopf site reached 80% in the beginning of February. It was resulted by the special selection of ROIs (Figure 5.2). As a deciduous forest, there were more gaps between the oak trunks than the spruce in Hundseck. Hence both the snow in the background and foreground

of the oak forest had high brightness in the digital pictures, leading to overestimated snow interception. Even some snow on the ground in far range might be misclassified as snow in canopies. The overlapped snow in the background and foreground could not reflect the snow interception dynamics. Therefore, three small ROIs at trunk-concentrated regions were determined (Figure 5.2), where the canopy snow had large contrast with the background, i.e., the dark oak trunks. The smaller sizes and special positions of the ROIs for the Hortenkopf oak forest resulted in higher snow interception indices (*SII*) during frequent snowfall periods. Consequently, the snow interception for different tree species derived from digital images cannot be compared with each other. According to the time-lapse photos, the intercepted snow quantities in spruce canopies were higher than those in oak canopies under the same condition. However, the derived *SII* time series showed high performance in demonstrating the temporal dynamics of the snow interception in canopies.

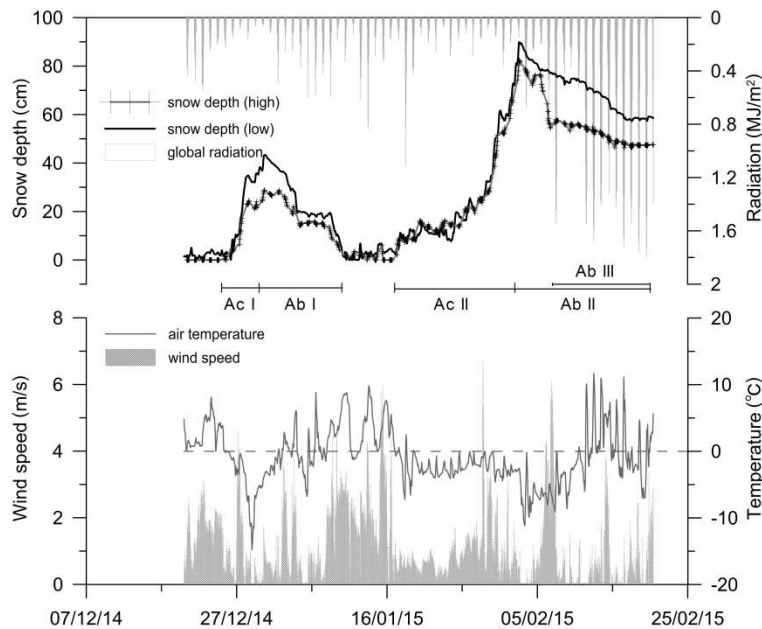


**Figure 5.12** Snow depth dynamics at Hundseck high and low open sites during the winter 2014/2015. Cross plots refer to the acquired digital images. Global radiation, air temperature and wind speed are shown for comparison. The phases (Ac I-II, Ab I-III) refer to the accumulation and ablation phases in Table 5.3.

### 5.3.3 Snow accumulation and ablation

Snow accumulation and ablation processes closely relate to meteorologic elements, such as air temperature, radiation and wind speed. The temporal variation of the snow depths in Hundseck high and low sites are shown in Figure 5.12. At the same time, the

global radiation, air temperature and wind speed observed by AWS are also displayed for comparison. It shows that the snow depth formed the first peak in a cold period when the air temperature even reached the minimum during the winter 2014/2015. The snow depth at the mountain base approached about 40 cm while it was approximately 30 cm at the mountain top. The complex topography and turbulence might promote snow accumulation at the base of the mountain. Incoming solar radiation and wind speed remained at low values as well. Then along with the rising temperature, the snow pack entered into a negative balance and melted completely after ten days. The second frequent-snow period started at about 14 January 2015 when the air temperature again declined below freezing. The snow depth reached the maximum at around 2 February 2015, with 82 cm and 67 cm for the Hundseck low and high sites respectively. After that the snow cover shifted to a negative balance with reduced snowfalls. At the same time, the air temperature rebounded above 0 °C and the incoming solar radiation was also increasing.

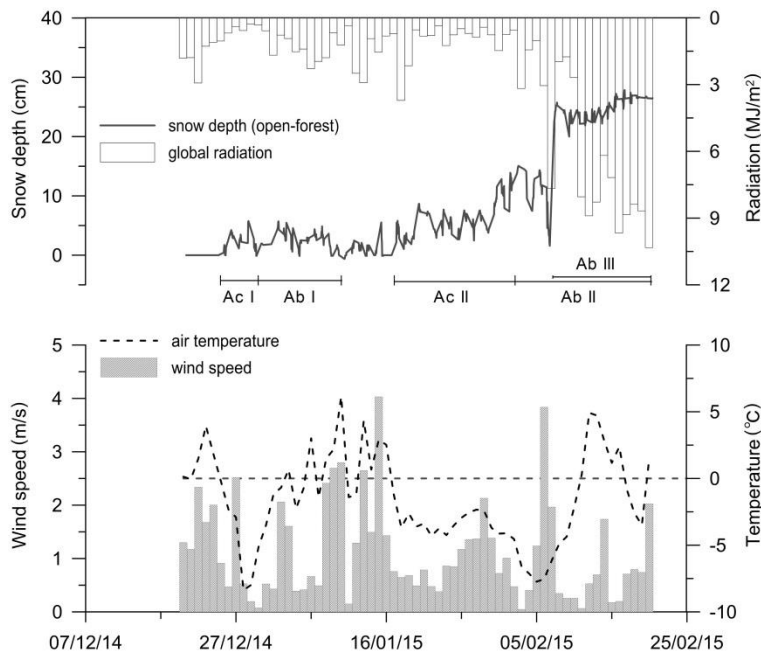


**Figure 5.13** The differences between daily snow depths at Hundseck high open and forest sites for the snow season 2014/2015. Global radiation, air temperature and wind speed are shown for comparison. The phases (Ac I-II, Ab I-III) refer to the accumulation and ablation phases in Table 5.3.

A special event occurred during 5–7 February 2015 should be noted. Both the snow depth of the open and forest sites at the mountain summit dropped markedly about 10–20 cm within the first two days, but the snow depth at the base of the mountain declined smoothly (Figure 5.7 and 5.12). In the third day, 7 February 2015, the snow

depth beneath the forest canopies further decreased 20 cm while the snow depth in the clearing increased 3 cm. According to the meteorological observations by the AWS at the base of the mountain, air temperature kept below freezing and the solar radiation rose up until 7 February (Figure 5.12). However, the wind speed was consistently high during the three days, and the maximum wind speed at the Hundseck low site even approached 16 m/s, which implied that the maximum wind speed might exceed 20 m/s at the mountain summit. Consequently, high wind most likely played the dominant role in the snowpack redistribution in this event. It was also supported by the results shown in Figure 5.13. Wind speed was highest from the afternoon on 6 February to the morning on 7 February, during which the snow depth difference between the open and forest sites at the mountain top firstly dropped quickly then went up sharply.

**Table 5.3** Snow accumulation and ablation on the ground in the winter 2014/2015.

Phases	Parameters	Hundseck high open	Hundseck high forest	Hundseck low open	Hortenkopf forest
Accumulation Phase I (Ac I)	SD (cm)	0.0	0.0	0.0	0.0
	Beginning	25/12/2014	25/12/2014	25/12/2014	27/12/2014
	SD (cm)	28.7	27.0	43.3	10.6
	Ending	30/12/2014	30/12/2014	30/12/2014	28/12/2014
	Duration(d)	10	10	10	2
	Rates(cm/d)	2.9	2.7	4.3	5.3
Accumulation Phase II (Ac II)	SD (cm)	0.0	0.0	0.0	0.0
	Beginning	17/1/2015	17/1/2015	17/1/2015	20/1/2015
	SD (cm)	82.3	67.3	89.9	22.3
	Ending	2/2/2015	2/2/2015	2/2/2015	4/2/2015
	Duration(d)	17	17	17	16
	Rates(cm/d)	4.8	4.0	5.3	1.4
Ablation Phase I (Ab I)	SD (cm)	28.7	27.0	43.3	10.6
	Beginning	30/12/2014	30/12/2014	30/12/2014	28/12/2014
	SD (cm)	0.0	0.0	0.0	0.0
	Ending	10/1/2015	10/1/2015	10/1/2015	8/1/2015
	Duration(d)	12	12	12	12
	Rates(cm/d)	2.4	2.3	3.6	0.9
Ablation Phase II (Ab II)	SD (cm)	82.3	67.3	89.9	22.3
	Beginning	2/2/2015	2/2/2015	2/2/2015	4/2/2015
	SD (cm)	47.5	21.0	58.5	0.8
	Ending	20/2/2015	20/2/2015	20/2/2015	22/2/2015
	Duration(d)	19	19	19	19
	Rates(cm/d)	1.8	2.4	1.7	1.1
Ablation Phase III (Ab III)	SD (cm)	56.6	34.2	76.8	20.1
	Beginning	7/2/2015	7/2/2015	7/2/2015	7/2/2015
	SD (cm)	47.5	21.0	58.5	0.8
	Ending	20/2/2015	20/2/2015	20/2/2015	22/2/2015
	Duration(d)	14	14	14	13
	Rates(cm/d)	0.7	0.9	1.3	1.2

Table 5.3 demonstrates the main snow accumulation and ablation phases in the study area during the winter 2014/2015. It lists the snow depths at the beginning and ending of two accumulation phases and three ablation phases. It should be noted that the ablation phase III is one part of the ablation phase II after the strong wind event during 5–7 February 2015. Table 5.3 shows that both the snowfall magnitude and accumulation rates in Hundseck low clearings were higher than those in the high clearings during the two accumulation phases. With a smaller elevation difference, the weaker wind abrasion and sudden wind slowdown might add the snow accumulation at the base of the mountain. At the Hundseck high site, the snow depths and accumulation rates in the forest were lower than those in the open field in the two accumulation phases because of interception. Compared to the snow accumulation in the Hundseck sites (Black Forest), the snowfall magnitude in the Hortenkopf site (Palatinate Forest) was significantly lower.

In the ablation phase I (Table 5.3), the snowpack in the Hundseck low clearing depleted more quickly than that in the high clearing, which might be resulted by higher temperatures. In contrast, the snow cover at the Hundseck low site showed a lower melting rate in the second ablation phase (2–20 February 2015). The sharp declines of snow depth in the two Hundseck high sites, because of the strong wind during 5–7 February 2015, was responsible for this reversion. It could be proved by the melting process in the ablation phase III, i.e. the latter part of phase II after the high-wind event, the snowpack in the Hundseck low site again melted faster than that at the high clearing. In addition, Table 5.3 also illustrates that the overall melting rate at the Hundseck high forest site was close to or even higher than that at the high open field. Figure 5.13 obviously demonstrates that the difference of snow depth in clearing and forest was increasing during the whole winter. It was similar to the results obtained by Woo and Giesbrecht (2000), who suggested that higher melt rates occurred beneath canopies compared to the clear-cuts, since the enhanced longwave radiation could offset the reduction in shortwave radiation, leading to an increased total energy budget available for melting. However, the snowpack beneath trees at Hundseck high site did not melt faster than that in clear-cuts in ablation phase I (Table 5.3). One reason might be the total snow depths after accumulation phase I were relatively low. Alternatively, the lower incoming solar radiation might weaken the disparity of energy budgets between the forest site and clearing (Figure 5.13). Compared to the snow ablation processes at the Hundseck sites, the snow cover in the Hortenkopf site melted slower in the ablation phase I and II (Table 5.3). As a deciduous forest, the sparse oak forest in Hortenkopf probably did not significantly increase the longwave radiation and delayed the snow ablation.

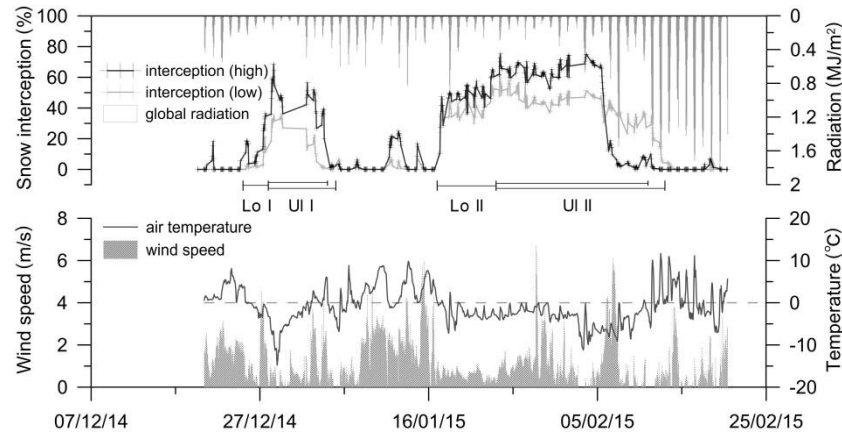


**Figure 5.14** Same as Figure 5.12, but for snow interception. The phases (Lo I-II, UI I-II) refer to the loading and unloading phases in Table 5.4.

**Table 5.4** Snow loading and unloading in canopy cover in the winter 2014/2015.

Phases	Parameters	Hundseck high	Hundseck low	Hortenkopf
Loading Phase I (Lo I)	Interception (%)	0.0	0.0	0.0
	Beginning	25/12/2014	25/12/2014	27/12/2014
	Interception (%)	68.6	35.1	35.9
	Ending	28/12/2014	28/12/2014	28/12/2014
	Duration (d)	4	4	2
	Rates (%/d)	17.2	8.8	18.0
Loading Phase II (Lo II)	Interception (%)	0.0	0.0	0.0
	Beginning	17/1/2015	17/1/2015	20/1/2015
	Interception (%)	75.2	61.2	80.8
	Ending	24/1/2015	24/1/2015	2/2/2015
	Duration (d)	8	8	14
	Rates (%/d)	9.4	7.7	5.8
Unloading Phase I (UI I)	Interception (%)	68.6	35.1	35.9
	Beginning	28/12/2014	28/12/2014	28/12/2014
	Interception (%)	0.0	0.0	0.0
	Ending	5/1/2015	4/1/2015	3/1/2015
	Duration (d)	9	8	7
	Rates (%/d)	7.6	4.4	5.1
Unloading Phase II (UI II)	Interception (%)	75.2	61.2	80.8
	Beginning	24/1/2015	24/1/2015	2/2/2015
	Interception (%)	0.0	0.0	0.0
	Ending	11/2/2015	13/2/2015	10/2/2015
	Duration (d)	19	21	9
	Rates (%/d)	4.0	2.9	9.0

Meteorological factors not only influenced the snowpack on the ground, but also the snow unloading processes in the canopies. Schmidt and Gluns (1991) suggested that

meteorologic conditions were more important than branch growth form in determining snow interception amounts on conifers. Figure 5.14 shows the snow interception dynamics in the Hundseck high and low sites, as well as the meteorologic conditions, such as the global radiation, air temperature and wind speed. Similar to the variation of the snow depths, snow interception in the canopy cover also had two main high-value periods. However, there were some differences between the two periods. In the first period, air temperature only kept below freezing for a short time then increased above 0 °C, and both the incoming solar radiation and wind speed were relatively low. The snow unloading from the canopy cover was most likely a melting process. In the second period, the intercepted snow remained in canopies for a longer time compared to the first one, because the air temperature was consistently below freezing. From 3 February 2015, snow accumulation in canopies turned to snow ablation with reduced snowfalls. Nevertheless, the unloading for the Hundseck high site was more quickly than that for the low site.

Figure 5.14 suggests that the strong-wind event during 6–7 February 2015 might accelerate the snow removal from the canopies at the mountain summit, and its intercepted snow completely disappeared on 9 February 2015. In contrast, the snow interception at the base of the mountain declined slowly during 3–10 February 2015 because of relatively lower wind speed. Since the air temperature was still below freezing during this time period, sublimation might mainly contribute to the snow interception unloading of the canopies in the Hundseck low site. From 11 February 2015, the intercepted snow in the canopies of the mountain base melted quickly and was completely removed until 13 February 2015 with high temperature and radiation. Therefore, the time-lapse photography monitoring revealed that each factor of air temperature, solar radiation and wind speed plays an important role in the snow unloading from the canopy cover. In high-temperature environment, melting process dominant the interception unloading, and sublimation mainly contributes to the snow unloading in freezing conditions, while strong wind can significantly speed up it, especially for mountain tops.

Table 5.4 illustrates the loading and unloading parameters of snow canopy interception at the three sites. Even though the interception index (*SII*) values cannot be compared among different sites, the duration time of snow interception in canopies still contained important information. Table 5.4 shows that the intercepted snow at the Hundseck high site unloaded more slowly than that at the low site in the unloading phase I, which might be led by a lower temperature. However, an opposite process occurred in the unloading phase II, as the high wind during 6–7 February 2015 promoted the unloading process in the Hundseck mountain top. Compared to the coniferous forest in Hundseck, the deciduous forest in Hortenkopf had shorter interception duration because of less leaf area (Table 5.4).

## 5.4 Discussion and conclusions

In this study, a digital camera network was utilized to monitor the snow processes in montane forest environments. It suggests that time-lapse photography is a cost saving and effective technique to execute continuous observations of snow depths and snow canopy interception. However, there are some limitations on this method, many of which have been concluded by Parajka et al. (2012a) and Garvelmann et al. (2013). This study has found some other problems that should be avoided to ensure a successful monitoring. The snow stakes should be fixed stably on the ground, and the branches and grass that are possible to shade the stakes in the camera view must be cleared. Otherwise, it may bring difficulties to the following snow depth interpretation. According to the simultaneous snow survey at the observation sites, the snow depths had high heterogeneity due to the irregularities in the terrain and wind-blow-snow as well as vegetation coverage variation. Therefore, more snow stakes installed in the camera view could contribute to the accuracy of snow depth monitoring with time-lapse photography. For the snow interception observation, it is better to select the canopies that cannot be directly irradiated by the sunshine, because the bright spots on canopies are prone to be misclassified as snow and lead to false snow interception. In addition, as the distance and orientation of the camera to canopies can significantly influence the calculated interception index (*SII*), arranging the cameras in similar positions is favorable for the comparison of snow interception derived from different cameras.

Only the digital images from three cameras were possible to be used, which is a shortage of this study. Fewer observation sites might decrease the representativeness of the data. Nevertheless, the time-lapse photography applied in this study showed a high performance. The digital pictures were utilized to reveal the complex interactions between snow and forest cover in mountainous regions. A semi-automatic procedure was developed to extract snow depths from the camera images, which showed a high consistency with the manual readings and station-based measurements. A mean precision of approximately  $\pm 2$  cm could be achieved, though some abnormal values should be manually corrected in accordance with the digital pictures by the researcher. To quantify the snow interception level, a snow interception index (*SII*) was defined as the mean percentage of snow pixels in the representative ROI polygons in the canopy cover of the camera image. The efficiency of six threshold-self-adaption classifiers (i.e., MaxEntropy, Huang, IsoData, Li, MinError, Otsu) commonly used in binary classification were evaluated in this study. MaxEntropy classification showed a superior performance in differentiating foreground snow from background and in quantifying the snow canopy interception in various illumination conditions. The thresholds selected by MaxEntropy classifier fitted better with the brightness change of

referential snow in the clearings than the other classifications. Thus MaxEntropy classifier is adopted to extract the snow interception information from the digital images.

The time-lapse photography recorded the snow accumulation and ablation processes on the ground as well as the snow loading and unloading in the canopy cover with high temporal resolution. The obtained time series of snow depth and snow interception illustrated that canopy interception responded to meteorologic factors more sensitively than snow depth on the ground. For instance, in the early stage of a snowfall or a frequent-snow period, snow interception can rise quickly to a maximum. In freezing and low-wind condition, the intercepted snow could remain in the canopies for a long time, and sublimation is the main route for the water stored in snow returning to the atmosphere. The upturn in air temperature can let sublimation give way to melting process and lead to higher unloading and ablation rates. Incoming solar radiation contributes to the sublimation and temperature rise. High wind can significantly redistribute the snowpack, e.g. abruptly removing the intercepted snow from the canopies and transporting it to the clearings. The digital images also provided some evidence about how forest cover and elevation influence snow processes. The results suggested that the snow cover underneath canopies has a relative higher ablation rate than that in clearings. The enhanced longwave radiation by the canopies might play an important role in this process. The unloading of intercepted snow in deciduous forest is faster than that in coniferous forest. With a lower elevation difference, the base of a mountain can accumulate more snow than the mountain top, which might be resulted by the terminal distribution of wind. However, higher temperatures in low elevations can accelerate the ablation process, compared to that occurred at mountain tops.

In this study, digital camera network proved to be an effective approach to monitor the particularly complicated snow processes in montane forest environment, which are important components in hydrological models. Therefore, time-lapse photography has the potential to collect valuable snow process information for the setup and validation of snowpack models in the future. Moreover, an extensive camera network in mountainous regions can also contribute to water resource assessment and snow-related disaster precaution.

## Chapter 6

### Summary and concluding remarks

In this thesis, the synergetic application of remote sensing, hydrological modeling and ground observations to the investigation of seasonal snow cover and snow processes has been demonstrated as a case study in the Upper Rhine Region of southwestern Germany. The snow research in this region is a challenging task because of the complicated topography and the consequent high variability in the snow cover. Besides, due to its temperate winters, the frequent alternations of rain and snow also add to the difficulty in studying the snow processes in this area.

As areal snow observations, remotely sensed MODIS snow cover products were selected to reveal the spatial and temporal patterns of the snow distribution, and they were also expected to evaluate the snow simulations by TRAIN model. However, a serious hindrance arose from the apparent snow misclassifications (e.g. snow/cloud confusion) in MODIS snow data. The high cloud fractions on the daily remotely sensed snow maps became another difficulty. Thus, in chapter 2 MODIS 8-day snow cover products were initially applied as substitutes because of their lower cloud coverage, though at the expense of temporal resolution. Ground-based meteorological observations were utilized to discriminate between real and false snow in the remotely sensed snow products. This method was inspired by the temperature-based identification scheme of precipitation phase, which is normally employed in hydrological models. Besides, surface-observed precipitation was also used to reject the overestimated snow of MODIS data for the period with low temperatures. Due to the short persistence of the snow cover over the study area, MODIS 8-day snow products showed some shortcomings in representing the snow time series. Therefore, another algorithm was developed to process MODIS daily snow cover products, as shown in chapter 3. In situ snow depth observations were applied to interpolate the large number of cloud pixels on the remotely sensed snow maps using a conditional probability technique, which showed high efficiency and filled all the cloud gaps of MODIS daily snow images. In addition, a meteorological composite filter was utilized to correct the snow misclassifications of MODIS snow data. This approach showed the ability to produce cloud-free remote sensing snow maps with higher accuracy than the original MODIS snow products. Then in chapter 4 the improved MODIS daily snow cover maps were used to evaluate the simulated snow covered area (SCA) by TRAIN model while the simulated snow water equivalent (SWE) was compared with ground

snow-depth measurements. Based on the SWE simulations for the period 1961-2008, the long-term dynamics of the seasonal snow cover in the study area were analyzed, and the response of snow to the changing temperature and precipitation was also detected. Finally, field observations (chapter 5) were employed to monitor the mountain snow processes, as a comparison with remote sensing and hydrological modeling. A monitoring network consisting of digital cameras and automatic weather stations was set up in two small catchments for this purpose. Time-lapse photography showed promise implementation in capturing the complex processes of snowfall in mountain forest environments, such as snow accumulation and ablation, snow canopy interception loading and unloading, as well as blowing snow. Quantitative information of snow parameters such as snow depth and snow interception was successfully interpreted from the digital pictures, indicating time-lapse photography can be applied as an operational technique for field snow monitoring.

The above four case studies clearly demonstrate both the advantages and shortcomings of field observations, remote sensing and hydrological models in investigating snow cover and snow processes. Sturm (2015) regarded the three methods for snow research as a system with three legs (Appendix B), and he described in a figure (Figure A1) how to combine the three approaches in revealing the snow reality. Sturm (2015) suggested the three snow measuring techniques can be connected for confirmation purpose, and both ground observations and remotely sensed snow data can be applied to force snow models; moreover, scale transformation should be considered in using any two methods of the three.

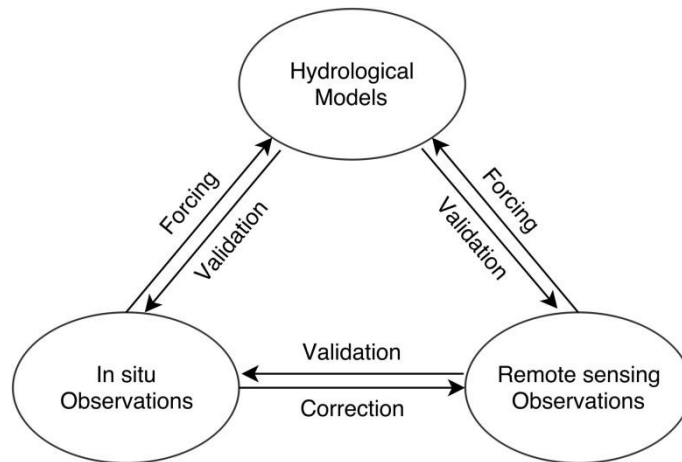


**Figure 6.1** Relations between in situ observations, hydrological models and remote sensing.

However, the two case studies in chapter 2 and 3 of this dissertation suggest that ground observations have the ability to correct remotely sensed hydrological datasets,

and they can also contribute to the cloud-gap-filling schemes of optical remote sensing products. Therefore, the "three-leg-system" should be adjusted to the one shown in Figure 6.1, i.e., there is an arrow from in situ observations to remote sensing observations, indicating the correction function of the former for the latter, which is the major contribution of this thesis.

Blöschl (2011) emphasized the scale issues in hydrology, which is also very important in snow studies. As two kinds of snow observations, in situ monitoring and remote sensing can provide the information of a snowpack at point-scale (1-D data) and areal-scale (2-D data), respectively. With the high reliability and accuracy of the modern meteorological instruments, field measurements can partly achieve "what you see is what you get" at point-scale, just as direct realist suggested for the people's sensing of the world; nonetheless it is always not true for areal-scale (e.g. basin scale) because of the large heterogeneity of hydrological variables. Due to the frequent errors, remotely sensed data are often "what you see is not what you get", even for the areal-scale. An available solution is to improve the remote sensing data to "what you see is what you get" in assistance with ground observations, the applicability of which has been proved in this dissertation. However, remote sensing cannot provide the most valuable snow information for hydrologists, e.g. snowmelt runoff, surface energy balance and snow prediction, which is the major advantage of snow models, i.e. providing "what you want". Because of the similarity between remote sensing and hydrological models (distributed models) in scales, remote-sensing-forced models possess more potential in presenting outstanding hydrological simulations in the future as compared to those forced by ground observations. Moreover, it is more appropriate to update the model output by assimilating remote sensing observations, instead of point-based ground measurements. Zhang et al. (2014) utilized remotely sensed data, alone, to force, calibrate, and update a hydrologic model towards streamflow simulations in an ungauged basin, and positive results were achieved. As great uncertainty still exists in the inversion algorithms of remote sensing for snow parameters, there is broad space for the development of remotely sensed snow products. Besides, more optimization is needed as well for snow hydrological models in the future snow studies.

However, hydrological models are unlikely to produce a snow "reality" due to the lack of local input, boundary data and local calibration, as suggested by Strum (2015). In situ observations and remote sensing are also difficult to reveal the snow "reality", because there are distinct "realities" at different scales. For example, a station located within a city did not observe a snowfall while it actually snowed in the surrounding mountains. The station record of "snow free" was the "reality" in the city, but not for the mountain area. A satellite-based sensor might capture the snow cover with labeling a coarse pixel as "snow covered"; nonetheless the snow absence in the city.

The snow "reality" for a city resident is "snow free", while the information of "snow covered" in the adjacent mountains is very important for a hydrologist, because the followed snowmelt will add to the runoff in the river. Therefore, what the hydrologists can do is to find the best approximation of the snow "reality" with the full utilization of the "three-leg-system" containing in situ observations, remote sensing and hydrological modeling.

As a concluding remark to this doctoral research, the author wishes to emphasize the significance of improving the quality of remotely sensed hydrological data sets with ground observations. Though the differentiated scales lead to a great gap between the two data sources, in situ meteorological records still have the potential to contribute to the error rejection and cloud removal of remote sensing data. Assimilation of remotely sensed observations is an effective technique for relieving the uncertainty of hydrological models, but inferior observations may deteriorate the model performance. Therefore, the fusion of ground-based and remotely sensed observations is indispensable to gain a superior data assimilation in hydrological research.

## Appendix A: Selected snow observation projects, remote sensing sensors and snow models

**Table A1** Selected international or national projects and datasets including in situ snow observations.

Project/Dataset name	Objectives/Observations	Organizers	Start time	References
Global Cryosphere Watch-CryoNet	Snow, Glaciers, Ice sheets, Sea/lake ice, Permafrost	WMO	2007	WMO, 2013
WMO Solid Precipitation Measurement Intercomparison	Snow	WMO-CIMO	1986	Goodison et al., 1998
Global Historical Climatology Network (GHCN)	Snow, Temperature, Precipitation	NOAA-NCDC	1992	Menne et al., 2012
WCRP- Climate and Cryosphere (CliC) International Project	Snow, Glaciers, Sea ice, Sea level	ICSU, WMO	2003	Barry, 2003
CMC-Daily Snow Depth Analysis Data	Snow depth, Snow water equivalent	Canada-CMC	1998	Brown and Brasnett, 2010
Historical Soviet Daily Snow Depth (HSDSD)	Snow depth	USA-NSIDC	2001	Armstrong, 2001
Historical Climatology Network (HCN)	Snow, Temperature, Precipitation	USA-CDIAC	1991	CDIAC et al., 1991
European Climate Assessment & Dataset	Snow depth and other climate elements	ESCN/EUME TNET	1998	Klein Tank et al., 2002

Table A2 Characteristics of optical sensors used for snow detection.

Satellite	Sensors	Spectral bands	Spectral range / $\mu\text{m}$	Spatial resolution /m	Temporal resolution /d	Launch time
Landsat 1-3	MSS	4	0.5-1.1	79	18	1972
Landsat 4-5	MSS/TM	4/7	0.5-1.1/0.45-12.5	30/120	16	1982
Landsat 7	ETM+/PAN	7/1	0.45-12.5	15/30/60	16	1999
Landsat 8	OLI/TIRS	9/2	0.43-2.29/10.6-12.51	15/30/100	16	2013
Terra	MODIS	36	0.4-14.4	250/500/1000	1	1999
Aqua	MODIS	36	0.4-14.4	250/500/1000	1	2002
NOAA	AVHRR	4/5/6	0.58-12.5	1090	1	1978
SPOT 1-3	XS/PAN	3/1	0.50-0.89	10/20	26	1986
SPOT 4/5	XS/PAN	4/1	0.48-1.75	2.5/5/10/20	26	1998
SPOT 6/7	XS/PAN	4/1	0.45-0.89	1.5/6	26	2012
IKONOS	XS/PAN	4/1	0.45-0.85	4/1	3	1999
ERS-2	ASTER-2	7	0.55-12.0	1000	2-3	1995
Envisat	AA/TSR/MERIS	7/15	0.55-12.0/0.39-1.04	1000/300	2-3	2002

**Table A3** Characteristics of passive (PM) and active (AM) microwave sensors used for snow detection.

Satellite	Sensor	Bands	Frequencies /GHz	Spatial resolution /km/m	Temporal resolution /d	Launch time
	Nimbus-7	5	6.6/10.7/18.0/21.0/37.0	30-160 km	1	1978
	DMSP	4	19.3/22.2/37.0/85.5	13-70 km	1	1987
PM	Aqua	6	6.9/10.7/18.7/23.8/36.5/89.0	5-50 km	1	2002
	ADEOS-II	8	6.9/10.7/18.7/23.8/36.5/89.0/50.3/52.8	5-50 km	1	2002
	GCOM-W1	7	6.9/7.3/10.7/18.7/23.8/36.5/89.0	5-50 km	1	2012
	ADEOS I	Ku	14	50 km	2	1996
	ADEOS II	Ku	13.4	25 km	1	2002
	QuickSCAT	Ku	13.4	25 km	1	1999
	MetOp	C	5.3	25/50 km	2	2005
	RADARSAT	C	5.3	8-100 m	24	1995
AM	RADARSAT-2	C	5.4	3-100 m	24	2007
	ERS 1-2	C	5.3	30 m	35	1991
	Envisat	C	5.3	30/150/1000 m	35	2001
	JERS-1	L	1.275	18 m	44	1992
	Terra	X	9.6	1/3/18 m	11	2007

**Table A4** Selected snow hydrological models (Rutter et al., 2009; Slater et al., 2001).

Snow Model	Identifier	Model
2LM	2LM	Yamazaki, (2001); Yamazaki et al., (2004)
ACASA	ACA	Pyles et al., (2000)
BATS	BATS	Dickinson et al. (1993); Yang et al., (1997)
CLASS	CLA	Bartlett et al., (2006); Verseghy (1991)
CLM2-TOP	CLI	Bonan et al., (2002); Niu and Yang (2003)
CLM3	CL3	Lewis et al., (2004); Oleson et al., (2004)
CRHM	CRH	Hedstrom et al., (2001); Pomeroy et al., (2007)
CROCUS	CROCUS	Brun et al., (1989, 1992)
ESCIMO	ESC	Strasser et al., (2002, 2008)
ISBA-ES	ISE	Boone and Etchevers (2001)
JULES	JUL	Blyth et al., (2006)
MATSIRO	MAT	Takata et al., (2003)
MOSES	MOS	Cox et al., (1999); Essery et al., (2003)
NCEP	NCEP	Koren et al., (1999)
NOAH-LSM	NOH	Ek et al., (2003)
PLACE	PLACE	Wetzel and Boone (1995)
RCA	RCA	Kjellström et al., (2005), Samuelsson et al., (2006)
SNOW-17	S17	Anderson (1973, 1976)
SAST	SAS	Jin et al., (1999a, 1999b)
SLAM	SLAM	Desborough (1999)
SNOWCAN	SNO	Tribbeck (2002), Tribbeck et al., (2004, 2006)
SNOWPACK	SNP	Bartelt and Lehning (2002); Lehning et al., (2002)
SRGM	SRG	Gelfan et al., (2004)
SSiB3	SSI	Xue et al., (2003)
SWAP	SWAP	Gusev and Nasonova (1998)
TRAIN	TRAIN	Menzel et al., (2009); Wimmer et al., (2009)
UGAMP	UGAMP	Gedney (1995)
VIC	VIC	Cherkauer et al., (2003)
UKMO	UKMO	Warrilow and Buckley (1989)

## Appendix B: Relations between ground observations, remote sensing and snow models

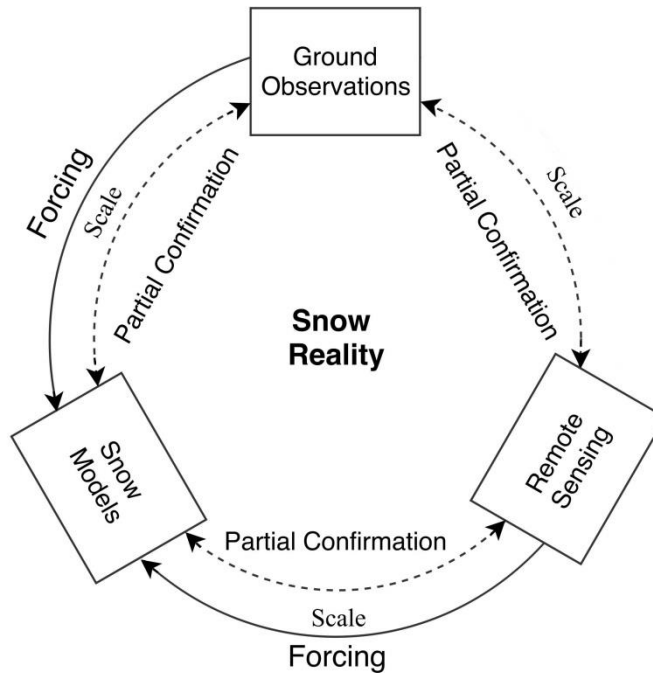


**Figure A1** Relations between ground snow observations, hydrological modeling and remote sensing, suggested by Sturm (2015).

The following excerpt is from Sturm (2015), which provides insightful guidance for our snow research in future: "Within the snow research community (including the snow remote sensing community) a consensus has been building that modeling ultimately achieves its best results (and greatest accuracy) when it is used as one of three legs of a system that consists of (1) field measurements, (2) remote sensing, and (3) modeling and data assimilation (Figure A1). Each of these legs has strengths and weaknesses, as suggested in the figure and alluded to in the preceding text. Field measurements can be in error, but more often provide good values. They are, however, frequently located in the wrong place as far as being representative, and they are usually sparse in number so they fail to capture the local heterogeneity. Nonetheless, they have the greatest reliability of the three legs and are essential to any successful modeling effort. Remote sensing products have the coverage (both in space and time) we need, but no sensor to date has been able to provide all of the snow parameters that are needed, and outright errors are frequent where reduction algorithms exceed their range of applicability. The products often lack the resolution needed by the modeling, requiring

subgrid approximations. The models themselves are the crucible where we see how well we understand the physics of the snow-covered world, but the real physics are still far more complicated than we can currently represent numerically, and even when we have mastered parts of that problem, we rarely know the boundary conditions and forcing functions for all grid cells in the model domain, again leading to errors. But when the strengths of each leg are used to compensate for the weaknesses in the other legs, the system (in principle) should converge toward results that are increasingly realistic, a goal that more and more researchers seem to be endorsing."

## Bibliography

- Aizen, E.M., Aizen, V.B., Melack, J.M., Krenke, A.N., 2000. Heat exchange during snow ablation in plains and mountains of Eurasia. *Journal of Geophysical Research*, 105, 013–027. doi:10.1029/2000JD900279.
- Aizen, V.B., Aizen, E.M., Melack, J., Nakamura, T., Kobayashi, S., 2002. Estimation of the energy used to melt snow in the Tien Shan mountains and Japanese Islands. *Global and Planetary Change*, 32, 349–359. doi:10.1016/S0921-8181(02)00075-9
- Anderson, E.A., 1973. National Weather Service River Forecast System-Snow Accumulation and Ablation Model. NOAA Tech. Memo. NWSHYDRO-17, 217 pp., U.S. Department of Commerce, Silver Spring, Md.
- Anderson, E.A., 1976. A point energy and mass balance model of a snowcover. NOAA Tech. Rep. 19, 150 pp., U.S. Department of Commerce, Silver Spring, Md.
- Andreadis, K.M., Lettenmaier, D.P., 2006. Assimilating remotely sensed snow observations into a macroscale hydrology model. *Advances in Water Resources*, 29, 872–886. doi:10.1016/j.advwatres.2005.08.004.
- Andreadis, K.M., Storck, P., Lettenmaier, D.P., 2009. Modeling snow accumulation and ablation processes in forested environments. *Water Resources Research*, 45, W05429. doi:10.1029/2008WR 007042.
- Armstrong, R., 2001. Historical Soviet daily snow depth version 2 (HSDSD). Boulder, CO: National Snow and Ice Data Center. CD-ROM. <http://dx.doi.org/10.7265/N5JW8BS3>.
- Armstrong, R.L., Brun, E., 2008. *Snow and Climate: Physical Processes, Surface Energy Exchange and Modeling*, Cambridge University Press. Cambridge, UK.
- Arnell, N.W., 1999. Climate change and global water resources. *Global Environmental Change*, 9, S31–S49.
- Ault, T. W., Czajkowski, K. P., Benko, T., Coss, J., Struble, J., Spongberg, A., Templin, M., Gross, C., 2006. Validation of the MODIS snow product and cloud mask using student and NWS cooperative station observations in the Lower Great Lakes Region. *Remote Sensing of Environment*, 105, 341–353. doi:10.1016/j.rse.2006.07.004.
- Barnes, W.L., Pagano, T.S., Salomonson, V.V., 1998. Prelaunch characteristics of the Moderate Resolution Imaging Spectroradiometer (MODIS) on EOS-AM1, *IEEE Transactions on Geoscience and Remote Sensing*, 36, 1088–1100.
- Barnett T.P., Adam, J.C., Lettenmaier, D.P., 2005. Potential impacts of a warming climate on water availability in snow-dominated regions, *Nature*, 438, 303–309. doi:10.1038/nature 04141.

- Barry, R.G., 2003. Mountain cryospheric studies and the WCRP climate and cryosphere (CliC) project. *Journal of Hydrology*, 282, 177–181. doi:10.1016/S0022-1694(03)00253-1.
- Bartelt, P., Lehning, M., 2002. A physical SNOWPACK model for the Swiss avalanche warning—Part I: Numerical model. *Cold Regions Science and Technology*, 35, 123–145. doi:10.1016/S0165-232X(02)00074-5.
- Bartlett, P.A., MacKay, M.D., Verseghy, D.L., 2006. Modified snow algorithms in the Canadian Land Surface Scheme: Model runs and sensitivity analysis at three boreal forest stands. *Atmosphere-Ocean*, 44, 207–222. doi:10.3137/ao.440301.
- Bewley, D., Essery, R., Pomeroy, J., Ménard, C., 2010. Measurements and modelling of snowmelt and turbulent heat fluxes over shrub tundra. *Hydrology and Earth System Sciences*, 14, 1331–1340. doi:10.5194/hess-14-1331-2010.
- Blanchet, J., Lehning, M., 2010. Mapping snow depth return levels: Smooth spatial modeling versus station interpolation. *Hydrology and Earth System Sciences*, 14, 2527–2544. doi:10.5194/hess-14-2527-2010.
- Blöschl, G., Kirnbauer, R., Gutknecht, D., 1991. Distributed snowmelt simulations in an alpine catchment: 1. Model evaluation on the basis of snow cover patterns. *Water Resources Research*, 27, 3171–3179.
- Blöschl, G., 2011. Scaling in hydrology. *Hydrological Processes*, 15, 709–711. doi:10.1002/hyp.432.
- Blyth, E., Best, M., Cox, P., Essery, R., Boucher, O., Harding, R., Prentice, C., 2006. JULES: A new community land surface model, *Global Change Newsletter*, 66, 9–11.
- BMUNR (Bundesministerium für Umwelt, Naturschutz und Reaktorsicherheit), 2003. *Hydrologischer Atlas von Deutschland*. Bonn/ Berlin, Germany.
- Bonan, G.B., Oleson, K.W., Vertenstein, M., Levis, S., Zeng, X.B., Dai, Y.J., Dickinson, R.E., Yang, Z.L., 2002. The land surface climatology of the community land model coupled to the NCAR community climate model. *Journal of Climate*, 15, 3123 – 3149.
- Boone, A., Etchevers, P., 2001. An intercomparison of three snow schemes of varying complexity coupled to the same land surface model: Local-scale evaluation at an Alpine site. *Journal of Geophysical Research*, 2, 374–394.
- Brown, L., Thorne, R., Woo, M.K., 2008. Using satellite imagery to validate snow distribution simulated by a hydrological model in large northern basins. *Hydrological Processes*, 22, 2777–2787. doi:10.1002/hyp.6999.
- Brown, R.D., 2000. Northern Hemisphere snow cover variability and change, 1915–97, *Journal of Climate*, 13, 2339–2355.
- Brown, R.D., Brasnett, B., 2010. Canadian Meteorological Centre (CMC) Daily Snow Depth Analysis Data. Environment Canada, 2010. Boulder, Colorado USA: National Snow and Ice Data Center.

- Brown, R., Derksen, C., and Wang, L., 2010. A multi-data set analysis of variability and change in Arctic spring snow cover extent, 1967–2008. *Journal of Geophysical Research*, 115, D16111. doi:10.1029/2010JD013 975.
- Brown, R.D., Mote P.W., 2009. The response of Northern Hemisphere snow cover to a changing climate, *Journal of Climate*, 22, 2124–2145, doi:10.1175/2008 JCLI2665.1.
- Brown, R.D. Robinson, D.A., 2011. Northern Hemisphere spring snow cover variability and change over 1922–2010 including an assessment of uncertainty. *The Cryosphere*, 5, 219–229. doi:10.5194/tc-5-219-2011, 2011.
- Brucker, L., Picard, G., Fily, M., 2010. Snow grain-size profiles deduced from microwave snow emissivities in Antarctica. *Journal of Glaciology*, 56, 514–526. doi:10.3189/002214310792447806.
- Brun, E., David, P., Sudul, M., 1992. A numerical model to simulate snow-cover stratigraphy for operational avalanche forecasting. *Journal of Glaciology*, 38, 13–22.
- Brun, E., Martin, E., Simon, V., Gendre, C., Coleou, C., 1989. An energy and mass model of snow cover suitable for operational avalanche forecasting. *Journal of Glaciology*, 35, 333–341.
- Bründl, M., 1997. Snow interception and meltwater transport in subalpine forests. Thesis, ETH Zürich, Switzerland.
- Brutel-Vuilmet, C., Menegoz, M., Krinner, G., 2013. An analysis of present and future seasonal Northern Hemisphere land snow cover simulated by CMIP5 coupled climate models. *The Cryosphere*, 7, 67–80. doi:10.5194/tc-7-67-2013.
- Carrera-Hernández, J.J., Gaskin, S.J., 2007. Spatio temporal analysis of daily precipitation and temperature in the Basin of Mexico. *Journal of Hydrology*. 336, 231–249. doi:10.1016/j.jhydrol.2006.12.021.
- CDIAC et al., 1991. Historical Climatology Network (HCN) Daily Temperature, Precipitation, and Snow Observations for 1871-1997. Research Data Archive at the National Center for Atmospheric Research, Computational and Information Systems Laboratory. <http://rda.ucar.edu/datasets/ds511.0/>.
- Cherkauer, K.A., Bowling, L.C., Lettenmaier D.P., 2003. Variable infiltration capacity cold land process model updates. *Global and Planetary Change*, 38, 151–159, doi:10.1016/S0921-8181(03)00025-0.
- Collins, T.J., 2007. ImageJ for microscopy. *Biotechniques*, 43, 25–30.
- Cox, P.M., Betts, R.A., Bunton, C.B., Essery, R.L.H., Rowntree, P.R., Smith, J., 1999. The impact of new land surface physics on the GCM simulation of climate and climate sensitivity. *Climate Dynamics*, 15, 183–203. doi: 10.1007/s00382005 0276.
- Davis, R.E., McKenzie, J.C., Jordan, R., 2006. Distributed snow process modeling: an image processing approach. *Hydrological Processes*, 9, 865–875. doi:10.1002/hyp. 3360090804.

- Deems J.S., Painter, T.H., Finnegan, D.C., 2013. Lidar measurement of snow depth: a review. *Journal of Glaciology*, 59, 467–479. doi:10.3189/2013JoG12J 154.
- D'Eon, R., 2004. Snow depth as a function of canopy cover and other site attributes in a forested ungulate winter range in southeast British Columbia. *BC Journal of Ecosystems and Management*, 3, 1–9.
- Déry, S.J., Salomonson, V.V., Stieglitz, M., Hall, D.K., Appel, I., 2005. An approach to using snow areal depletion curves inferred from MODIS and its application to land-surface modelling in Alaska. *Hydrological Processes*, 19, 2755–2774. doi:10.1002/hyp5784.
- Desborough, D.E., 1999, Surface energy balance complexity in GCM land surface models. *Climate Dynamics*, 15, 389–403.
- DeWalle, D.R., Rango, A., 2008. *Principles of snow hydrology*. Cambridge University Press. Cambridge, UK.
- Dickinson, R.E., Henderson-Sellers, A., Kennedy, P.J., 1993. Biosphere–Atmosphere Transfer Scheme (BATS) Version 1e as coupled to the NCAR Community Climate Model. NCAR Tech. Note TN-387 1 STR, 72 pp.
- Dietz, A.J., Kuenzer, C., Gessner, U., Dech, S., 2012. Remote sensing of snow – a review of available methods, *International Journal of Remote Sensing*, 33, 4094–4134. [http:// dx.doi.org/10.1080/01431161.2011.640964](http://dx.doi.org/10.1080/01431161.2011.640964).
- Dietz, A.J., Wohner, C., Kuenzer, C., 2012. European Snow Cover Characteristics between 2000 and 2011 Derived from Improved MODIS Daily Snow Cover Products. *Remote Sensing*, 4, 2432–2454. doi:10.3390/rs4082432.
- Domine, F., 2011. Physical properties of snow. In: *Encyclopedia of snow, ice and glaciers*. Edited by: Singh, V.P., Singh, P., Haritashya, U.K., Springer, Dordrecht. The Netherlands. pp. 859–862.
- Dong, C., Menzel, L., 2016a. Improving the accuracy of MODIS 8-day snow products with in situ temperature and precipitation data. *Journal of Hydrology*, 534, 466–477. <http://dx.doi.org/10.1016/j.jhydrol.2015.12.065>.
- Dong, C., Menzel, L., 2016b. Producing cloud-free MODIS snow cover products with conditional probability interpolation and meteorological data. in press.
- Dong, J.R., Peters-Lidard, C., 2010. On the relationship between temperature and MODIS snow cover retrieval errors in the Western US. *IEEE Journal of Selected Topics in Applied Earth Observations and Remote Sensing*, 3, 132–140. doi:10.1109/JSTARS.2009.2039698.
- Dressler, K.A., Leavesley, G.H., Bales, R.C., Fassnacht, S.R., 2006. Evaluation of gridded snow water equivalent and satellite snow cover products for mountain basins in a hydrologic model. *Hydrological Processes*, 20, 673–688. doi:10.1002/hyp.6130.

- Dyck, S., Peschke, G., 1995. *Grundlagen der Hydrologie*, 3 ed., Verlag für Bauwesen, Berlin, Germany, 536 pp.
- Ek, M.B., Mitchell, K.E., Lin, Y., Rogers, E., Grunmann, P., Koren, V., Gayno, G., Tarpley, J.D., 2003. Implementation of Noah land surface model advances in the National Centers for Environmental Prediction operational mesoscale Eta model. *Journal of Geophysical Research*, 108, 8851. doi:10.1029/2002JD003296.
- Essery, R.L.H., Best, M.J., Betts, R.A., Cox, P.M., Taylor, C.M., 2003. Explicit representation of subgrid heterogeneity in a GCM land surface scheme. *Journal of Hydrometeorology*, 4, 530–543.
- Essery, R., Morin, S., Lejeune, Y., Ménard, C., 2012. A comparison of 1701 snow models using observations from an alpine site. *Advances in Water Resources*, 55, 131–148. <http://dx.doi.org/10.1016/j.advwatres.2012.07.013>.
- Essery, R., Morin, S., Lejeune, Y., Ménard, C.B., 2013. A comparison of 1701 snow models using observations from an alpine site, *Advances in Water Resources*, 55, 131–148. doi:10.1016/j.advwatres.2012.07.013.
- Essery, R., Pomeroy, J., Parvianen, J., Storck, P., 2003. Sublimation of snow from coniferous forests in a climate model. *Journal of Climate*, 16, 1855–1864.
- Estilow, T.W., Young, A.H., Robinson, D.A., 2015. A long-term Northern Hemisphere snow cover extent data record for climate studies and monitoring. *Earth System Science Data*, 7, 137–142. doi:10.5194/essd-7-137-2015.
- Feng, S., Hu, Q., 2007. Changes in winter snowfall/precipitation ratio in the contiguous United States, *Journal of Geophysical Research*, 112, D15109. doi:10.1029/2007JD008397.
- Fitzharris, B.B., 1996. The cryosphere: Changes and their impacts. In: *Climate Change 1995: Impacts, Adaptions, and Mitigation of Climate Change: Scientific-Technical Analyses*. Edited by: Watson, R.T., Zinyowera, M.C., Moss, R.H., IPCC (WMO, UNEP). Cambridge University Press. Cambridge, UK. pp. 241–265.
- Floyd, W., Weiler, M., 2008. Measuring snow accumulation and ablation dynamics during rain-on-snow events: innovative measurement techniques. *Hydrological Processes*, 22, 4805–4812. doi:10.1002/hyp.7142.
- Foppa, N., Seiz, G., 2012. Inter-annual variations of snow days over Switzerland from 2000–2010 derived from MODIS satellite data. *The Cryosphere*, 6, 331–342. doi:10.5194/tc-6-331-2012.
- Foppa, N., Stoffel, A., Meister, R., 2007. Synergy of in situ and space borne observation for snow depth mapping in the Swiss Alps. *International Journal of Applied Earth Observation and Geoinformation*, 9, 294–310. doi:10.1016/j.jag.2006.10.001.
- Foster, J., Sun, C., Walker, J.P., Kelly, R., Chang, A., Dong, J., Powell, H., 2005. Quantifying the uncertainty in passive microwave snow water equivalent

- observations. *Remote Sensing of Environment*, 94, 187–203. doi:10.1016/j.rse.2004.09.012.
- Franz, K.J., Karsten, L.R., 2013. Calibration of a distributed snow model using MODIS snow covered area data. *Journal of Hydrology*, 494, 160–175. <http://dx.doi.org/10.1016/j.jhydrol.2013.04.026>.
- Gafurov, A., Bárdossy, A., 2009. Cloud removal methodology from MODIS snow cover product. *Hydrology and Earth System Sciences*, 13, 1361–1373. doi:10.5194/hess-13-1361-2009.
- Gafurov, A., Vorogushyn1, S., Farinotti1, D., Duethmann1, D., Merkushev, A., Merz1, B., 2015. Snow-cover reconstruction methodology for mountainous regions based on historic in situ observations and recent remote sensing data. *The Cryosphere*, 9, 451–463. doi:10.5194/tc-9-451-2015.
- Gallet, J.C., Domine, F., Zender, C., Picard, G., 2009. Measurement of the specific surface area of snow using infrared reflectance in an integrating sphere at 1310 and 1550 nm. *The Cryosphere*, 3, 167–182. doi:10.5194/tc-3-167-2009.
- Gao, Y., Xie, H., Lu, N., Yao, T., Liang, T., 2010. Toward advanced daily cloud-free snow cover and snow water equivalent products from Terra–Aqua MODIS and Aqua AMSR-E measurements. *Journal of Hydrology*, 385, 23–35. doi:10.1016/j.jhydrol.2010.01.022.
- Gao, Y., Lu, N., Yao, T.D., 2011. Evaluation of a cloud-gap-filled MODIS daily snow cover product over the Pacific Northwest USA. *Journal of Hydrology*, 404, 157–165. doi:10.1016/j.jhydrol.2011.04.026.
- Garvelmann, J., Pohl, S., Weiler, M., 2013. From observation to the quantification of snow processes with a time-lapse camera network. *Hydrology and Earth System Sciences*, 17, 1415–1429. doi:10.5194/hess-17-1415-2013.
- Gedney, N., 1995. Development of a land surface scheme and its application to the Sahel. Thesis, University of Reading, UK.
- Gelfan, A.N., Pomeroy, J.W., Kuchment, L.S., 2004. Modeling forest cover influences on snow accumulation, sublimation, and melt. *Journal of Hydrometeorology*, 5, 785–803.
- Gilbert, R.O., 1987. Sen's nonparametric estimator of slope. In: *Statistical methods for environmental pollution monitoring*. Edited by: Gilbert, R.O., John Wiley and Sons, pp. 217–219.
- Gillan, B.J., Harper, J.T., Moore, J.N., 2010. Timing of present and future snowmelt from high elevations in northwest Montana. *Water Resources Research*, 46, W01507. doi:10.1029/2009WR007861.
- Goodison, B.E., Louie, P.Y.T., Yang, D., 1998. WMO Solid Precipitation Measurement Intercomparison - Final Report, (WMO/TD-No. 872, IOM 67).

- Grody, N.C., Basist, A.N., 1996. Global identification of snow cover using SSM/I measurements. *IEEE Transactions on Geoscience and Remote Sensing*, 34, 237–249.
- Grusson, Y., Sun, X., Gascoin, S., Sauvage, S., Srinivasan, R., Anctil, F., Sánchez-Pérez, J.M., 2015. Assessing the capability of the SWAT model to simulate snow, snow melt and streamflow dynamics over an alpine watershed. *Journal of Hydrology*, 531, 574–588. doi:10.1016/j.jhydrol.2015.10.070.
- Gusev, Ye.M., Nasonova, O.N., 1998. The land surface parameterization scheme SWAP: Description and partial validation. *Global and Planetary Change*, 19, 63–86.
- Hall, D.K., Foster, J.L., DiGirolamo, N., Riggs, G.A., 2012. Snow cover, snowmelt timing and stream power in the Wind River Range, Wyoming. *Geomorphology*, 137, 87–93. <http://dx.doi.org/10.1016/j.geomorph.2010.11.011>.
- Hall, D.K., Martinec, J., 1985. *Remote Sensing of Ice and Snow*, Chapman and Hall, London, United Kingdom and New York, USA.
- Hall, D.K., Riggs, G.A., Salomonson, V.V., DiGirolamo, N.E., Bayr, K.J. 2002. MODIS snow-cover products. *Remote Sensing of Environment*, 83, 181–194.
- Hall, D.K., Riggs, G.A., 2007. Accuracy assessment of the MODIS snow products. *Hydrological Processes*, 21, 1534–1547. doi:10.1002/hyp.6715.
- Hall, D.K., Riggs, G.A., Foster, J.L., Kumar, S.V., 2010. Development and validation of a cloud-gap filled MODIS daily snow-cover product, *Remote Sensing of Environment*, 114, 496–503. doi:10.1016/j.rse.2009.10.007.
- Hedstrom, N.R., Granger, R.J., Pomeroy, J.W., Gray, D.M., Brown T., Little. J.L., 2001. Enhanced indicators of land use change and climate variability impacts on prairie hydrology using the Cold Regions Hydrological Model. *Proceedings of the 58th Eastern Snow Conference*, Ottawa, Ontario, Canada.
- Hinterding, A., 2003. Entwicklung hybrider Interpolationsverfahren für den automatisierten Betrieb am Beispiel meteorologischer Größen, *Inst. f. Geoinformatik, Westfälische Wilhelms Universität Münster, IfGI prints*, 19, Münster, Germany. (in German)
- Hirabayashi, Y., Kanae, S., Motoya, K., Masuda, K., Döll, P., 2008. A 59-year (1948-2006) global meteorological forcing data set for land surface models. Part II: Global snowfall estimation. *Hydrological Research Letters*, 2, 65–69. doi:10.3178/HRL.2.65.
- Hirsch, R.M., Slack, J.R., 1984. A nonparametric trend test for seasonal data with serial dependence. *Water Resources Research*, 20, 727–32.
- Hirsch R.M., Slack J.R., Smith, R.A., 1982. Techniques of trend analysis for monthly water quality data. *Water Resources Research*, 18, 107–21.
- Homan, J.W., Luce, C.H., McNamara, J.P., Glenn, N.F., 2011. Improvement of distributed snowmelt energy balance modeling with MODIS-based NDSI-derived fractional snow-covered area data, *Hydrological Processes*, 25, 650–660. doi:10.1002/hyp.7857.

- Huang, L. K., and Wang, M.J., 1995. Image thresholding by minimizing the measure of fuzziness. *Pattern Recognition*, 28, 41–51.
- Hüsler, F., Jonas, T., Riffler, M., Musial, J.P., Wunderle, S., 2014. A satellite-based snow cover climatology (1985-2011) for the European Alps derived from AVHRR data. *The Cryosphere*, 8, 73–90. doi:10.5194/tc-8-73-2014.
- IPCC., 2007. *Climate Change 2007: The Physical Science Basis. Contribution of Working Group I to the Fourth Assessment Report of the Intergovernmental Panel on Climate Change*. Edited by: Solomon, S., Qin, D., Manning, M., Chen, Z., Marquis, M., Averyt, K. B., Tignor, M., Miller, H. L., Cambridge University Press, Cambridge, United Kingdom and New York, NY, USA, 996 pp.
- IPCC., 2013. *Climate Change 2013: The Physical Science Basis. Contribution of Working Group I to the Fifth Assessment Report of the Intergovernmental Panel on Climate Change*. Edited by Stocker, T.F., Qin, D., Plattner, G.K., Tignor, M., Allen, S.K., Boschung, J., Nauels, A., Xia, Y., Bex, V., Midgley, P.M., Cambridge University Press, Cambridge, United Kingdom and New York, USA. doi:10.1017/CBO9781107415324.
- Jarvis, C.H., Stuart, N., 2001. A comparison among strategies for interpolating maximum and minimum daily air temperatures. Part II: The interaction between number of guiding variables and the type of interpolation method. *Journal of Applied Meteorology*, 40, 1075–1084.
- Jasper, K., Gurtz, J., Lang, H., 2002. Advanced flood forecasting in Alpine watersheds by coupling meteorological observations and forecasts with a distributed hydrological model. *Journal of Hydrology*, 267, 40–52. doi:10.1016/S0022-1694(02)00138-5.
- Jedlovec, G., 2009. Automated detection of clouds in satellite imagery. In: *Advances in Geoscience and Remote Sensing*. Edited by: Jedlovec G., InTech, <http://www.intechopen.com/books/advances-in-geoscience-and-remote-sensing/automated-detection-of-clouds-in-satellite-magery>.
- Jin, J., Gao, X. Sorooshian, S., Yang, Z.L., Bales, R., Dickinson, R.E., Sun, S.F., Wu G.X., 1999a. One-dimensional snow water and energy balance model for vegetated surfaces. *Hydrological Processes*, 13, 2467–2482.
- Jin, J., Gao, X., Yang, Z.L., Bales, R.C., Sorooshian, S., Dickinson R.E., 1999b. Comparative analyses of physically based snowmelt models for climate simulations. *Journal of Climate*, 12, 2643–2657.
- Jin, S.G., Qian, X.D., Kutoglu, H., 2016. Snow depth variations estimated from GPS-Reflectometry: A case study in Alaska from L2P SNR data, *Remote Sensing*, 8, 63. doi:10.3390/rs8010063.
- Jin, Z., Charlock, T.P., Yang, P., Xie, Y., Miller, W., 2008. Snow optical properties for different particle shapes with application to snow grain size retrieval and

- MODIS/CERES radiance comparison over Antarctica. *Remote Sensing of Environment*, 112, 3563–3581. doi:10.1016/j.rse.2008.04.011.
- Kapur, J.N., Sahoo, P.K., Wong, A.K.C., 1985. A new method for gray-level picture thresholding using the entropy of the histogram. *Computer Vision, Graphics, and Image processing*, 29, 273–285.
- Kelly, R.E., Chang, A.T., Tsang, L., Foster, J.L., 2003. A prototype AMSR-E global snow area and snow depth algorithm. *IEEE Transactions on Geoscience and Remote Sensing*, 41, 230–242.
- Kendall, M.G., 1975. Rank correlation measures. Charles Griffin, London, UK.
- Kendall, M.G., Gibbons, J.D., 1990. Rank correlation methods. Edward Arnold, London, UK.
- Kirchner, P.B., Bales, R.C., Molotch, N.P., Flanagan, J., Guo, Q., 2014. LiDAR measurement of seasonal snow accumulation along an elevation gradient in the southern Sierra Nevada, California, *Hydrology and Earth System Sciences*, 18, 4261–4275. doi:10.5194/hess-18-4261-2014.
- Kittler, J., Illingworth, J., 1986. Minimum error thresholding, *Pattern Recognition*, 19, 41–47.
- Kjellström, E., Bärring, L., Gollvik, S., Hansson, U., Jones, C., Samuelsson, P., Rummukainen, M., Ullerstig, A., Willén, U., Wyser, K., 2005. A140-year simulation of European climate with the new version of the Rossby Centre regional atmospheric climate model (RCA3). Rep. Meteorol. Climatol., 108, 54 pp., Swedish Meteorological and Hydrological Institute, Norrköping, Sweden.
- Klein, A.G., Barnett, A.C., 2003. Validation of daily MODIS snow cover maps of the Upper Rio Grande River Basin for the 2000-2001 snow year. *Remote Sensing of Environment*, 86, 162–176. doi:10.1016/S00344257(03)00097-X.
- Klein Tank, A.M.G. et al., 2002. Daily dataset of 20th-century surface air temperature and precipitation series for the European Climate Assessment. *International Journal of Climatology*, 22, 1441–1453. doi:10.1002/joc.773.
- Knowles, N., Dettinger, M.D., Cayan, D.R., 2006. Trends in snowfall versus rainfall in the Western United States. *Journal of Climate*, 19, 4545–4559. <http://dx.doi.org/10.1175/JCLI3850.1>.
- Koenig, L.S., Steig, E.J., Wienbrenner, D.P., Shuman, C.A., 2007. A link between microwave extinction length, firn thermal diffusivity, and accumulation rate in West Antarctica. *Journal of Geophysical Research*, 112, F03018. doi:10.1029/2006JF000716.
- Koivusalo, H., Kokkonen, T., 2002. Snow processes in a forest clearing and in a coniferous forest. *Journal of Hydrology*, 262, 145–164. doi:10.1016/S0022-1694(02)00031-8.

- König, M., Sturm, M., 1998. Mapping snow distribution in the Alaskan Arctic using aerial photography and topographic relationships. *Water Resources Research*, 34, 3471–3483.
- König, M., Winther, J. G., Isaksson, E., 2001. Measuring snow and glacier ice properties from satellite. *Reviews of Geophysics*, 39, 1–27.
- Koren, V., Schaake, J., Mitchell, K., Duan, Q.Y., Chen, F., Baker, J.M., 1999. A parameterization of snowpack and frozen ground intended for NCEP weather and climate models. *Journal of Geophysical Research*, 104, 19569–19585.
- Kostadinov, T.S., Lookingbill, T.R., 2015. Snow cover variability in a forest ecotone of the Oregon Cascades via MODIS Terra products. *Remote Sensing of Environment*, 164, 155–169. <http://dx.doi.org/10.1016/j.rse.2015.04.002>.
- Krajčí, P., Holko, L., Perdigão, R. A. P., Parajka, J., 2014. Estimation of regional snowline elevation (RSLE) from MODIS images for seasonally snow covered mountain basins. *Journal of Hydrology*, 519, 1769–1778. doi:10.1016/j.jhydrol.2014.08.064.
- Latnenser, M., Schneebeli, M., 2003. Long-term snow climate trends of the Swiss Alps (1931–99), *International Journal of Climatology*, 23, 733–750. doi:10.1002/joc.912.
- Lee, S., Klein, A.G., Over, T.M., 2005. A comparison of MODIS and NOHRSC snow-cover products for simulating streamflow using the Snowmelt Runoff Model. *Hydrological Processes*, 19, 2951–2972. doi:10.1002/hyp.5810.
- Lehning, M., Bartelt, P., Brown, B., Fierz, C., 2002. A physical SNOWPACK model for the Swiss avalanche warning—Part III: Meteorological forcing, thin layer formation and evaluation. *Cold Regions Science and Technology*, 35, 169–184. doi:10.1016/S0165-232X(02)00072-1.
- Leo, S., 2010. Monitoring snowmelt at high temporal and spatial resolution: a method using standard digital camera images. Thesis, University of Tübingen, Germany.
- Lewis, S., Bonan, G.B., Vertenstein, M., Oleson, K.W., 2004. The Community Land Model's Dynamic Global Vegetation Model (CLMDGVM): Technical description and user's guide. NCAR Tech. Note 459+IA, 50 pp., National Center for Atmospheric Research, Boulder, Colorado.
- Li, C.H., Tam, P.K.S., 1998. An iterative algorithm for minimum cross entropy thresholding. *Pattern Recognition Letters*, 19, 771–776.
- Liang, T.G., Huang, X.D., Wu, C.X., Li, W.L., Guo, Z.G., Ren, J.Z., 2008a. An application of MODIS data to snow cover monitoring in a pastoral area: A case study in Northern Xinjiang, China. *Remote Sensing of Environment*, 112, 1514–1526. doi:10.1016/j.rse.2007.06.001.
- Liang, T.G., Zhang, X.T., Xie, H.J., Wu, C.X., Feng, Q.S., Huang, X.D., Chen, Q.G., 2008b. Toward improved daily snow cover mapping with advanced combination of

- MODIS and AMSR-E measurements. *Remote Sensing of Environment*, 112, 3750–3761. doi:10.1016/j.rse.2008.05.010.
- Liu, J.F., Chen, R.S., Wang, G., 2015. Snowline and snow cover monitoring at high spatial resolution in a mountainous river basin based on a time-lapse camera at a daily scale. *Journal of Mountain Science*, 12, 60–69. doi:10.1007/s11629-013-2842-y.
- López-Burgos, V., Gupta, H.V., Clark, M., 2013. Reducing cloud obscuration of MODIS snow cover area products by combining spatio-temporal techniques with a probability of snow approach, *Hydrology and Earth System Sciences*, 17, 1809–1823. doi:10.5194/hess-17-1809-2013.
- López-Moreno, J.I., Nogués-Bravo, D., 2006. Interpolating local snow depth data: an evaluation of methods. *Hydrological Processes*, 20, 2217–2232. doi:10.1002/hyp.6199.
- Malcher, P., Floricioiu, D., Rott, H., 2003. Snow mapping in Alpine areas using medium resolution spectrometric sensors. *Geoscience and Remote Sensing Symposium, 2003. IGARSS Proceedings. IEEE International*, 4, 2835–2837.
- Mann, H.B., 1945. Non-parametric tests against trend. *Econometrica*, 13, 245–259.
- Marks, D., Kimball, J., Tingey, D., Link, T., 1998. The sensitivity of snowmelt processes to climate conditions and forest cover during rain-on-snow: a case study of the 1996 Pacific Northwest flood. *Hydrological Processes*, 12, 1569–1587.
- Maurer, E.P., Rhoads, J.D., Dubayah, R.O., Lettenmaier, D.P., 2003. Evaluation of the snow-covered area data product from MODIS. *Hydrological Processes*, 17, 59–71. doi:10.1002/hyp.1193.
- McCabe, G.J., Wolock, D.M., 2010. Long-term variability in Northern Hemisphere snow cover and associations with warmer winters. *Climatic Change*, 99, 141–153. doi:10.1007/s10584-009-9675-2.
- McCreight, J.L., Small, E.E., Larson K.M., 2014. Snow depth, density, and SWE estimates derived from GPS reflection data: Validation in the western U. S. *Water Resources Research*, 50, 6892–6909. doi:10.1002/2014WR015561.
- Menne, M.J., Durre, I., Vose, R.S., Gleason, B.E., Houston, T.G., 2012. An Overview of the Global Historical Climatology Network-Daily Database. *Journal of Atmospheric and Oceanic Technology*, 29, 897–910. doi:10.1175/JTECH-D-11-00103.1.
- Menzel, L., 1999. Flächenhafte Modellierung der Evapotranspiration mit TRAIN (areal simulation of evapotranspiration using TRAIN, in German). *PIK-Report*, 54, Potsdam.
- Menzel, L., 2007. Model based simulation of the water balance of forests on different spatial scales. In: *The role of forests and forest management in the water cycle, Progress in Hydro Sciences and Engineering*. Edited by: Feger, K.H., Wang, Y., Bernhofer, C., Seeger, J., Dresden Water Center, Dresden, Germany, 309–319.

- Menzel, L., Koch, J., Onigkeit, J., Schaldach, R., 2009. Modelling the effects of land-use and land- cover change on water availability in the Jordan River region. *Advances in Geosciences*, 21, 73–80. [www.adv-geosci.net/21/73/2009/](http://www.adv-geosci.net/21/73/2009/).
- Menzel, L., Lang, H., 2005. Spatial heterogeneity of snow conditions and evapotranspiration in the Swiss Alps. In: *Global Change in Mountain Regions – An Overview of Current Knowledge*. Edited by: Huber, U.M., Bugmann, H.K.M., Reasoner, M.A., Springer, Berlin, Heidelberg, New York, 275–282. doi:10.1007/1-4020-3508-X\_28.
- Meromy, L., Molotch, N.P., Link, T.E., Fassnacht, S.R., Rice, R., 2013. Subgrid variability of snow water equivalent at operational snow stations in the western United States. *Hydrological Processes*, 27, 2383–2400. doi:10.1002/hyp.9355.
- Mizukami, N., Perica, S., Hatch, D., 2011. Regional approach for mapping climatological snow water equivalent over the mountainous regions of the western United States. *Journal of Hydrology*. 400, 72–82. doi:10.1016/j.jhydrol.2011.01.019.
- MODIS Reprojection Tool (MRT), 2008. User's manual, release 4.0 (pp. 62). [https://lpdaac.usgs.gov/lpdaac/content/.../MRT\\_Users\\_Manual.pdf](https://lpdaac.usgs.gov/lpdaac/content/.../MRT_Users_Manual.pdf).
- Molotch, N.P., 2009. Reconstructing snow water equivalent in the Rio Grande headwaters using remotely sensed snow cover data and a spatially distributed snowmelt model. *Hydrological Processes*, 23, 1076–1089. doi:10.1002/hyp.7206.
- Molotch, N.P., Brooks, P.D., Burns, S., Litvak, M., Monson, R.K., McConnell, J.R., Musselman, K., 2009. Ecohydrological controls on snowmelt partitioning in mixed-conifer sub-alpine forests. *Ecohydrology*. 2, 129–142. doi:10.1002/eco.48.
- Molotch, N.P., Colee, M.T., Bales, R.C., Dozier, J., 2005. Estimating the spatial distribution of snow water equivalent in an alpine basin using binary regression tree models: the impact of digital elevation data and independent variable selection. *Hydrological Processes*, 19, 1459–1479. doi:10.1002/hyp.5586.
- Molotch, N.P., Margulis, S.A., 2008. Estimating the distribution of snow water equivalent using remotely sensed snow cover data and a spatially distributed snowmelt model: A multi-resolution, multi-sensor comparison. *Advances in Water Resources*, 31, 1503–1514. doi:10.1016/j.advwatres.2008.07.017.
- Monteith, J.L., 1965. Evaporation and environment. *Symposia of the Society for Experimental Biology*, 19, 205–234.
- Montpetit, B., Royer, A., Langois, A., Chum, M., Cliche, P., Roy, A., Champollion, N., Picard, G., Dominé, F., Obbard, R., In-situ measurements for snow grain size and shape characterization using optical methods. *Proceedings of 68th Eastern Snow Conference*. McGill University, Montreal, Quebec. June 14-16, 2011.
- Morán-Tejeda, E., López-Moreno, J.I., Beniston, M., 2013. The changing roles of temperature and precipitation on snowpack variability in Switzerland as a function of altitude. *Geophysical Research Letters*, 40, 1–6. doi:10.1002/grl.50463.

- Mote, P.W., 2003. Trends in snow water equivalent in the Pacific Northwest and their climatic causes. *Geophysical Research Letters*, 30, 1601. doi:10.1029/2003GL017258.
- Musselman, K.N., Molotch, N.P., Margulis, S.A., Lehning, M., Gustafson, D., 2012. Improved snowmelt simulations with a canopy model forced with photo-derived direct beam canopy transmissivity. *Water Resources Research*, 48, W10509. doi: 10.1029/2012WR012285.
- Niu, G.Y., Yang, Z.L., 2003. The versatile integrator of surface atmospheric processes - Part 2: Evaluation of three topography-based runoff schemes. *Global and Planetary Change*, 38, 191–208. doi:10.1016/S0921-8181(03)00029-8.
- Oleson, K.W., Dai, Y., Bonan, G., et al., 2004. Technical description of the Community Land Model (CLM), NCAR Tech. Note 461+STR, 174 pp., National Center for Atmospheric Research, Boulder, Colorado.
- Otsu, N., 1979. A thresholding selection method from gray-level histograms. *IEEE Transactions on Systems, Man, and Cybernetics*, 9, 62–66.
- Painter, T.H., Barrett, A.P., Landry, C.C., Neff, J.C., Cassidy, M.P., Lawrence, C.R., McBride, K.E., Farmer, G.L., 2007. Impact of disturbed desert soils on duration of mountain snow cover. *Geophysical Research Letters*, 34, L12502. doi:10.1029/2007GL030284.
- Painter, T.H., Rittger, K., Mckenzie, C., Slaughter, P., Davis, R.E., Dozier, J., 2009. Retrieval of subpixel snow covered area, grain size, and albedo from MODIS. *Remote Sensing of Environment*, 113, 868–879. doi:10.1016/S0034-4257(02)00187-6.
- Parajka, J., Blöschl, G., 2006. Validation of MODIS snow cover images over Austria. *Hydrology and Earth System Sciences*, 10, 679–689. doi:10.5194/hess-10-679-2006.
- Parajka, J., Blöschl, G., 2008a. Spatio-temporal combination of MODIS images - potential for snow cover mapping. *Water Resources Research*, 44, W03406, doi:10.1029/2007WR006204.
- Parajka, J., Blöschl, G., 2008b. The value of MODIS snow cover data in validating and calibrating conceptual hydrologic models. *Journal of Hydrology*, 358, 240–258. doi:10.1016/j.jhydrol.2008.06.006.
- Parajka, J., Haas, P., Kirnbauer, R., Jansa, J., and Blöschl, G., 2012a. Potential of time-lapse photography of snow for hydrological purposes at the small catchment scale. *Hydrological Processes*, 26, 3327–3337. doi:10.1002/hyp.8389
- Parajka, J., Holko, L., Kostka, Z., Blöschl, G., 2012b. MODIS snow cover mapping accuracy in a small mountain catchment - comparison between open and forest sites. *Hydrology and Earth System Sciences*, 16, 2365–2377. doi:10.5194/hess-16-2365-2012.
- Paudel, K. P., Andersen, P., 2011. Monitoring snow cover variability in an agropastoral area in the Trans Himalayan region of Nepal using MODIS data with improved

- cloud removal methodology. *Remote Sensing of Environment*, 115, 1234–1246. doi:10.1016/j.rse.2011.01.006.
- Peters, G. Van Balen, R.T., 2007. Tectonic geomorphology of the northern Upper Rhine Graben, Germany. *Global Planetary Change*, 58, 310–334. doi:10.1016/j.gloplacha.2006.11.041.
- Pomeroy, J.W., Brun, E., 2001. Physical properties of snow. In: *Snow Ecology: an Interdisciplinary Examination of Snow-covered Ecosystems*, Edited by: Jones, H.G., Pomeroy, J.W., Walker, D.A., Hoham, R.W., Cambridge University Press, Cambridge, UK, pp. 45–118.
- Pomeroy, J.W., Granger, R.J., Pietroniro, A., Elliot, J., Toth, B., Hedstrom, N., 1997. Hydrological Pathways in the Prince Albert Model Forest. NHRI Environment Canada, Saskatoon, Saskatchewan.
- Pomeroy, J.W., Parviainen, J., Hedstrom, N., Gray, D.M., 1998. Coupled modelling of forest snow interception and sublimation. *Hydrological Processes*, 12, 2317–2337.
- Pomeroy, J.W., Gray, D.M., Brown, T., Hedstrom, N.R., Quinton, W.L., Granger, R.J., Carey, S.K., 2007. The Cold Regions Hydrological Model, a platform for basing process representation and model structure on physical evidence. *Hydrological Processes*, 21, 2650–2667. doi:10.1002/hyp.6787.
- Pomeroy, J.W., Schmidt, R.A., 1993. The use of fractal geometry in modelling intercepted snow accumulation and sublimation. *Proceedings of the 50th Eastern Snow Conference, Québec*, pp. 1–10.
- Powell, C., Blesius, L., Davis, J., Schuetzenmeister, F., 2011. Using MODIS snow cover and precipitation data to model water runoff for the Mokelumne River Basin in the Sierra Nevada, California (2000–2009). *Global and Planetary Change*, 77, 77–84. doi:10.1016/j.gloplacha.2011.03.005.
- Pu, Z., Xu, L., Salomonson, V., 2007. MODIS/Terra observed seasonal variations of snow cover over the Tibetan Plateau. *Geophysical Research Letters*, 34, L06706. doi:10.1029/2007GL029262.
- Pyles, R.D., Weare, B.C., Pawu, K.T., 2000. The UCD advanced canopy-atmosphere-soil algorithm: Comparisons with observations from different climate and vegetation regimes. *Quarterly Journal of the Royal Meteorological Society*. 126, 2951–2980. doi:10.1002/qj.49712656917.
- Raleigh, M.S., Rittger, K., Moore, C.E., Henn, B., Lutz, J.A., Lundquist, J.D., 2013. Ground-based testing of MODIS fractional snow cover in subalpine meadows and forests of the Sierra Nevada. *Remote Sensing of Environment*, 128, 44–57. <http://dx.doi.org/10.1016/j.rse.2012.09.016>.
- Ramsay, B.H., 1998. The interactive multisensor snow and ice mapping system. *Hydrological Processes*, 12, 1537–1546.

- Ridler, T.W., Calvard, S., 1978. Picture thresholding using an iterative selection method. *IEEE transactions on Systems, Man and Cybernetics*, 8, 630–632.
- Riggs, G. A., Hall, D. K. 2003. Reduction of cloud obscuration in the MODIS snow data product. *Proceedings of the 60th Eastern Snow Conference*, Sherbrooke, Québec, 4–6 June, 2003, pp. 205–212.
- Riggs, G.A., Hall, D.K., Salomonson, V.V., 2006. MODIS snow products user guide to collection 5. [https://nsidc.org/data/docs/daac/modis\\_v5/Dorothy\\_snow\\_doc.pdf](https://nsidc.org/data/docs/daac/modis_v5/Dorothy_snow_doc.pdf).
- Riggs, G.A., Hall, D.K., 2010. MODIS Snow Cover Mapping Decision Tree Technique: Snow and Cloud Discrimination. *Proceedings of the 67th Eastern Snow Conference*, Hancock, MA, USA, 8–10 June, 2010, pp. 41–50.
- Robinson, D.A., Dewey, K.F., Heim Jr., R.R., 1993. Global snow cover monitoring: an update. *Bulletin of the American Meteorological Society*, 74, 1689–1696.
- Rodgers, J.L., Nicewander, W.A., 1988. Thirteen ways to look at the correlation coefficient. *The American Statistician*, 42, 59–66.
- Roesch, A., 2006. Evaluation of surface albedo and snow cover in AR4 coupled climate models. *Journal of Geophysical Research*. 111, D15111, doi:10.1029/2005JD006473.
- Rutter, N. et al., 2009. Evaluation of forest snow processes models (SnowMIP2). *Journal of Geophysical Research*, 114, D06111. doi:10.1029/2008JD011063.
- Samuel, J., Coulibaly, P., Dumedah, G., Moradkhani, H., 2014. Assessing model state and forecasts variation in hydrologic data assimilation. *Journal of Hydrology*. 513, 127–141. doi:10.1016/j.jhydrol.2014.03.048.
- Samuelsson, P., Gollvik, S., Ullerstig, A., 2006. The land-surface scheme of the Rossby Centre regional atmospheric climate model (RCA3). *Rep. Meteorol.* 122, 25 pp., Swedish Meteorological and Hydrological Institute, Norrköping, Sweden.
- Sauter, T., Weitzenkamp, B., Schneider, C., 2010. Spatio-temporal prediction of snow cover in the Black Forest mountain range using remote sensing and a recurrent neural network. *International Journal of Climatology*, 30, 2330–2341. doi:10.1002/joc.2043.
- Schmidt, R.A., Gluns, D.R., 1991. Snowfall interception on branches of three conifer species. *Canadian Journal of Forest Research*, 21, 1262–1269.
- Schmucki, E., Marty, C., Fierz, C., Lehning, M., 2014. Evaluation of modelled snow depth and snow water equivalent at three contrasting sites in Switzerland using SNOWPACK simulations driven by different meteorological data input. *Cold Regions Science and Technology*. 99, 27–37. doi:10.1016/j.coldregions.2013.12.004.
- Sen, P.K., 1968. Estimates of the regression coefficient based on Kendall's tau. *Journal of the American Statistical Association*, 63, 1379–89.
- Serquet, G., Marty, C., Dulex, J.P., Rebetez, M., 2011. Seasonal trends and temperature dependence of the snowfall/precipitation-day ratio in Switzerland. *Geophysical Research Letters*, 38, L07703. doi:10.1029/2011GL046976.

- Shrestha, M., Wang, L., Koike, T., Xue, Y., Hirabayashi, Y., 2014. Correcting basin-scale snowfall in a mountainous basin using a distributed snowmelt model and remote-sensing data. *Hydrology and Earth System Sciences*, 18, 747–761. doi:10.5194/hessd-10-11711-2013.
- Shamir, E., Georgakakos, K.P., 2006. Distributed snow accumulation and ablation modeling in the American River Basin. *Advances in Water Resources*. 29, 558–570. doi:10.1016/j.advwatres.2005.06.010.
- Simic, A., Fernandes, R., Brown, R., Romanov, P., Park, W., 2004. Validation of VEGETATION, MODIS, and GOES+SSM/I snow-cover products over Canada based on surface snow depth observations. *Hydrological Processes*, 18, 1089–1104. doi:10.1002/hyp.5509
- Singh, P., Singh, V.P., *Snow and glacier hydrology*. Kluwer Academic Publishers, Dordrecht, The Netherlands, pp. 104.
- Slater, A.G., Clark, M., 2006. Snow data assimilation via an ensemble Kalman filter. *Journal of Hydrometeorology*, 7, 478–493. <http://dx.doi.org/10.1175/JHM505.1>
- Slater, A.G., et al. 2001. The representation of snow in land surface schemes: Results from PILPS 2(d). *Journal of Hydrometeorology*, 2, 7–25.
- Spearman, C., 1904. The proof and measurement of association between two things. *The American Journal of Psychology*, 15, 72–101.
- Strasser, U., Bernhardt, M., Weber, M., Liston, G.E., Mauser, W., 2008. Is snow sublimation important in the alpine water balance? *The Cryosphere*, 2, 53–66. doi:10.5194/tc-2-53-2008.
- Strasser, U., Etchevers, P., Lejeune, Y., 2002. Inter-comparison of two snow models with different complexity using data from an alpine site. *Nordic Hydrology*, 33, 15–26.
- Street, R.B., Melnikov, P.I., 1990. Seasonal snow, cover, ice and permafrost, In: *Climate Change: The IPCC Impacts Assessment*, Edited by Tegart, W.J.McG., Sheldon, G.W., Griffiths, D.C., Australian Government Publishing Service, Canberra, Australia.
- Sturm, M., 2015, White water: Fifty years of snow research in WRR and the outlook for the future. *Water Resources Research*, 51, 4948–4965. doi:10.1002/2015WR017242.
- Tahir, A.A., Chevallier, P., Arnaud, Y., Ashraf, M., Bhatti, M.T., 2015. Snow cover trend and hydrological characteristics of the Astore River basin (Western Himalayas) and its comparison to the Hunza basin (Karakoram region). *Science of the Total Environment*, 505, 748–761. <http://dx.doi.org/10.1016/j.scitotenv.2014.10.065>.
- Takata, K., Emori, S., Watanabe, T., 2003. Development of the minimal advanced treatments of surface interaction and runoff. *Global and Planetary Change*, 38, 209–222. doi:10.1016/S0921-8181(03)00030-4.

- Thompson, J.A., Paull, D.J., Lees, B.G., 2015. An improved liberal cloud-mask for addressing snow/cloud confusion with MODIS. *Photogrammetric Engineering & Remote Sensing*, 81, 119–129. doi:10.14358/PERS.81.2.23.
- Tong, J., Déry, S. J., Jackson, P. L., 2009. Topographic control of snow distribution in an alpine watershed of western Canada inferred from spatially-filtered MODIS snow products. *Hydrology and Earth System Sciences*, 13, 319–326. doi:10.5194/hess-13-319-2009.
- Törnros, T., Menzel, L., 2014. Addressing drought conditions under current and future climates in the Jordan River region. *Hydrology and Earth System Sciences*, 18, 305–318. doi:10.5194/hess-18-305-2014.
- Tribbeck, M.J., 2002. Modelling the effect of vegetation on the seasonal snow cover. Ph.D. thesis, 221 pp., Univ. of Reading, Reading, U. K.
- Tribbeck, M.J., Gurney, R.J., Morris, E.M., Pearson, D.W.C., 2004. A new Snow-SVAT to simulate the accumulation and ablation of seasonal snow cover beneath a forest canopy. *Journal of Glaciology*, 50, 171–182. doi:10.3189/172756504781830187.
- Tribbeck, M.J., Gurney, R.J., Morris, E.M., 2006. The radiative effect of a fir canopy on a snowpack. *Journal of Hydrometeorology*, 7, 880–895. doi:10.1175/JHM528.1.
- Uehlinger U., Wantzen K.M., Leuven, R.S.E.W., Arndt H., 2008. The Rhine River Basin. In: *Rivers of Europe*. Edited by: Tockner, K., Robinson, C.T., and Uehlinger, U., Academic Press, London, pp. 199–245.
- Varhola, A., Coops, N.C., Weiler, M., Moore, R.D., 2010. Forest canopy effects on snow accumulation and ablation: an integrative review of empirical results. *Journal of Hydrology*, 2010, 392, 219–233. doi:10.1016/j.jhydrol.2010.08.009.
- Verseghy, D.L., 1991. CLASS-A Canadian Land Surface Scheme for GCMs. 1. Soil model. *International Journal of Climatology*, 11, 111–133.
- Verzano, K., Menzel, L., 2009. Snow conditions in mountains and climate change—a global view. In: Marks, D. (Ed.): *Hydrology in Mountain Regions: Observations, Processes and Dynamics*. IAHS Publication 326, Wallingford, 147–154.
- Wang, X.W., Xie, H.J., Liang, T.G., 2008. Evaluation of MODIS snow cover and cloud mask and its application in Northern Xinjiang, China. *Remote Sensing of Environment*, 112, 1497–1513. doi:10.1016/j.rse.2007.05.016.
- Wang, X.W., Xie, H.J., Liang, T.G., Huang, X.D., 2009. Comparison and validation of MODIS standard and new combination of Terra and Aqua snow cover products in northern Xinjiang, China. *Hydrological Processes*, 23, 419–429. doi:10.1002/hyp.7151.
- Warren, S.G., 1982. Optical properties of snow. *Reviews of Geophysics*, 20, 67–89. doi: 10.1029/RG020i001p00067.
- Warrilow, D.A., Buckley, E., 1989. The impact of land surface processes on the moisture budget of a climate model. *Annals of Geophysics*, 7, 439–450.

- Wetzel, P., Boone, A., 1995. A parameterization for land–atmosphere–cloud exchange (PLACE): Documentation and testing of a detailed process model of the partly cloudy boundary layer over heterogeneous land. *Journal of Climate*, 8, 1810–1837.
- Wilks, D. S. (2006). *Statistical Methods in the Atmospheric Sciences*. 2nd Edition, Academic Press, London, United Kingdom.
- Wimmer, F., Schläffer, S., Aus der Beek, T., Menzel, L., 2009. Distributed modelling of climate change impacts on snow sublimation in Northern Mongolia. *Advances in Geosciences*, 21, 117–124. [www.adv-geosci.net/21/117/2009/](http://www.adv-geosci.net/21/117/2009/).
- WMO, 2013. CryoNet Implementation Meeting, 1st Session, final report. World Meteorological Organization GCW (Global Cryosphere Watch), Vienna, Austria, 20-22 November 2012. GCW Report 2 (2013), 94 pp.
- Woo, M., Giesbrecht, M. A. (2000). Simulation of snowmelt in a subarctic spruce woodland: 1. Tree model. *Water Resources Research*, 36, 2275–2285.
- Xia, Q., Gao, X., Chu, W., Sorooshian, S., 2012. Estimation of daily cloud-free, snow-covered areas from MODIS based on variational interpolation. *Water Resources Research*, 48, WR011072. doi:10.1029/2011WR011072.
- Xie, H. J., Wang, X.W., Liang, T.G., 2009. Development and assessment of combined Terra and Aqua snow cover products in Colorado Plateau, USA and northern Xinjiang, China. *Journal of Applied Remote Sensing*, 3, 033559. doi:10.1117/1.3265996.
- Xue, Y.K., Sun, S.F., Kahan, D.S., Jiao, Y.J., 2003. Impact of parameterizations in snow physics and interface processes on the simulation of snow cover and runoff at several cold region sites. *Journal of Geophysical Research*, 108, 8859. doi:10.1029/2002JD003174.
- Yamazaki, T., 2001. A one-dimensional land surface model adaptable to intensely cold regions and its application in eastern Siberia. *Journal of the Meteorological Society of Japan*, 79, 1107–1118.
- Yamazaki, T., Yabuki, H., Ishii, Y., Ohta, T., Ohata, T., 2004. Water and energy exchanges at forests and a grassland in eastern Siberia evaluated using a one-dimensional land surface model. *Journal of Hydrometeorology*, 5, 504–515.
- Yang, Z.L., Dickinson, R.E., Robock, A., Vinnikov, Ya.K., 1997. On validation of the snow sub-model of the biosphere–atmosphere transfer scheme with Russian snow cover and meteorological observational data. *Journal of Climate*, 10, 353–373.
- Yue, S., Pilon, P., Phinney, B., Cavadias, G., 2002. The influence of auto-correlation on the ability to detect trend in hydrological series. *Hydrological Processes*, 16, 1807–1829. doi:10.1002/hyp.1095.
- Zhang, Y., Hong, Y., Gourley, J.J., Wang, X., Brakenridge, G.R., Groeve T.D., Vergara, H., 2014. Impact of assimilating spaceborne microwave signals for improving hydrological predictions ungauged basins. In: *Remote Sensing of the Terrestrial*

- Water Cycle. Edited by: Lakshmi, V., Alsdorf, D., Anderson, M., Biancamaria, S., Cosh, M., Entin, J., Huffman, G., Kustas, W., van Oevelen, P., Painter, T., Parajka, J., Rodell, M., Rüdiger, C., John Wiley & Sons, Inc, Hoboken, NJ., USA. doi: 10.1002/9781118872086.ch27.
- Zhou, H., Aizen, E., Aizen V., 2013. Deriving long term snow cover extent dataset from AVHRR and MODIS data: Central Asia case study. *Remote Sensing of Environment*, 136, 146–162. doi:10.1016/j.rse.2013.04.015.
- Zhou, X., Xie, H., Hendrickx, J.M.H., 2005. Statistical evaluation of remotely sensed snow cover products with constraints from streamflow and SNOTEL measurements. *Remote Sensing of Environment*, 94, 214–231. doi:10.1016/j.rse.2004.10.007.

## **Acknowledgment**

This dissertation has been accomplished in Heidelberg University Hydrology and Climatology Research Group on “Rhine-Transect: An interdisciplinary, long-term research project across the Upper Rhine Valley”.

First and foremost, I am sincerely grateful to my supervisor Prof. Dr. Lucas Menzel for his generous support and guidance during the past four years. He has provided me with particular encouragement, inspiring discussions, and the opportunity to develop my skills and broaden my knowledge as a hydrological researcher. Many thanks also go to my current and erstwhile colleagues for their valuable comments and suggestions that improved the presentation and contents of this dissertation. Special thanks go to my colleague Matthias Stork for his kind support in revising the German abstract.

I would like to thank my wife Jie Guo for her patience and support, and for standing beside me throughout my graduate study. Special thanks are given to my parents, my sister and my brother for encouraging me to pursue my career and to realize my potential.

I also wish to acknowledge the financial support from the China Scholarship Council (CSC) and the German Academic Exchange Service (DAAD). The author is grateful to the German Weather Service (DWD) and National Snow and Ice Data Center (NSIDC) for data supply.

*Chunyu Dong*

Heidelberg, Spring 2016

**Eidesstattliche Versicherung gemäß § 8 der Promotionsordnung  
der Naturwissenschaftlich-Mathematischen Gesamtfakultät  
der Universität Heidelberg**

1. Bei der eingereichten Dissertation zu dem Thema

Assessing the availability of remote sensing, hydrological modeling and in situ  
observations in snow cover research

---

handelt es sich um meine eigenständig erbrachte Leistung.

2. Ich habe nur die angegebenen Quellen und Hilfsmittel benutzt und mich keiner unzulässigen Hilfe Dritter bedient. Insbesondere habe ich wörtlich oder sinngemäß aus anderen Werken übernommene Inhalte als solche kenntlich gemacht.

3. Die Arbeit oder Teile davon habe ich wie folgt/bislang nicht<sup>1)</sup> an einer Hochschule des In- oder Auslands als Bestandteil einer Prüfungs- oder Qualifikationsleistung vorgelegt.

Titel der Arbeit: \_\_\_\_\_

Hochschule und Jahr: \_\_\_\_\_

Art der Prüfungs- oder Qualifikationsleistung: \_\_\_\_\_

4. Die Richtigkeit der vorstehenden Erklärungen bestätige ich.

5. Die Bedeutung der eidesstattlichen Versicherung und die strafrechtlichen Folgen einer unrichtigen oder unvollständigen eidesstattlichen Versicherung sind mir bekannt.

Ich versichere an Eides statt, dass ich nach bestem Wissen die reine Wahrheit erklärt und nichts verschwiegen habe.

Heidelberg, 4, Mai 2016  
Ort und Datum

Chunyu Dong  
Unterschrift

<sup>1)</sup> Nicht Zutreffendes streichen. Bei Bejahung sind anzugeben: der Titel der andernorts vorgelegten Arbeit, die Hochschule, das Jahr der Vorlage und die Art der Prüfungs- oder Qualifikationsleistung.